

**DEVELOPMENT OF BIOCONJUGATES AND THEIR
MODUL CONSTRUCTS FOR TARGETED THERAPY
OF CANCERS WITH HIGH MORTALITY**

Excerpt from the results obtained in frame of the grant

NVKP_16-1-2016-0036

supported by the National Research, Development and Innovation Office

ISBN 978-963-489-286-1

Budapest, 2020



TABLE OF CONTENTS

Preface: Development of bioconjugates and their module constructs for targeted therapy of cancers with high mortality (<i>Gábor Mező</i>)	3
Optimization of homing peptide sequence selected by phage display for HT-29 colon cancer cells to improve the antitumor activity (<i>Krisztina Kiss, Beáta Biri-Kovács, Rita Szabó, Kata Nóra Enyedi, Murányi József, Gitta Schlosser, Ivan Randelović, József Tóvári, Gábor Mező</i>)	5
New GnRH-III derivative as homing peptide for potential drug targeting in cancer therapy (<i>Sabine Schuster, Beáta Biri-Kovács, Ivan Randelović, József Tóvári, Gábor Mező</i>)	10
Comparison of the apoptotic effects of different GnRH-based conjugates with or without butyrylated Lys in position 4 on colon carcinoma cells (<i>Eszter Lajkó, Rózsa Hegedüs, Gábor Mező, László Kőhidai</i>)	17
Structural and binding characteristics of HER2 receptor targeting peptides (<i>Beáta Biri-Kovács, Afrodité Adorján, Ildikó Szabó, Bálint Szeder, Szilvia Bősze, Gábor Mező</i>)	23
Development of novel cyclic NGR peptide–daunomycin conjugates with dual targeting property (<i>Andrea A.P. Tripodi, Kata Nóra Enyedi, Beáta Biri-Kovács, Ivan Randelović, Szilárd Tóth, Bálint Szeder, Gergely Szakács, József Tóvári, Gábor Mező</i>)	28
Design, synthesis and characterization of Pancreatic Ductal Adenocarcinoma (PDAC) targeting antitumor daunomycin-peptide conjugates (<i>Levente E. Dókus, Eszter Lajkó, Orsolya Láng, Diána Mező, Zsófia Szász, Angéla Takács, László Kőhidai, Gitta Schlosser, Ivan Randelović, József Tóvári, Gábor Mező</i>)	34
Synthesis and <i>in vitro</i> evaluation of drug containing melanoma specific peptide conjugates (<i>Ildikó Szabó, Szilvia Bősze, Gábor Mező</i>)	39
Optimization of the structure of targeted Daunomycin conjugates against non-small cell lung cancer (<i>Zoltán Bánóczi, Ildikó Szabó, Gábor Mező</i>)	45
Peptide based delivery vehicles for tumor tissue targeting (<i>Zsuzsa Baranyai, Katalin Uray, Beáta Biri-Kovács, Lilla Horváth, Szilvia Bősze</i>)	50

Tandem mass spectrometry of daunorubicin-containing peptide conjugates (<i>Gitta Schlosser, Mohammed Al-Majidi, Adina Borbély, Lilla Pethő, Dániel Szabó, Levente Dókus, Gábor Mező</i>)	55
Effect of ionization conditions in electrospray ionization mass spectrometry of daunorubicin-tuftsins peptide conjugates (<i>Lilla Pethő, Gábor Mező, Gitta Schlosser</i>)	60
Synthesis of drug-peptide conjugates using bifunctional spacers (<i>Lea Várhegyi, Lilla Pethő, Kata Nóra Enyedi</i>)	65
<i>In vitro</i> anti-tumor effect of cinchona-chalcone hybrids with 1,4- or 1,5-disubstituted 1,2,3-triazole linker (<i>Rita Oláh-Szabó, Tamás Jernei, Ildikó Szabó, Gábor Mező, Antal Csámpai</i>)	70
<i>In vitro</i> antitumor effect and structure–activity relationships of ferrocene-containing imipridone hybrids (<i>Rita Oláh-Szabó, Péter Bárány, Imre Kovács, Tamás Czucz, Szilvia Bősze, Antal Csámpai</i>)	75
The <i>in vitro</i> antitumor effect of ONC201 derivatives in pancreatic and in colorectal cancer cell lines (<i>Angéla Takács, Zsófia Szász, Eszter Lajkó, Márton Kalabay, Diána Mező, Nóra Fekete Éva Pállinger, Péter Bárány, Antal Csámpai, Orsolya Láng, László Kőhidai</i>)	81
Bortezomib has antitumor effect in melanoma cells that can be inhibited by alpha-lipoic acid (<i>Angéla Takács, Eszter Lajkó, Orsolya Láng, Ildikó Istenes, László Kőhidai</i>)	86
Design and synthesis of novel apoptosis-inducing cytotoxic drug leads for conjugation with carrier molecules and development of Tumor Targeting Drug Conjugates (<i>Béla Bertók, György Dormán, László Kőhidai, Orsolya Láng, Csaba Magyar</i>)	92

Development of bioconjugates and their module constructs for targeted therapy of cancers with high mortality

Preface

Gábor Mező^{1,2}

¹Institute of Chemistry, Eötvös Loránd University, Budapest, Hungary

²MTA-ELTE Research Group of Peptide Chemistry, Hungarian Academy of Sciences, Eötvös L. University, Budapest, Hungary

Cancer is currently the second leading cause of death worldwide. Global cancer statistics estimate over 18 million new cases and close to 10 million deaths for 2018. One of the main therapeutic approaches for cancer is chemotherapy. However, chemotherapy is not always effective and induces severe toxic side effects, as the applied drugs affect not only cancer cells but also normal tissues. To overcome this drawback, targeted therapeutic possibilities have been investigated for increasing tumor selectivity. For this purpose, the anticancer drugs are attached either to antibodies or small molecules like homing peptides that can recognize specifically the tumor-specific or overexpressed receptors on cancer cells. The other advantage of this type of therapy is the avoidance of multidrug resistance. Although some antibody–drug conjugates (ADCs) are investigated to the market for tumor treatment, besides their benefits (*e.g.* high specificity and slow elimination from the circulation) they have some limitations as well (*e.g.* pure tumor tissue penetration and high cost). Therefore, there is increased interest in small molecule drug conjugates (SMDCs) especially in peptide drug conjugates (PDCs). Appropriate homing peptides can recognize tumor-specific or overexpressed receptors on tumor cells with high affinity even if they might not be as selective as ADCs, moreover, they are not immunogen and the preparation of PDC is easier and more cost-effective. However, in many cases, the cell surface components that could be attacked are not well known. In this case, peptides with specific binding properties can be selected by the aid of phage display. The second most important problem is the selection of efficient anti-cancer agents to be bound to the peptide through an appropriate linkage allowing the release of the free drug or its active metabolite in cancer cells. There are several promising peptide-based drug conjugates for targeted tumor therapy in Clinical Trial phases. However, many different types of cancers exist, therefore a few structures of peptide drug conjugates are not enough for the treatment of a broad range of malignant diseases. The recent trend of personalized oncology needs a significant number of versatile drug delivery systems (DDSs)

with high selectivity and efficacy to the special tumor types. Furthermore, a combination of DDSs might increase the therapeutic effect.

In the frame of the project “Development of bioconjugates and their module constructs for targeted therapy of cancers with high mortality” supported by Hungarian National Research, Development and Innovation Office (grant number: NVKP_16-1-2016-0036) our goal was to develop new peptide drug conjugates for the treatment of different types of tumors especially for the ones that cause high mortality (*e.g.* pancreatic, lung, colon, metastatic melanoma, glioma and HER2 positive breast cancers). For this purpose, three libraries of compounds: a) anticancer agents, b) homing peptides, and c) bifunctional linkers that are suitable for connection of the two previous ones) were developed. The final aim of this project was to prepare appropriate modules that can be combined easily for the development of numerous different DDSs for targeted tumor therapy (Figure 1).

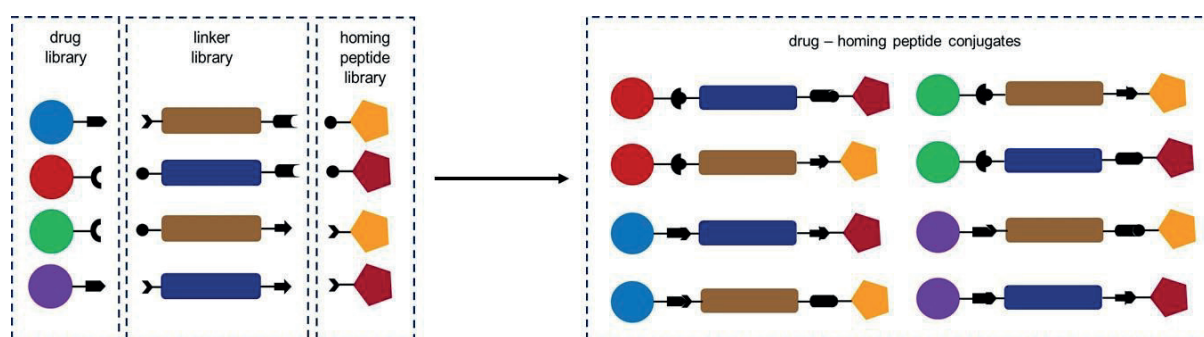


Figure 1. Schematic presentation of module libraries and their combination in conjugates

This booklet provides an overview for readers about the results obtained in the frame of the project by the consortium members. The consortium members are Eötvös Loránd University, Institute of Chemistry including the Research Group of Peptide Chemistry, Semmelweis University and ComInnex, Inc. We believe that this concept may provide a new strategy and our results make a stride towards efficient personalized tumor chemotherapy.

Optimization of homing peptide sequence selected by phage display for HT-29 colon cancer cells to improve the antitumor activity

Krisztina Kiss^{1,2}, Beáta Biri-Kovács^{1,2}, Rita Szabó¹, Kata Nóra Enyedi^{1,2}, Murányi József³, Gitta Schlosser^{1,2}, Ivan Randelović⁴, József Tóvári⁴, Gábor Mező^{1,2}

¹MTA-ELTE Research Group of Peptide Chemistry, Hungarian Academy of Sciences, Eötvös L. University, Budapest, Hungary

²Institute of Chemistry, Eötvös L. University, Budapest, Hungary

³MTA-SE Pathobiochemistry Research Group, Semmelweis University, Budapest, Hungary

⁴Department of Experimental Pharmacology, National Institute of Oncology, Budapest, Hungary

Introduction

Colon cancer has become the third most commonly diagnosed cancer and the fourth leading cause of death related to cancer in the world.^{1,2} Besides the conventional treatments of colon cancer (surgery, radiation therapy and chemotherapy) targeted therapy is one of the main therapeutic approaches that might have a significant role in the future.³ The most remarkable advantages of targeted cancer therapy over the conventional chemotherapy are the specificity towards cancer cells while sparing toxicity to off-target cells and the avoidance of multi-drug resistance (MDR), which are the major obstacles in cancer chemotherapy.⁴ The concept of selective drug targeting is based on the high expression of certain cell surface components on tumors or the tumor neovasculature.⁵ Therefore, the search of new tumor homing peptides that recognize them is a hot topic in targeted cancer therapy.⁶ One of the approaches often used to explore new peptides is a technique belonging to *in vitro* evolution methods: phage display is a useful tool to identify tumor-specific peptides that can be used efficiently for anticancer drug targeting.⁷

Zhang and his co-workers selected HT-29 human colon cancer-specific heptapeptides by phage display technology.¹ In the *in vitro* panning experiment a 7-mer phage-display peptide library containing 10^{11} pfu was used (*ca.* 100 clones belong to one peptide sequence). After 3 rounds of panning using colon cancer cell lines and 2 rounds of subtractive screening, the peptide sequences of 50 randomly picked phage clones were analyzed by cell – enzyme-linked immunosorbent assay. The heptapeptide VHLGYAT was found as the most selective peptide to HT-29 colon cancer cell line. It has to be noted that the receptor recognized by this peptide was not identified. We believed that during the random selection of 50 clones from the panned and screened phages after three rounds of panning, some compounds with higher

affinity and/or selectivity were lost. Thus, Ala scan and positional scan procedures were used to find more active conjugates in this study.

Results

Daunomycin (Dau) conjugate of VHLGYAT peptide amide (Dau=Aoa-LRRYVHLGYAT-NH₂) was prepared. Dau as an anticancer agent was attached to the homing peptide *via* oxime linkage through an aminooxyacetic moiety (Aoa) which was connected to a Cathepsin B cleavable spacer (LRRY). This spacer was investigated to avoid the release of different metabolites from the conjugates, because the oxime bond is stable, and the smallest metabolite that can be released is Dau=Aoa-Xxx-OH (where Xxx is the amino acid whose amino group is acylated with aminooxyacetic acid).⁸ The peptide chain was built up by SPPS, and Dau was conjugated to the aminooxy acetylated peptide in solution (Figure 1).

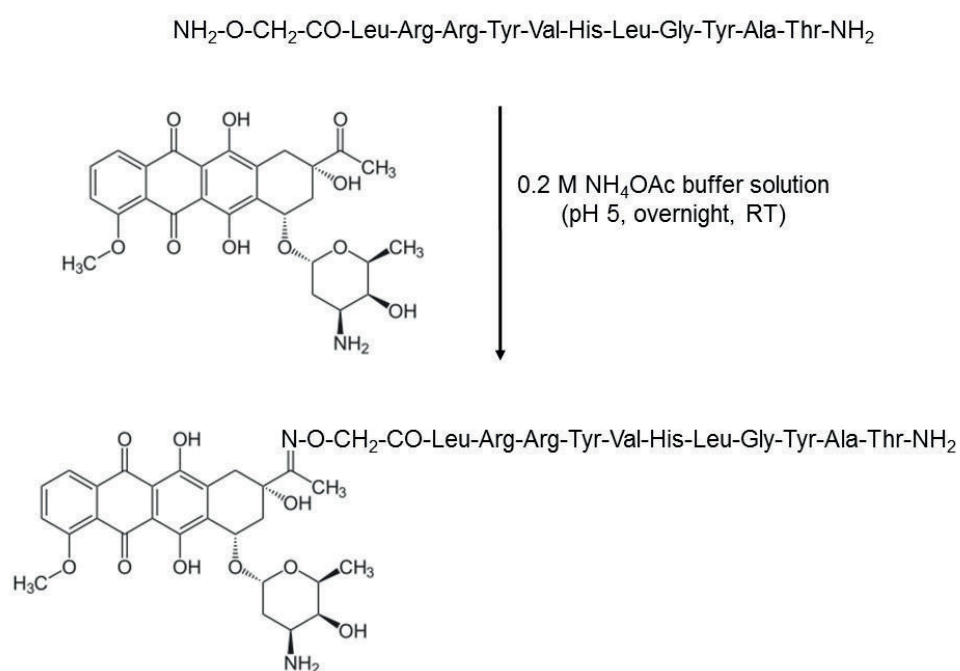


Figure 1. Conjugation of daunomycin to the aminooxyacetylated homing peptide

The conjugate showed moderate cytostatic effect (Table 1).⁹ In the next step Ala scan was made and all amino acid in the basic heptapeptide sequence was replaced by Ala step by step. The cytotoxic effect of the new conjugates was measured on HT-29 colon adenocarcinoma cells. The results indicated that the replacement of Val, Leu or Tyr to Ala (V/A, L/A, Y/A) in the sequence of the homing peptide is not allowed without loss of cytostatic effect (IC₅₀ > 100 μM). When Thr was changed to Ala (T/A) the anti-tumour effect

decreased a bit, while the modification of His (H/A) in the sequence resulted in a slightly more active conjugate (Table 1). The replacement of Gly to Ala (G/A) increased the cytostatic effect significantly (from $IC_{50} = 46.9 \pm 9.4 \mu\text{M}$ to $24.1 \pm 1.6 \mu\text{M}$) in this experiment. The differences in antitumor activity of the conjugates could be explained by their different cellular uptake propensity measured by flow cytometry. Therefore, further different types of amino acids were incorporated in this position. Lys as a basic, Glu as an acidic amino acid, Thr, Ser and Asn as polar and Phe, Leu as nonpolar (aromatic and nonaromatic) amino acids were incorporated. Furthermore, Pro that might break the conformation of the peptide was investigated.

Table 1. Characteristics of conjugates modified by Ala and positional scanning

Compounds (code)	RP-HPLC	ESI-MS	ESI-MS	IC ₅₀ ^c
	R _t (min) ^a	calc	meas ^b	(μM)
Dau=Aoa-LRRY-AHLGYAT-NH ₂ (1)	28.2	1930.1	1929.9	46.9±9.4
Dau=Aoa-LRRY-AHLGYAT-NH ₂ (2)	27.7	1901.5	1901.8	>100
Dau=Aoa-LRRY-VALGYAT-NH ₂ (3)	29.0	1863.5	1864.0	36.8±0.4
Dau=Aoa-LRRY-VHAGYAT-NH ₂ (4)	27.2	1887.5	1887.8	>100
Dau=Aoa-LRRY-VHLAYAT-NH ₂ (5)	28.6	1943.6	1943.9	24.1±1.6
Dau=Aoa-LRRY-VHLGAAT-NH ₂ (6)	27.4	1837.5	1837.8	>100
Dau=Aoa-LRRY-VHLGYAA-NH ₂ (7)	28.0	1899.8	1899.9	70.9±3.8
Dau=Aoa-LRRY-VHLKYAT-NH ₂ (8)	28.2	2000.7	2000.8	50.3±3.0
Dau=Aoa-LRRY-VHLEYAT-NH ₂ (9)	29.3	2001.6	2001.7	29.5±6.3
Dau=Aoa-LRRY-VHLLYAT-NH ₂ (10)	31.1	1985.7	1986.0	7.5±3.5
Dau=Aoa-LRRY-VHLFYAT-NH ₂ (11)	31.2	2019.7	2019.8	6.6±2.9
Dau=Aoa-LRRY-VHLSYAT-NH ₂ (12)	28.9	1959.6	1959.8	24.8±7.4
Dau=Aoa-LRRY-VHPTYAT-NH ₂ (13)	29.0	1973.6	1974.0	21.7±6.5
Dau=Aoa-LRRY-VHLYAT-NH ₂ (14)	29.0	1986.6	1987.9	28.0±19.4
Dau=Aoa-LRRY-VHLPYAT-NH ₂ (15)	31.2	1969.7	1970.1	>50
Dau=Aoa-LRRY-VHLYAT-NH ₂ (16)	30.8	2036.2	2036.1	38.4±17.7
Dau=Aoa-LRRY-VHLCpaYAT-NH ₂ (17)	31.3	2053.6	2053.8	3.6±0.1

^aRP-HPLC: column: Phenomenex Aeris Peptide XB-C18 column (250 mm x 4.6 mm) with 3.6 μm ; eluents: 0.1% TFA in water (A) and 0.1% TFA in MeCN-water (80:20, v/v) (B); gradient: 0 min 0% B, 5 min 0% B, 50 min 90% B; flow rate: 1 mL/min; detection: $\lambda = 220 \text{ nm}$.

^bESI-MS: Esquire 3000+ ion trap mass spectrometer

^cMTT assay on HT-29 colon adenocarcinoma cells; 24 h treatments + 48 h further incubation

All conjugates except the Pro containing one (**15**) showed cytostatic effect in the measured range. The incorporation of Lys (**8**) in this position decreased the cytostatic effect ($IC_{50} = 50.3 \pm 3.0 \mu\text{M}$) compared to both G/A, and the native conjugates. No significant difference in cytostatic effect was observed when the Ala was replaced Glu, Ser, Thr, Asn (**9**,

12, 13, 14). However, it is worth mentioning that the change of Ala to Ser (12) increased the water solubility of the conjugate that might be useful in drug development. The results indicated that the incorporation of Leu (10) or Phe (11) gives the best conjugates having 4-5 times higher cytostatic effect than the G/A ($IC_{50} = 6.6 \pm 2.9 \mu\text{M}$ and $7.5 \pm 3.5 \mu\text{M}$, respectively). When the Phe was substituted with OH group (Tyr, 16) the antitumor effect was decreased, while Cl substitution (Cpa: *p*-chloro-phenylalanine, 17) enhanced the activity to $IC_{50} = 3.6 \pm 0.1 \mu\text{M}$ (but decreased the solubility of the conjugate). Thus Phe was applied in this position in the further studies. It was also indicated that the efficiency of cellular uptake is the main factor for the antitumor activity of the conjugates.

The parent conjugate (Dau=Aoa-LRRYVHLGYAT-NH₂) and the Phe substituted version (Dau=Aoa-LRRYVHLFYAT-NH₂) were investigated for *in vivo* studies on orthotopically developed HT-29 colon tumor bearing mice. It was indicated that the conjugate with modified sequence have higher antitumor effect also *in vivo* (89% tumor growth inhibition) compared to the conjugate with unmodified sequence (65% inhibition), and its inhibition effect was similar to the activity of the free Dau (84%) (Figure 2A). However, Dau decreased the liver weight by 28% while the conjugates did not show significant toxic side effect suggesting the suitability of conjugates over the free drug in tumor therapy (Figure 3B). The difference in antitumor effect of the conjugates can be explained by the tumor proliferation index calculated in tumor tissues treated with the different conjugates (58% vs. 86%). Dau did not influence significantly the proliferation of tumor tissues (94%).

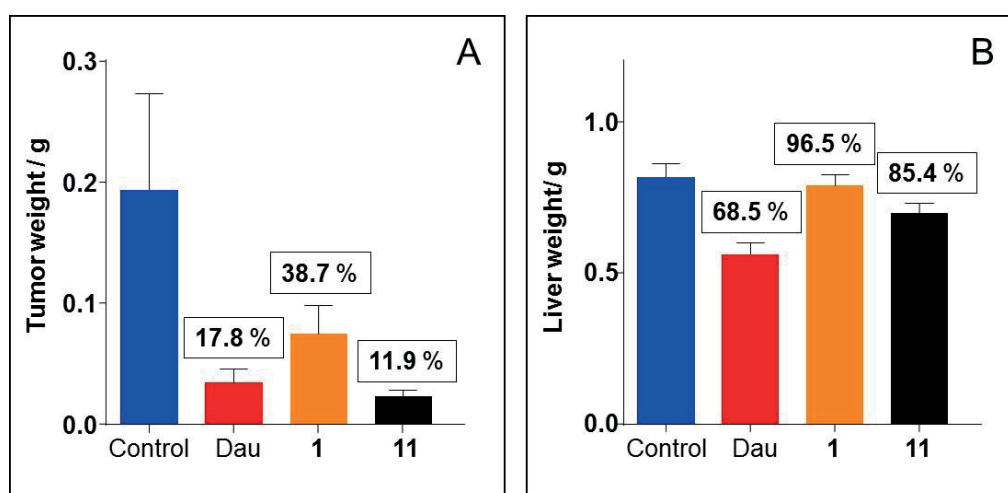


Figure 2. Antitumor effect and liver toxicity of Free Dau and conjugates 1 and 11

The *in vitro* cytostatic effect of these two conjugates was measured on 22 different cancer cell lines and on MRC-5 normal fibroblast as a negative control. On all cancer cells the

Phe containing conjugate showed 2-5 times higher activity than the parent conjugate, and its effect was significantly higher on tumor cells than on MRC-5, indicating the tumor selectivity of the conjugates. Interestingly, the conjugates were active not only on HT-29 but also on other types of tumors, especially on lung, oral and prostate cancers and melanomas. Therefore we made effort to figure out the cell surface compartment that is recognized by this peptide sequence. By the aid of affinity chromatography and proteomic methods, Hsp70 which takes part in the immune recognition of tumors could be identified as a potential receptor for cell targeting of the conjugates. In addition, several HSP70 binding peptide sequences (A6R (ASHLGLAR) and HbS (VHLTPVEK)) showing sequential similarity to our lead peptide could be found in the literature.¹⁰

In conclusion, in this study, we demonstrated that homing peptides selected by phage display can be improved by sequence modification for more efficient targeted tumor therapy. Furthermore, it seems that the oxime linked Dau conjugates are potential drug candidates for tumor treatment. In addition, it was indicated that membrane-bound Hsp70 is a potential target in targeted tumor therapy.

References

1. Zhang Y, Chen J, Zhang Y, Hu Z, Hu D, Pan Y, Ou S, Liu G, Yin X, Zhao J, Ren L, Wang J. *J Biomol Screen* **12**:429-435 (2007)
2. Lin C, Ng HL, Pan W, Chen H, Zhang G, Bian Z, Lu A, Yang Z. *Int J Mol Sci* **16**: 26936-26952 (2015)
3. Mishra J, Dromund J, Quazi SH, Karanki SS, Shaw JJ, Chen B, Kumar N. *Crit Rev Oncol Hematol* **86**: 232-250 (2013)
4. Padma VV. *Biomedicine (Taipei)* **5**: e46 (2015)
5. Baudino TA *Curr Drug Discov Technol* **12**: 3-20 (2015)
6. Kapoor P, Singh H, Gautam A, Chaudhary K, Kumar R, Raghava GPS. TumorHoPe: *PLoS ONE* **7**: e35187 (2012)
7. Hyvönen M, Laakkonen P. *Methods Mol Biol* **1324**: 205-222 (2015)
8. Orbán E, Mező G, Schlage P, Csík G, Kulić Z, Ansorge P, Fellingner E, Möller HM, Manea M. *Amino Acids* **41**: 469-483 (2011)
9. Kiss K, Biri-Kovács B, Szabó R, Randelović I, Enyedi KN, Schlosser G, Orosz Á, Kapuvári B, Tóvári J, Mező G. *Eur J Med Chem* **176**: 105-116 (2019)
10. Fourie AM, Sambrook JF, Gething MJ. *J Biol Chem* **269**: 30470-30478 (1994)

New GnRH-III derivative as a homing peptide for potential drug targeting in cancer therapy

**Sabine Schuster², Beáta Biri-Kovács^{1,2}, Ivan Randelović³, József Tóvári³,
Gábor Mező^{1,2}**

¹MTA-ELTE Research Group of Peptide Chemistry, Hungarian Academy of Sciences, Eötvös L. University, Budapest, Hungary

²Institute of Chemistry, Eötvös L. University, Budapest, Hungary

³Department of Experimental Pharmacology, National Institute of Oncology, Budapest, Hungary

Introduction

Targeted cancer therapy is a promising tool to overcome the drawbacks of classical chemotherapy like the lack of selectivity, toxicity to healthy tissue and the development of multidrug resistance forced by high dose treatments.¹ In general, ligands with high binding affinities to tumor-specific receptors or receptors which are overexpressed on the surface of cancer cells can be used as carriers for anticancer drugs enabling the selective delivery of an effective cytotoxic agent or radionuclides to tumor cells. Many regulatory peptides (*e.g.* gonadotropin-releasing hormone (GnRH), somatostatin, bombesin, neurotensin) have membrane-bound receptors on different types of tumor.² These receptors are usually overexpressed on tumor cells in comparison with normal tissues. Therefore, they might be good targets in targeted tumor therapy. Based on these findings, efficient cytotoxic GnRH-I derivatives were developed in Schally's laboratory. The most prominent conjugate AEZS-108 (ZoptrexTM, previously AN-152) consists of a GnRH-I-[⁶D-Lys] targeting moiety and the antitumor agent doxorubicin (Dox), which was conjugated to the side chain of the ⁶D-Lys through an ester bond by insertion of a glutaryl spacer.³ It has been demonstrated that AEZS-108 internalizes selectively in GnRH-R expressing cells followed by an intracellular release of the drug by tumor-specific carboxylesterases. Thus, the antitumor effect of AEZS-108 was intensively studied *in vitro* and *in vivo* revealing a significant tumor growth inhibition and regression of several tumor types *in vivo*.⁴ Due to the positive results, preclinical studies and clinical trials were performed up to phase III. Unfortunately, AEZS-108 could not achieve its primary endpoint in clinical phase III studies on endometrial cancer, which was caused by the lack of a significant difference in the median period of overall survival of patients treated with ZoptrexTM as compared to patients treated with doxorubicin.⁵ The main reason for this might be the poor enzymatic stability (against carboxylesterases) of the conjugate in circulation. Therefore, more stable oxime-linked daunomycin (Dau) – GnRH conjugates were

investigated in our laboratories.⁶ Instead of GnRH-I (<EHWSYGWLPG-NH₂, where <E is pyroglutamic acid) GnRH-III (<EHWSHDWKPG-NH₂) was applied in these conjugates, because this natural GnRH isoform (isolated from sea lamprey) has good affinity to GnRH receptors on tumor cells, but its endocrine effect is significantly lower in mammals which results in lower hormonal side effects during the treatment of hormone-independent tumors (e.g. colon cancers).^{7,8} Numerous GnRH-III – Dau conjugates had been developed up to the beginning of this project. Our lead compound was <EHWSK(Bu)DWK(Dau=Aoa)PG-NH₂ in which Ser in position 4 was replaced by side-chain butyrylated Lys and the Dau was attached to the side chain of Lys in position 8 *via* an oxime linkage.⁹ From this conjugate the released smallest metabolite was H-Lys(Dau=Aoa)-OH that also bound to the DNA efficiently resulting in significant tumor growth inhibition.¹⁰ In this project our plan was to make further modifications in the sequence of the homing peptide for increasing the antitumor activity of peptide-drug conjugates.

Results

Twenty new GnRH-III – Dau conjugates were developed. First, Asp in position 6 was replaced by D-Asp, D-Glu and D-Trp in both the native GnRH-III (Ser in position) and in our lead compound **K2** ([⁴Lys(Bu)]-GnRH-III(⁸Lys(Dau=Aoa))).¹¹ These conjugates showed lower cytostatic effect than the basic prime conjugates which was related to the lower cellular uptake of the new conjugates both on MCF-7 human breast (hormone-dependent) and HT-29 human colon (hormone-independent) adenocarcinoma. Considering the fact that the incorporation of ⁶D-Aaa did not lead to an improved antitumor activity of the GnRH-III-Dau conjugates, further amino acid substitutions, and their effect on cancer cell proliferation have been investigated. The applied sequence modifications have been selected based on the findings of previously reported structure-related activity studies of unconjugated GnRH-III derivatives.¹² According to this, ⁷Trp was changed to D-Trp and/or ³Trp was replaced by D-Trp or D-Tic (1,2,3,4-tetrahydroisoquinoline-3-carboxylic acid), an unnatural amino acid. D-Tic is a secondary amine (enclosed in a cycle) similarly to Pro, therefore the attachment of the following amino acid (His) was not easy, and a significant amount of His deleted peptide could be detected in the crude mixture. Therefore, we prepared conjugates from [²ΔHis, ³D-Tic]-GnRH-III and [²ΔHis, ³D-Tic, ⁴Lys(Bu)]-GnRH-III derivatives as well. Interestingly, [²ΔHis, ³D-Tic, ⁴Lys(Bu)]-GnRH-III(⁸Lys(Dau=Aoa)) conjugate showed significantly (2-5 times) higher cytostatic effect on many different tumor cell lines than our previous lead

compound (Table 1).¹³ The elevated activity of the new lead compound could be explained by its higher cellular uptake by tumor cells (Figure 1).

Table 1. Anti-proliferative effect of free drug Dau and GnRH-III-Dau conjugates **K2** and **16** on various cell lines.

Tumor type	Cell line	IC ₅₀ ¹ 24h + 48h			Relative efficiency ²	
		Dau (nM)	K2 (μM)	16 (μM)	K2/Dau	16/Dau
Breast	MDA-MB-231	54.6 ± 7.4	5.8 ± 0.8	1.9 ± 0.2	106.2	34.8
Breast	MCF-7	63.9 ± 21.0	16.5 ± 1.2	4.0 ± 0.8	258.2	62.6
Mice breast	4T1	56.0 ± 14.7	6.3 ± 0.9	1.8 ± 0.1	112.5	32.1
Colon	HT-29	202.9 ± 1.0	15.5 ± 1.7	7.3 ± 0.3	76.4	36.0
Mice colon	C26	117.5 ± 8.6	10.6 ± 0.2	2.6 ± 0.7	90.2	22.1
Prostate	DU145	16.3 ± 4.6	5.3 ± 0.4	2.1 ± 0.2	325.2	128.8
Prostate	PC-3	32.7 ± 4.7	6.3 ± 0.3	2.4 ± 0.6	192.7	73.4
Glioblastoma	U87MG	126.4 ± 53.7	9.0 ± 0.8	2.3 ± 0.1	71.2	18.2
Ovarian	A2780	10.4 ± 1.6	1.4 ± 1.1	2.1 ± 0.5	134.6	201.9
Ovarian	OVCAR-3	404.0 ± 9.4	46.0 ± 1.3	8.2 ± 0.5	113.9	20.3
Ovarian	OVCAR-8	185.6 ± 99.8	5.7 ± 0.8	9.5 ± 0.8	30.7	51.2
Liver	HepG2	22.9 ± 1.4	6.8 ± 0.3	2.2 ± 0.7	296.9	96.1
Melanoma	A2058	35.1 ± 14.9	8.4 ± 0.3	2.6 ± 0.5	239.3	74.1
Melanoma	WM983b	49.8 ± 22.9	12.7 ± 1.5	2.6 ± 0.6	255.0	52.2
Melanoma	HT168-M1/9	27.5 ± 9.1	13.5 ± 1.1	2.9 ± 0.6	490.9	105.5
Melanoma	M24	118.8 ± 25.0	16.2 ± 0.2	3.5 ± 0.6	136.4	29.5
Mice melanoma	B16	26.0 ± 8.0	3.2 ± 0.8	1.1 ± 0.2	123.1	42.3
Head and neck	PE/CA-PJ41	45.6 ± 33.5	4.7 ± 0.8	1.7 ± 0.5	103.1	37.3
Head and neck	PE/CA-PJ15	50.5 ± 38.7	7.4 ± 0.8	2.9 ± 0.6	146.5	57.4
Lung	H1975	20.9 ± 2.7	4.1 ± 0.1	2.3 ± 0.7	196.2	110.0
Lung	H1650	50.3 ± 13.4	10.5 ± 1.1	4.0 ± 0.8	208.7	79.5
Lung	A549	69.3 ± 23.5	9.7 ± 0.6	4.3 ± 0.4	140.0	62.0
Pancreas	PANC-1	525.9 ± 24.7	>100	56.4 ± 4.5	>190.2	107.2
Normal fibroblast	MRC-5	287.6 ± 35.1	41.9 ± 3.8	19.7 ± 1.2	145.7	68.5

¹ IC₅₀ values (average ± SD). ² Relative potency = IC₅₀ conjugate / IC₅₀ Dau.

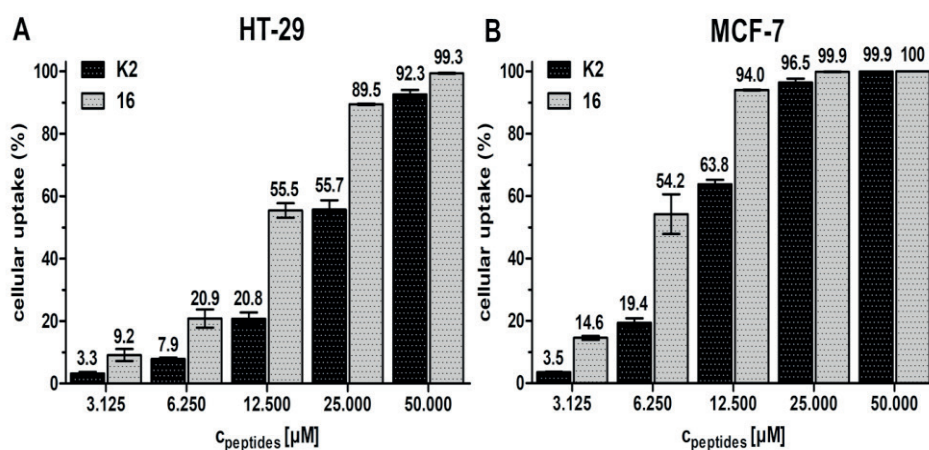


Figure 1. Cellular uptake of GnRH-III-Dau conjugates [⁴Lys(Bu)]-GnRH-III(⁸Lys(Dau=Aoa) **K2** and [²ΔHis, ³D-Tic, ⁴Lys(Bu)]-GnRH-III(⁸Lys(Dau=Aoa) **16** by flow cytometry. **A:** HT-29 and **B:** MCF-7 cancer cells after 6 h treatment.

In metabolism studies, it was also indicated that the modification resulted in the improvement of enzyme stability of the new conjugates, but the efficiency of the active metabolite release was not influenced by this sequence modification. These two conjugates were investigated for *in vivo* studies, too. Mice with orthotopically developed HT-29 colon carcinoma were treated with free Dau once a week (3 times, 1 mg/kg dose) and with conjugates two times/week (7 times, 10 mg Dau content/kg dose).¹³ The mice in free Dau treated group exhibited a significantly decreased bodyweight, whereby the experiment was terminated on day 23 after tumor transplantation (day 17 of treatment). The bodyweight of the mice in the control group was significantly decreased on day 30 after tumor transplantation which was the reason for experiment termination (Figure 2A). Tumor weights indicated similar growth inhibition in all treated groups compared to the control (84.3% for Dau (one week earlier stage), 80.8% for **K2** and 87.1% for **16** (Figure 2B). However, the conjugates did not show liver toxicity in comparison with the free Dau treatment (Figure 2C).

In addition, *in vivo* experiments in orthotopic 4T1 mice breast carcinoma and in MDA-MB-231 human breast carcinoma bearing mice indicated significant inhibition (40-50%) of macro- and micrometastasis formation compared to the control that was higher than in the case of free Dau treatment. Conjugate **16** showed slightly better antimetastatic effect than conjugate **K2** suggesting that the new lead compound can be more effective not only *in vitro*, but also *in vivo*. In addition, we can conclude that the oxime linked Dau – GnRH-III conjugates might be good candidates for targeted tumor therapy.¹³

These two conjugates were investigated for *in vivo* studies, too. Mice with orthotopically developed HT-29 colon carcinoma were treated with free Dau once a week (3

times, 1 mg/kg dose) and with conjugates two times/week (7 times, 10 mg Dau content/kg dose).¹³ The mice in free Dau treated group exhibited a significantly decreased bodyweight, whereby the experiment was terminated on day 23 after tumor transplantation (day 17 of treatment). The bodyweight of the mice in the control group was significantly decreased on day 30 after tumor transplantation which was the reason for experiment termination (Figure 2A). Tumor weights indicated similar growth inhibition in all treated groups compared to the control (84.3% for Dau (one week earlier stage), 80.8% for **K2** and 87.1% for **16** (Figure 2B). However, the conjugates did not show liver toxicity in comparison with the free Dau treatment (Figure 2C).

In addition, *in vivo* experiments in orthotopic 4T1 mice breast carcinoma and in MDA-MB-231 human breast carcinoma bearing mice indicated significant inhibition (40-50%) of macro- and micrometastasis formation compared to the control that was higher than in the case of free Dau treatment. Conjugate **16** showed slightly better antimetastatic effect than conjugate **K2** suggesting that the new lead compound can be more effective not only *in vitro*, but also *in vivo*. In addition, we can conclude that the oxime linked Dau – GnRH-III conjugates might be good candidates for targeted tumor therapy.¹³

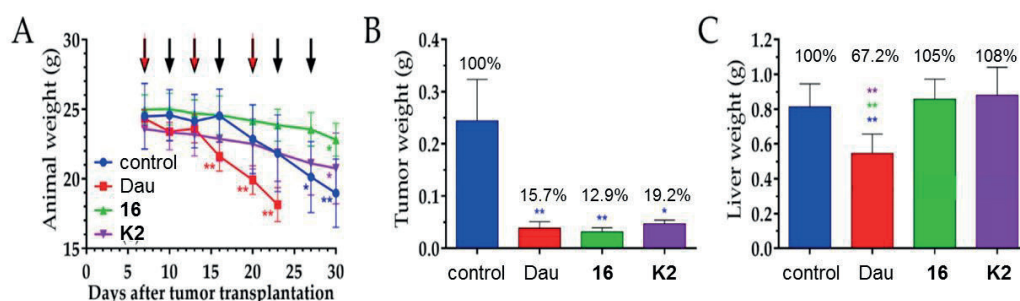


Figure 2. Effect of Dau and conjugate **16** and **K2** on animal weight (A), tumor growth (B) and their toxicity on the liver (C)

Considering the favorable results of conjugates **16** and **K2**, the corresponding peptide sequences have been selected as targeting moieties for the further conjugates, and the classical anticancer drugs Dau and PTX were used as payloads. The drugs were attached to the homing peptides through self-immolative linker (Val-Ala-PABC and Val-Cit-PABC, where Cit is citrulline and PABC is *para*-aminobenzyloxy carbonyl) that allow the release of free drugs in the presence of lysosomal enzyme Cathepsin B.¹⁴ In addition conjugates with non-cleavable linkers were investigated for comparative studies (Figure 3).¹⁵

The *in vitro* cytostatic effect of the conjugates indicated that PTX-containing conjugates are more potent on both A2780 ovarium carcinoma (high GnRH-R level) and

PANC-1 pancreatic cancer (low GnRH-R level) than the Dau conjugates (Table 2.). The free PTX has also one order of magnitude higher antitumor effect on the cells than Dau. There was a significant difference between the antitumor activity of conjugates with self-immolative spacer and non-cleavable spacer in all cases. However, the type of self-immolative linker and the homing peptide had no significant influence on the effect in the case of PTX conjugates, while Val-Ala-PABC linker and the [$^2\Delta$ His, 3 D-Tic, 4 Lys(Bu)]-GnRH-III homing peptide resulted in higher cytostatic effect compared with the application of Val-Cit-PABC and the [4 Lys(Bu)]-GnRH-III carrier. Interestingly the Dau conjugates with self-immolative linker did not show higher antitumor activity *in vitro* than the oxime linked version which does not serve the free drug release. This could be explained by the binding affinity of the conjugates to GnRH receptors. The oxime linked Dau conjugate had higher affinity to the receptor than the conjugate with a self-immolative linker. The reason might be the steric hindrance of the larger Val-Ala/Cit-PABC spacer over the aminoxyacetyl moiety.

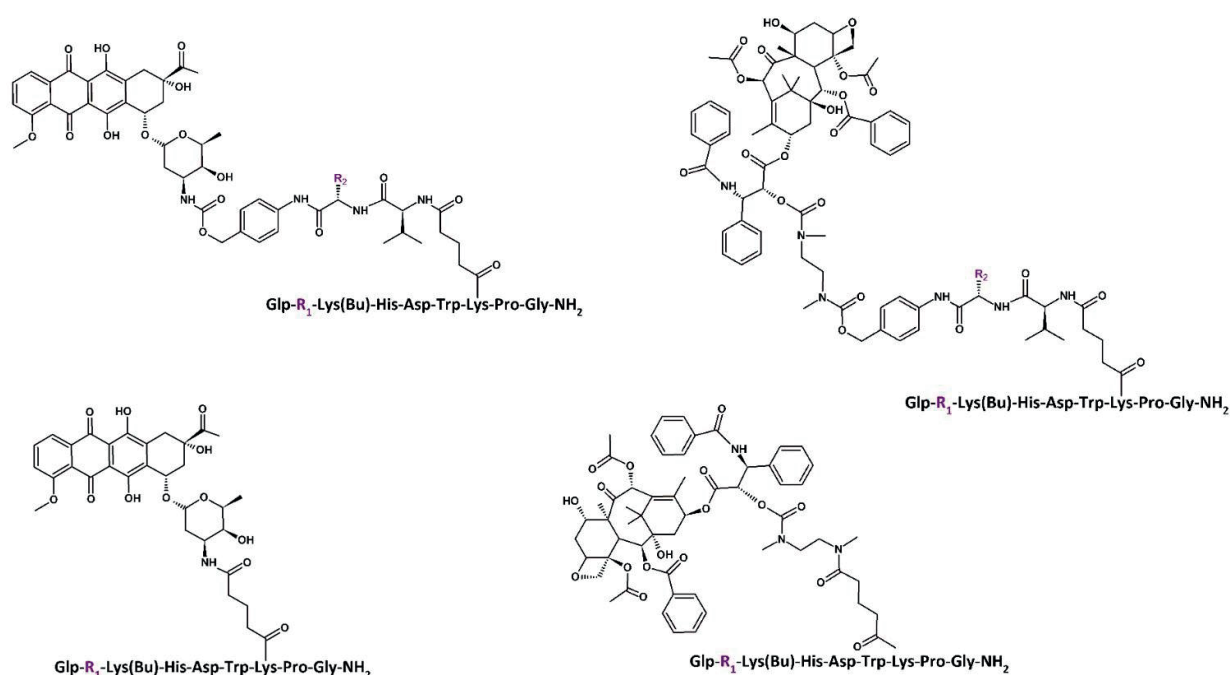


Figure 3. Chemical structure of Dau- and PTX-GnRH-III derivative conjugates with self-immolative spacers and non-cleavable spacers (R_1 is D-Tic or His-Trp and R_2 is Val-Ala or Val-Cit)

In conclusion, these experiments indicated that there are many factors that can influence the antitumor effect of the conjugates developed for targeted tumor therapy. These can be the efficacy of the drugs, the structure of the homing peptide, the binding affinity and cellular uptake of the peptide – drug conjugate, the release of the free drug or active metabolite from the conjugates in lysosomes (linker strategy). Therefore, during the development of drug

delivery systems, we have to study all of these factors to get appropriate drug candidates for targeted tumor therapy.

Table 2. Cytostatic effect of GnRH-III derivative Dau (left) and PTX (right) conjugates with the self-immolative linker and the non-cleavable linker

Code	R ₁	Cleavage site	A2780 (+) IC ₅₀ [μM] (ovarian)	Panc-1 (-) IC ₅₀ [μM] (pancreatic)
Dau			0.21±0.01	2.43±0.58
Sch79	His-Trp	-Val-Cit-	11.18±0.38	85.57±24.33
Sch90	His-Trp	-Val-Ala-	7.48±0.66	56.19±17.28
Sch107	His-Trp	none	67.88±25.36	>100
Sch89	D-Tic	-Val-Cit-	4.24±1.09	>100
Sch91	D-Tic	-Val-Ala-	2.85±0.90	>100
Sch108	D-Tic	none	48.14±0.47	>100

Code	R ₁	Cleavage site	A2780 (+) IC ₅₀ [μM] (ovarian)	Panc-1 (-) IC ₅₀ [μM] (pancreatic)
PTX			0.02±0.001	0.17±0.01
Sch93	His-Trp	-Val-Cit-	0.67±0.07	5.03±1.91
Sch100	His-Trp	-Val-Ala-	0.66±0.18	4.89±1.08
Sch112	His-Trp	none	41.52±9.83	> 100
Sch99	D-Tic	-Val-Ala-	0.77±0.08	8.15±3.22
Sch101	D-Tic	-Val-Cit-	0.51±0.11	6.44±1.22
Sch113	D-Tic	none	> 100	> 100

References

- Dai L, Liu J, Luo Z, Li M, Cai K. *J Mater Chem B* **4**: 6758-6772 (2016)
- Mező G, Manea M. *Expert Opin Drug Deliv* **7**: 79-96 (2010)
- Schally AV, Nagy A. *Life Sci* **72**: 2305-2320 (2003)
- Engel J, Emons G, Pinski J, Schally AV. *Expert Opin Investig Drugs* **21**: 891-899 (2012)
- <https://www.businesswire.com/news/home/20170501005409/en/Aeterna-Zentaris-Announces-ZoptEC-Phase-3-Clinical> (2017)
- Szabó I, Manea M, Orbán E, Csámpai A, Bősze S, Szabó R, Tejada M, Gaál D, Kapuvári B, Przybylski M, Hudecz F, Mező G. *Bioconjug Chem* **20**: 656-665 (2009)
- Sower SA, Chiang YC, Lovas S, Conlon JM. *Endocrinology* **132**: 1125-1131 (1993).
- Kovács M, Vincze B, Horváth JE, Seprődi J. *Peptides* **28**: 821-829 (2007)
- Hegedüs R, Manea M, Orbán E, Szabó I, Kiss E, Sipos E, Halmos G, Mező G. *Eur J Med Chem* **56**: 155-165 (2012)
- Orbán E, Mező G, Schlage P, Csík G, Kulić Z, Ansorge P, Fellingner E, Möller HM, Manea M. *Amino Acids* **41**: 469-483 (2011)
- Schuster S, Biri-Kovács B, Szeder B, Farkas V, Buday L, Szabó Z, Halmos G, Mező G. *Beilstein J Org Chem* **14**: 756-771 (2018)
- Schuster S, Biri-Kovács B, Szeder B, Buday L, Gardi J, Szabó Z, Halmos G, Mező G. *Pharmaceutics* **10**: 223 (2018)
- Randelović I, Schuster S, Kapuvári B, Fossati G, Steinkühler C, Mező G, Tóvári J. *Int J Mol Sci* **20**: 4763 (2019)
- Dubowchik GM, Firestone RA, Padilla L, Willner D, Hofstead SJ, Mosure K, Knipe JO, Lasch SJ, Trail PA. *Bioconjug Chem* **13**: 855-869 (2002)
- Schuster S. Synthesis of GnRH and somatostatin cytotoxic drug conjugates (PhD thesis) (2019)

Comparison of the apoptotic effects of different GnRH-based conjugates with or without butyrate Lys in position 4 on colon carcinoma cells

Eszter Lajkó¹, Rózsa Hegedüs², Gábor Mező^{2,3}, László Kóhidai¹

¹Department Genetics, Cell- and Immunobiology, Semmelweis University, Budapest, Hungary

²Research Group of Peptide Chemistry, Hungarian Academy of Sciences, Eötvös Loránd University, Budapest, Hungary

³Institute of Chemistry, Eötvös L. University, Budapest, Hungary

Introduction

Targeted tumor therapy represents a promising strategy to improve the selectivity and efficacy of chemotherapy, by delivering a cytotoxic drug covalently linked to a targeting unit which is selective to a tumor's overexpressed receptors. Gonadotropin-releasing hormone (GnRH) is one of the hormone peptides extensively studied and used for drug delivery. As for targeting units, several native and synthetic GnRH analogs were shown to efficiently affect only the tumor cells with GnRH receptor (GnRH-R) and spare the healthy cells with no or limited number of GnRH-R.^{1,2}

There are three main types of the decapeptide GnRH: GnRH-I (<EHWSYGWLPG-NH₂, where <E is pyroglutamic acid) and GnRH-II (<EHWSHGWYPG-NH₂) can be found in the human body,^{3,4} while GnRH-III (<EHWSHDWKPG-NH₂) is a non-human isoform; however, it can specifically bind to different human GnRH receptor-expressing tumor cells.⁵ GnRH peptides, as part of drug-delivery systems, have some valuable properties such as (i) having a tumor growth inhibitory effect on their own, (ii) providing an easy way of modification and conjugation due to the well-studied structure-activity relationships.⁶ One of the fundamental limitations of GnRH-based targeting is the relatively rapid proteolytic degradation of the peptide part.^{6,7} The modification of GnRH-I and GnRH-II in position 6 with D-amino acid could increase their affinity to the GnRH-R,⁴ their enzymatic stability as well as influence their antitumor activity.^{8,9} One of the most effective strategies to improve the antitumor activity and other biochemical properties (*e.g.* enzymatic stability) of GnRH-III and its conjugate was the replacement of Ser in position 4 with butyrate Lys.^{7,10}

It has been suggested that the apoptosis is involved in the antitumor activity of different anthracycline-GnRH conjugates.^{11,12} Depending on the target cells and the type of GnRH built in the anthracycline-GnRH conjugates, they could exhibit apoptotic activity with different extent.^{9,13} Our recent results on melanoma cells indicated that in the case of the GnRH-III conjugate modified with butyrate ⁴Lys (GnRH-III[⁴Lys(Bu),⁸Lys(Dau=Aoa)],

where Dau is daunomycin and Aoa is aminooxyacetyl moiety providing an oxime linkage between the drug and homing peptide), its antitumor effect was rather attributed to apoptotic activity than, in contrast to the GnRH-III[⁸Lys(Dau=Aoa)] possessing ⁴Ser, where the cell cycle blocking effect (arrest in G2/M phase) was shown to be more prominent.¹⁴ Although an increasing number of studies have focused on the determination of the apoptosis induced by different cytotoxic drug-containing GnRH conjugates, there are only a few data on the underlying molecular mechanism.

The aim of our work was to compare the apoptotic activity of different GnRH-based, Dau-containing conjugates by impedimetry (xCELLigence SP System), flow cytometry and quantitative real-time RT-PCR in HT-29 human colon carcinoma cell line.

Results

Three GnRH analogs (GnRH-I-[⁶D-Lys], GnRH-II-[⁶D-Lys] and GnRH-III), previously proven to be effective in Dau-delivery, were selected to compare the apoptotic activity of their conjugates. Two sets of conjugates were synthesized by attaching Dau directly to the ⁶D-Lys or ⁸Lys (depending on the GnRH analog) *via* oxime linkage; one group with Ser in position 4 and a second group, where this Ser was replaced with butyrate Lys (Table 1).

First, the cytotoxic/antiproliferative effect of the conjugates with different native GnRH isoforms and the effect of the substitution of butyrate Lys in position 4 were studied by using a more sophisticated, impedance-based method (xCELLigence SP System). In case of the conjugates built on native GnRH conjugates, the II-[⁴Ser,⁶D-Lys(Dau)] proved to be the most potent one followed by the I-[⁴Ser,⁶D-Lys(Dau)] and III-[⁴Ser,⁸Lys(Dau)] (the applied codes can be seen in Table 1). The substitution with ⁴Lys(Bu) proved to modify the cytotoxic effect of the conjugates depending on the type of GnRH analog. In the case of the GnRH-III based conjugates, this modification led to a more than one order of magnitude smaller IC₅₀ value (Table 1) and a stronger antitumor activity with an earlier onset. In the case of GnRH-I conjugates, the replacement of ⁴Ser by ⁴Lys(Bu) could cause only a slight increase in the potency (smaller IC₅₀ value) after 72 h, but the onset of the cytotoxic activity took less time. On the contrary, IC₅₀ values of GnRH-II conjugate with ⁴Lys(Bu) (II-[⁴Lys(Bu),⁶D-Lys(Dau)]) were more than two times higher than that of II-[⁴Ser,⁶D-Lys(Dau)] (Table 1).

In general, the conjugates had minor or no apoptotic effect. The apoptotic cell death induced by 24 h incubation with GnRH conjugates was measured by detecting the binding of FITC-conjugated Annexin V. In the case of conjugates with Ser⁴ only the GnRH-II conjugate

could elicit a slight, but significant apoptotic effect and the incorporation of $^4\text{Lys}(\text{Bu})$ diminished this activity (Table 1). Among the tested conjugates, III- $[\text{}^4\text{Lys}(\text{Bu}), \text{}^8\text{Lys}(\text{Dau})]$ had the maximal apoptotic effect (Table 1).

Table 1. IC_{50} values and apoptotic effects of Dau-GnRH- $[\text{}^4\text{Ser}/\text{}^4\text{Lys}(\text{Bu})]$ conjugates determined on HT-29 cell line

Conjugate	Code	IC_{50}^1 (μM)	Ratio of apoptotic cells ² [%]	
			(cont.: 8.91 ± 0.58)	
			72 h	24 h
GnRH-I- $[\text{}^4\text{Ser}, \text{}^6\text{D-Lys}(\text{Dau}=\text{Aoa})]$	I- $[\text{}^4\text{Ser}, \text{}^6\text{D-Lys}(\text{Dau})]$	21.94 ± 1.54		12.46 ± 1.1
GnRH-II- $[\text{}^4\text{Ser}, \text{}^6\text{D-Lys}(\text{Dau}=\text{Aoa})]$	II- $[\text{}^4\text{Ser}, \text{}^6\text{D-Lys}(\text{Dau})]$	19.73 ± 2.51		$15.05^* \pm 0.94$
GnRH-III- $[\text{}^4\text{Ser}, \text{}^8\text{Lys}(\text{Dau}=\text{Aoa})]$	III- $[\text{}^4\text{Ser}, \text{}^8\text{Lys}(\text{Dau})]$	56.82 ± 5.44		9.21 ± 0.76
GnRH-I- $[\text{}^4\text{Lys}(\text{Bu}), \text{}^6\text{D-Lys}(\text{Dau}=\text{Aoa})]$	I- $[\text{}^4\text{Lys}(\text{Bu}), \text{}^6\text{D-Lys}(\text{Dau})]$	16.18 ± 1.75		12.08 ± 1.36
GnRH-II- $[\text{}^4\text{Lys}(\text{Bu}), \text{}^6\text{D-Lys}(\text{Dau}=\text{Aoa})]$	II- $[\text{}^4\text{Lys}(\text{Bu}), \text{}^6\text{D-Lys}(\text{Dau})]$	48.08 ± 6.89		9.52 ± 1.06
GnRH-III- $[\text{}^4\text{Lys}(\text{Bu}), \text{}^8\text{Lys}(\text{Dau}=\text{Aoa})]$	III- $[\text{}^4\text{Lys}(\text{Bu}), \text{}^8\text{Lys}(\text{Dau})]$	4.56 ± 0.27		$17.00^{**} \pm 1.25$

¹ IC_{50} values represent the mean \pm SD of three parallel measurements and were calculated by fitting a sigmoidal dose-response curve with OriginPro 2016 software.

² For the treatment, the conjugates were applied at 10^{-4} M concentration for 24 h. Only the viable cells were taken into consideration to determine the ratio of apoptotic cells (percentage of Annexin V positive cells). Data shown are mean of two parallels \pm SD. The significance levels are the followings: *: $p < 0.05$, **: $p < 0.01$.

To investigate the molecular background of the HT-29 cell death induced by GnRH conjugates, a human apoptosis gene PCR array (RealTime ready Custom panel, Roche Applied Science, Mannheim, Germany) containing 23 apoptosis-related genes was used. GnRH-I and GnRH-III conjugates with ^4Ser increased the expression of *TP53* after 24 h incubation (Figure 1/A and C). All of the conjugates containing ^4Ser could increase the expression of genes involved in the intrinsic pro-apoptotic pathway, but with a different activity. The ^4Ser conjugates caused the most remarkable increase in case of the *TNF* expression, especially after 24 h (I- $[\text{}^4\text{Ser}, \text{}^6\text{D-Lys}(\text{Dau})]$): 40.57 fold, II- $[\text{}^4\text{Ser}, \text{}^6\text{D-Lys}(\text{Dau})]$: 18.33 fold, III- $[\text{}^4\text{Ser}, \text{}^8\text{Lys}(\text{Dau})]$: 50.45 fold) (Figure 1). Only the I- $[\text{}^4\text{Ser}, \text{}^6\text{D-Lys}(\text{Dau})]$ could influence (increase) the expression of *CASP9*, 7 and 3. All of the ^4Ser conjugates upregulated the expression of *FASL* and *STAT1* with comparable activity. The expression of other tested genes involved in the growth factor signaling pathway was reduced while the expression of

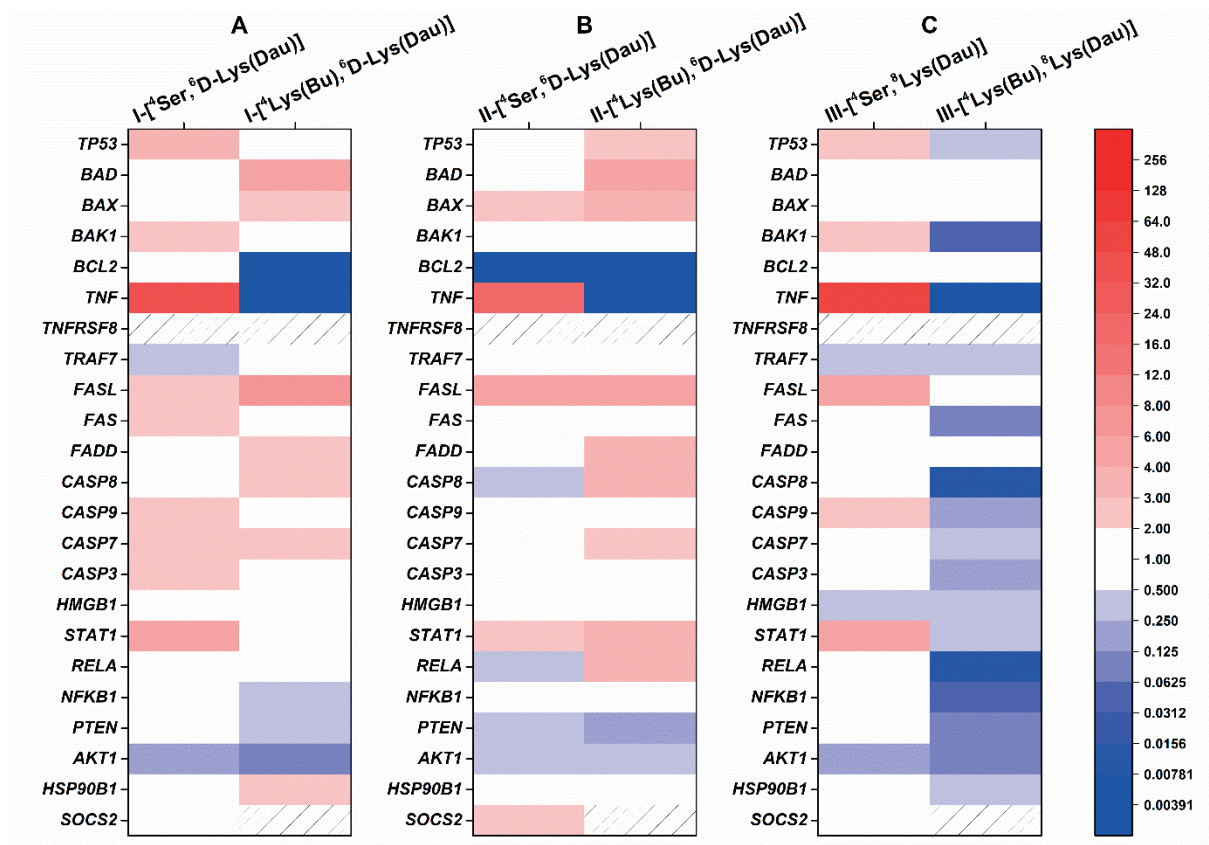


Figure 1. Comparison of the expression of human apoptosis-related genes in HT-29 cells treated with GnRH-[⁴Ser] and GnRH-[⁴Lys(Bu)] conjugates for 24 h. Effects of the conjugates pairs of GnRH-I (A), GnRH-II (B), GnRH-III (C) on gene expression were analyzed by a human apoptosis gene PCR array (RealTime ready Custom panel).

Colors of heatmap showed significant fold changes in gene expression compared to control. Fold changes ≥ 2 and $p < 0.05$ were considered as significant. Hashed zone means invalid PCR results.

TP53: tumor protein p53 data; *BAD*: BCL2-associated agonist of cell death; *BAX*: BCL2-associated X protein; *BAK1*: BCL2-antagonist/killer 1; *BCL2*: B-cell CLL/lymphoma 2; *TNF*: TNF-alpha, Tumor necrosis factor ligand superfamily member 2; *TNFRSF8*: Tumor necrosis factor receptor superfamily, member 8; *TRAF7*: TNF receptor-associated factor 7; *FASL*: Fas ligand, TNF superfamily member 6 (*TNFSF6*); *FAS*: TNF receptor superfamily member 6 (*TNFRSF6*); *FADD*: Fas (*TNFRSF6*)-associated via death domain; *CASP7*: caspase 7; *CASP3*: caspase 3; *CASP9*: caspase 9; *CASP8*: caspase 8; *HMGB1*: high-mobility group box 1; *NFKB1*: nuclear factor of kappa light polypeptide gene enhancer in B-cells 1; *RELA*: v-rel reticuloendotheliosis viral oncogene homolog A; *AKT1*: v-akt murine thymoma viral oncogene homolog 1; *PTEN*: phosphatase and tensin homolog; *STAT1*: signal transducer and activator of transcription 1; *SOCS2*: suppressor of cytokine signaling 2; *HSP90B1*: heat shock protein 90kDa beta (Grp94) member 1.

anti-apoptotic genes was elevated by II-[⁴Ser,⁶D-Lys(Dau)]. The replacement of ⁴Ser by ⁴Lys(Bu) led to significant changes in the expression of apoptosis-related genes as shown in Figure 1. When the cells were treated with ⁴Lys(Bu) containing GnRH-I or GnRH-III, the expression of the *TP53* was decreased to the control level or below in comparison with ⁴Ser derivatives (Figure 1/A and C). Similar to ⁴Ser conjugates, all of the conjugates with ⁴Lys(Bu) increased the level of *BAD* and *BAX* as well as abolished *BCL2* expression. The most

remarkable difference between the ⁴Ser and ⁴Lys(Bu) conjugates were detected in the expression of *TNF*. Due to the 24 h treatment with the ⁴Lys(Bu) conjugates the expression of *TNF* was not detectable. The cells treated with ⁴Lys(Bu) derivatives could also overexpress the *FASL* (Figure 1). Gene expression of the effector proteins and members of the growth factor signaling pathway were greatly reduced by III-[⁴Lys(Bu),⁸Lys(Dau)] (Figure 1/C). Contradiction with the ⁴Ser counterparts, GnRH-I and GnRH-II conjugates with ⁴Lys(Bu) caused an increase in the expression of *CASP8* and *CASP7* after 24 h incubation (Figure 1/A and C). I-[⁴Lys(Bu),⁶D-Lys(Dau)] and III-[⁴Lys(Bu),⁸Lys(Dau)] downregulated *HMGB1* expression by *ca.* 3-fold change (Figure 1/A and C). The expression of *STAT1* was changed in parallel with the *TP53*. Except for *RELA* and *NFKB1* in the II-[⁴Lys(Bu),⁶D-Lys(Dau)] treated group, all of the genes involved in the growth factor signaling pathway were reduced by the ⁴Lys(Bu) conjugates (Figure 1).

In summary, we demonstrated that modification with Lys(Bu) in position 4 increased the cytotoxic and apoptotic effect of GnRH-I and GnRH-III conjugates containing an oxime-linked Dau. Although the conjugates had a minor apoptotic effect, they could regulate the expression of several apoptosis-related factors, and this activity proved to be sensitive to the GnRH isoforms and the presence of the ⁴Lys(Bu), especially in case of *TNF*, *TP53* and members of the growth factor signaling pathway. Nevertheless, it is worth mentioning that independently of this modification, all of the investigated conjugates could increase the expression of *FASL* and the mitochondrial pro-apoptotic factors (e.g. *BAD* and *BAX*), which indicates the general importance of the FAS-dependent pathway and the mitochondrial apoptotic pathway in the antitumor effect of different GnRH conjugates. By detecting the expression of 23 apoptosis-related genes we could find further evidence that the GnRH-I and GnRH-III conjugates acted in a more or less similar way. Our comprehensive PCR results could show that the stronger cytotoxic activity of I-[⁴Lys(Bu),⁶D-Lys(Dau)], III-[⁴Lys(Bu),⁸Lys(Dau)] and II-[⁴Ser,⁶D-Lys(Dau)] was associated with a stronger and a more immediate inhibitory effect on the expression of elements of growth factor signaling comparing to their counterparts, where the upregulation of the expression *TP53*, *TNF* and caspases (e.g. *CASP9*) probably had a more important role. Our results also suggest the significance of ⁴Lys(Bu) in the anti-tumor activity of GnRH-I and GnRH-III conjugates, while in case of GnRH-II conjugates, the native Ser in position 4 appeared to be more important.

References

1. Engel JB, Tinneberg HR, Rick FG, Berkes E, Schally AV, *Curr Drug Targets* **17**: 488-494 (2016)
2. Szabó I, Manea M, Orbán E, Csámpai A, Bősze S, Szabó R, Tejada M, Gaál D, Kapuvári B, Przybylski M, Hudecz F, Mező G, *Bioconjug Chem* **20**: 656-665 (2009)
3. Cheng CK, Leung PCK, *Endocr Rev* **26**: 283-306 (2005)
4. Millar RP, Lu ZL, Pawson AJ, Flanagan CA, Morgan K, Maudsley SR, *Endocr Rev* **25**: 235-275 (2004)
5. Manea M, Mező G, *Protein Pept Lett* **20**: 439-449 (2013)
6. Mező G, Manea M, *Expert Opin Drug Deliv* **7**: 79-96 (2010)
7. Manea M, Leurs U, Orbán E, Baranyai Z, Ohlschlager P, Marquardt A, Schulcz A, Tejada M, Kapuvári B, Tóvári J, Mező G, *Bioconjug Chem* **22**: 1320-1329 (2011)
8. Sealfon SC, Weinstein H, Millar RP, *Endocr Rev* **18**: 180-205 (1997)
9. Szabó I, Bősze S, Orbán E, Sipos E, Halmos G, Kovács M, Mező G, *J Pept Sci* **21**: 426-435 (2015)
10. Hegedüs R, Manea M, Orbán E, Szabó I, Kiss E, Sipos E, Halmos G, Mező G, *Eur J Med Chem* **56**: 155-165 (2012)
11. Moretti RM, Montagnani Marelli M, Taylor DM, Martini PG, Marzagalli M, Limonta P, *PLoS One* **9**: e93713 (2014)
12. Zhang N, Qiu J, Zheng T, Zhang X, Hua K, Zhang Y, *Oncol Rep* **39**: 1034-1042 (2018)
13. Gunthert AR, Grundker C, Bongertz T, Schlott T, Nagy A, Schally AV, Emons G, *Am J Obstet Gynecol* **191**: 1164-1172 (2004)
14. Lajkó E, Spring S, Hegedüs R, Biri-Kovács B, Ingebrandt S, Mező G, Köhidai L, *Beilstein J Org Chem* **14**: 2495-2509 (2018)

Structural and binding characteristics of HER2 receptor targeting peptides

Beáta Biri-Kovács^{1,2}, Afrodité Adorján^{1,2}, Ildikó Szabó², Bálint Szeder³, Szilvia Bősze²,
Gábor Mező^{1,2}

¹Institute of Chemistry, Eötvös L. University, Budapest, Hungary

²MTA-ELTE Research Group of Peptide Chemistry, Hungarian Academy of Sciences, Eötvös L. University, Budapest, Hungary

³Institute of Enzymology, Research Centre for Natural Sciences, Hungarian Academy of Sciences, Budapest, Hungary

Introduction

HER2 (ErbB2) is overexpressed in 15-30% of breast cancers and is also amplified in several other cancers (gastric, ovarian, prostate), its increased expression prognoses high mortality rate and the development of metastases. HER2 is a transmembrane glycoprotein that belongs to the epidermal growth factor receptor tyrosine kinase protein family and plays role in mitogenic signaling. HER2 is the only receptor in the protein family that does not have a known ligand, its activation occurs through the formation of homo- or heterodimers (formed with other members of the protein kinase family). Its increased level results in uncontrollable tumor growth due to the excessive formation of HER2-containing dimers leading to enhanced cell proliferation and survival.^{1,2}

As HER2 is an important target in breast cancer research, several therapies have been developed during the last decades that include the use of monoclonal antibodies, small molecule tyrosine kinase inhibitors and antibody-drug conjugates. Despite successful anti-HER2 agents that achieved improvement in tumor therapy, some patients suffer from serious side effects or have developed resistance, thus, new approaches in HER2-targeting are needed.³ Moreover, for selection of the appropriate therapeutical agent, new, fast, reliable and quantitative diagnostical tools are also required.

Tumor targeting peptides have become an important field in targeted tumor therapy due to their low molecular weight, easy synthesis, high receptor recognition rate and better tissue penetration characteristics. With the use of peptide bacteriophage display technology, Karasseva *et al.* identified a hexapeptide (KCCYSL) that bound with high affinity and specificity to HER2-expressing cells.⁴ Hence, we chose this peptide as a starting point of our study to design new, modified peptides with increased HER2 binding affinity.

Geng *et al.* used the method of molecular dynamics simulation to identify peptides involved in the dimerization at the extracellular domain of HER2. These peptides were used

to build a „One bead one compound” (OBOC) library and were screened for specificity and affinity resulting in 17-mer peptides binding with high affinity to HER2 receptor.⁵ Parts of the peptides with the strongest binding ability show similarities with the KCCYSL peptide. Thus, we decided to synthesize combined peptides where the modified KCCYSL sequence precedes GYYNPN (taken from the OBOC library) and compare their binding to HER2 expressing cells.⁶

Results

A set of hexa- and 12-mer peptide analogues were synthesized by solid-phase peptide synthesis on Rink Amide MBHA resin using Fmoc/tBu protocol. In the last step, 5(6)-carboxyfluorescein (CF) as fluorescent dye was attached to the N-terminus of the peptidyl resins. The compounds were analyzed by analytical RP-HPLC, their molecular weight was identified by ESI-MS (Table 1).

Table 1. List of HER2 binding compounds, their codes and chemical characteristics.

Compound	Code	RP-HPLC R _t (min) ¹	ESI-MS MW (calculated)	ESI-MS MW (measured) ²
CF-KCCYSL-NH ₂	P(CC)	29.9 ^a	1072.9	1072.3
CF-KCGCYSL-NH ₂	P(CGC)	29.4 ^a	1129.9	1129.8
CF-KCGGCYSL-NH ₂	P(CGGC)	31.7 ^a	1186.0	1187.0
CF-KC _(AcM) C _(AcM) YSL-NH ₂	P(C _(AcM) C _(AcM))	28.8 ^a	1214.5	1214.0
CF-KCSYSL-NH ₂	P(CS)	29.7 ^a	1056.7	1056.4
CF-KSCYSL-NH ₂	P(SC)	29.5 ^a	1056.7	1056.4
CF-KSSYSL-NH ₂	P(SS)	27.7 ^a	1040.8	1040.5
CF-KAAYSL-NH ₂	P(AA)	28.8 ^a	1007.8	1008.4
CF-GYYNPT-NH ₂	P(YY)	30.0 ^a	1070.8	1070.4
CF-KAAYSLGYYNPT-NH ₂	cP(AA)_P(YY)	21.4 ^b	1704.5	1704.6
CF-KSCYSLGYYNPT-NH ₂	cP(SC)_P(YY)	21.4 ^b	1751.8	1752.2
CF-YSLGYYNPT-NH ₂	P(short)_P(YY)	22.7 ^b	1433.8	1433.8
CF-TAKLYPGYANYS-NH ₂	scr_P(AA)_YY)	21.1 ^b	1704.5	1704.0
CF-GYYNPTKAAYSL-NH ₂	cP(YY)_P(AA)	21.6 ^b	1704.5	1704.6
H-KAAYSLGYYNPT-NH ₂	Unlabeled cP(AA)_P(YY)	19.4 ^b	1345.7	1346.0
H-KSCYSLGYYNPT-NH ₂	Unlabeled cP(SC)_P(YY)	19.4 ^b	1393.6	1394.0

¹ RP-HPLC: ^a: column: Phenomenex Aeris Peptide XB-C18 column (250 x 4.6 mm) with 3.6 μm silica; eluents: 0.1% TFA in water (A) and 0.1% TFA in acetonitrile-water (80:20, v/v) (B); gradient: 0 min 0% B, 5 min 0% B, 50 min 90% B; flow rate: 1 mL/min; detection: λ= 220 nm, ^b: column: Macherey–Nagel Nucleosil C18 column (250 x 4.6 mm) with 5 μm silica (100 Å pore size); eluents: 0.1% TFA in water (A) and 0.1% TFA/ acetonitrile –water (80:20 v/v) (B); gradient 0 min 2% B, 5 min 2% B, 30 min 90% B; flow rate 1 mL/min; detection: 220 nm

² ESI-MS: Esquire 3000+ ion trap mass spectrometer (Bruker Daltonics)

Cellular uptake was measured by flow cytometry using HER2-overexpressing breast cancer cells. HER2 expression was detected by Western blot (Figure 1A), as a result, MDA-MB-453 breast adenocarcinoma cell line was chosen for further studies. First, variations of the KCCYSL hexapeptide (role of cysteine residues, distance between them) were studied based on the measured fluorescence intensity after incubation of the cells with CF-labeled peptides for 3 h. Consequently, the two most promising analogues (P(AA) and P(SC)) were chosen for further experiments and the design of combined peptides. The next cellular uptake study demonstrated that combined peptide cP(AA)_P(YY) shows ten times higher fluorescence intensity values compared to the P(AA) hexapeptide (Figure 1B).

Cellular localization was detected by confocal microscopy, as expected, peptides could be detected at the membrane of MDA-MB-453 cells suggesting their binding to the extracellular domain of HER2 (Figure 1C).

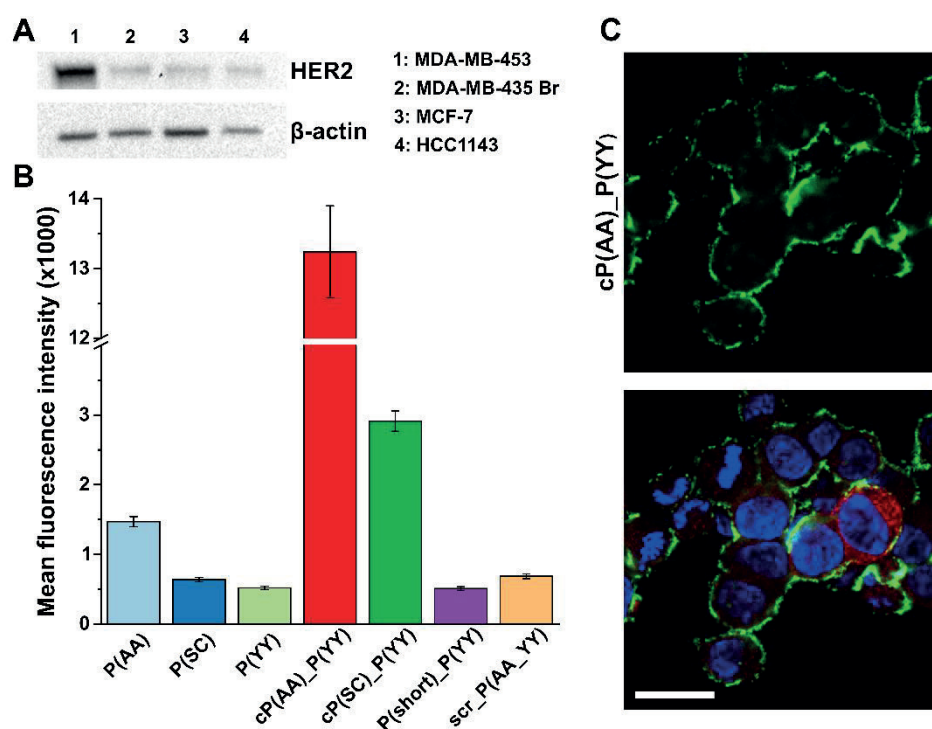


Figure 1. (A) Western blot analysis of breast cancer cells for HER2 expression. (B) Cellular uptake profile of CF-labeled peptides measured by flow cytometry on MDA-MB-453 cells. (C) Confocal microscopy imaging of MDA-MB-453 cells incubated with cP(AA)_P(YY) peptide (green), nuclei were stained with DAPI (blue), HER2 was visualized by immunofluorescence staining (red), scale bar represents 20 μ m.

To monitor specificity, cells were pre-incubated with unlabeled peptides before addition of CF-labeled derivatives. Cellular uptake and microscopic measurements demonstrated that fluorescent signal was decreased supporting that peptides bind to a specific

receptor on the surface of cells (Figure 2A and 2B). The most promising combined peptide (cP(AA)_P(YY)) was also studied for specificity by designing and analysing a reversed version of it (cP(YY)_P(AA)). Flow cytometric and confocal microscopic analysis confirms the importance of the order of the two hexapeptides as the reversed peptide bound to cells at a much lower extent (Figure 2C and 2D).

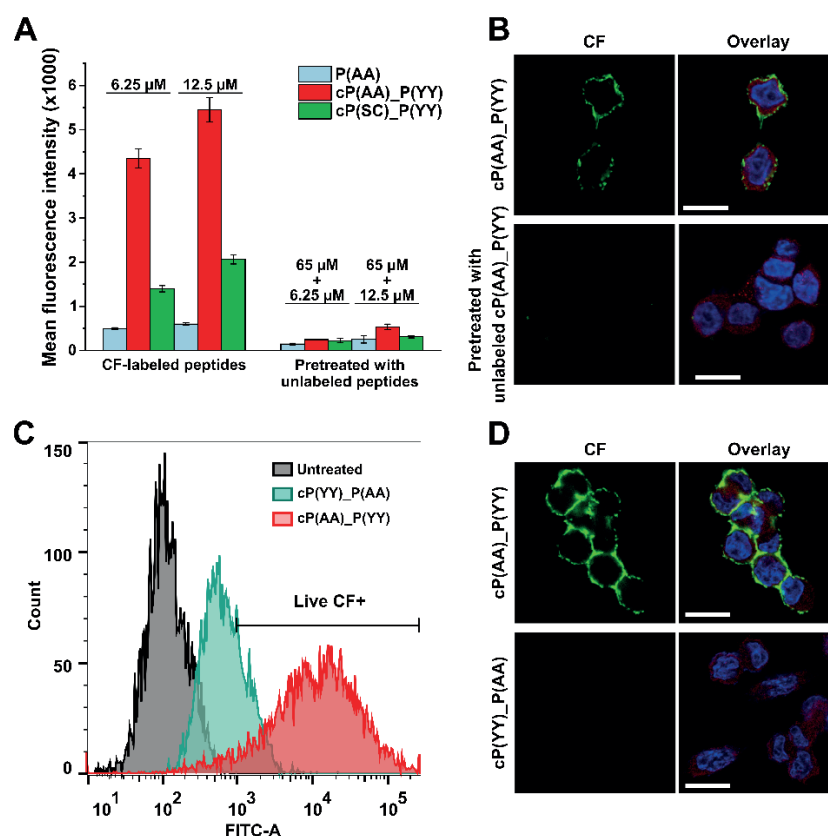


Figure 2. (A, B) Cellular uptake and confocal microscopic imaging of CF-labeled peptides using MDA-MB-453 cells pre-incubated with corresponding unlabeled peptide. (C, D) Study of cellular uptake of the reversed combined peptide by flow cytometry and confocal microscopy (green: CF, blue: nuclei, red: HER2, scale bars: 20 μ m).

Finally, the secondary structure of the peptides was predicted using the PEP-FOLD algorithm.⁷ The predicted helix formation is quite low for the negative control scrambled peptide, however, it increases in case of peptides binding with a higher rate to HER2-expressing cells and the highest is in case of the most promising combined peptide (Figure 3).

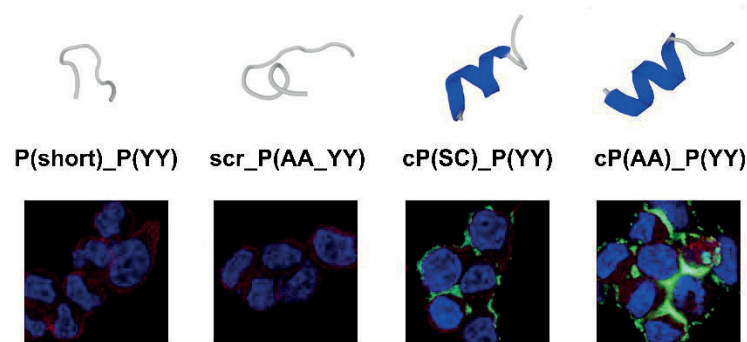


Figure 3. The estimated α -helical content of HER2-binding peptides is proportional to the fluorescence intensity detected on the surface of MDA-MB-453 cells incubated with CF-labeled peptides.

In conclusion, we developed targeting peptides against the extracellular domain of HER2 receptor. We generated new analogues by modifying and combining two sets of known HER2-binding peptides that resulted in the revealing of a 12-mer peptide that binds to HER2 overexpressing cells with high affinity and specificity. Microscopy experiments validated extracellular localization; specificity was verified by preincubation of cells with unlabeled peptides. Secondary structure prediction revealed the importance of the α -helical structure of the conjugates. This combined homing peptide with high affinity and specificity for HER2 extracellular domain can be applied in further studies for tumor diagnostics and drug targeting.⁶

References

1. Lv Q, Meng Z, Yu Y, Jiang F, Guan D, Liang C, Zhou J, Lu A, Zhang G. *Int J Mol Sci* **17**: 2095 (2016)
2. Hsu JL, Hung MC. *Cancer Metastasis Rev* **35**: 575-588 (2016)
3. Escriva-de-Romani S, Arumi M, Bellet M, Saura C. *Breast*. **39**: 80-88 (2018)
4. Karasseva NG, Glinsky VV, Chen NX., Komatireddy R, Quinn TP. *J Prot Chem* **21**: 287-96. (2002)
5. Geng L, Wang Z, Jia X, Han Q, Xiang Z, Li D, Yang X, Zhang D, Bu X, Wang W, Hu Z, Fang Q. *Theranostics*. **6**: 1261-1273 (2016)
6. Biri-Kovács, B, Adorján A, Szabó I, Szeder B, Bősze S., Mező G. *Biomolecules* **10**: 183 (2020)
7. Shen Y, Maupetit J, Derreumaux P, Tuffery P. *J Chem Theory Comput* **10**: 4745-4758 (2014)

Development of novel cyclic NGR peptide–daunomycin conjugates with dual targeting property

Andrea A.P. Tripodi^{1,2}, Kata Nóra Enyedi^{1,2}, Beáta Biri-Kovács^{1,2}, Ivan Randelović³, Szilárd Tóth⁴, Bálint Szeder⁴, Szakács G⁴, József Tóvári³, Gábor Mező^{1,2}

¹MTA-ELTE Research Group of Peptide Chemistry, Hungarian Academy of Sciences, Eötvös L. University, Budapest, Hungary

²Institute of Chemistry, Eötvös L. University, Budapest, Hungary

³Department of Experimental Pharmacology, National Institute of Oncology, Budapest, Hungary

⁴Research Center for Natural Sciences, Hungarian Academy of Sciences

Introduction

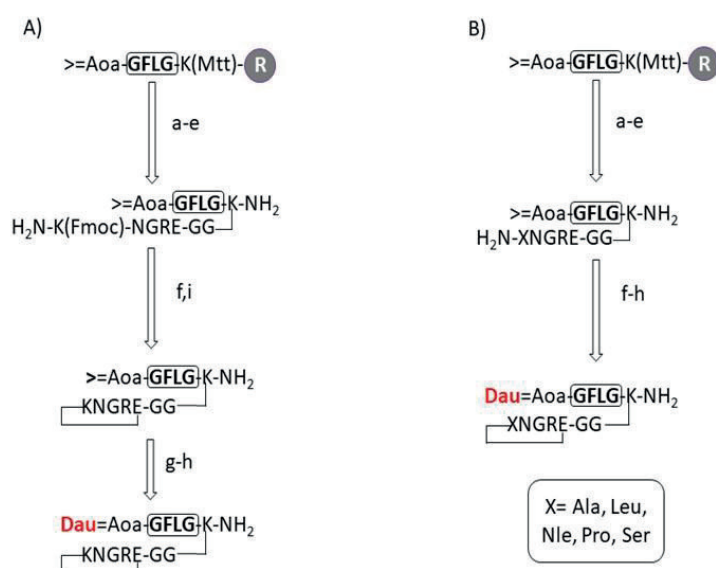
Targeted chemotherapy is one of the most promising approaches for selective cancer treatment that may decrease the toxic side effects of anticancer drugs. This therapeutic approach is based on the fact that tumor-specific receptors are highly expressed on cancer cells/tissues. NGR-motif (Asn-Gly-Arg) containing peptides identified by phage display are suitable candidates for selective drug delivery. NGR peptides bind to CD13-receptors on tumor cells and tumor-related angiogenic blood vessels.¹ However, it is known that the Asn-Gly moiety is subject to Asn deamidation through succinimide formation leading to isoaspartic acid (*isoAsp*, *isoD*) and aspartic acid derivatives usually in a ratio of 3:1 after hydrolysis.² *IsoDGR* peptides are bound to RGD-integrin receptors with high affinity.³ Due to their function in tumor proliferation, metastasis and angiogenesis, integrin-receptors are also promising targets for cancer therapy. Thus, NGR-peptide homing devices may provide dual-targeted delivery of anticancer drugs.

In our previous studies, cyclic NGR derivatives with different bonds (amide, disulfide or thioether) in the cycle were applied for drug targeting. Special attention was paid to the chemostability and *in vitro* biological activity of the compounds.^{4,5} Our results indicated that the conjugates had an antitumor effect on both the CD13(+) HT-1080 human fibrosarcoma cells and the CD13(-) HT-29 human colon adenocarcinoma cells. Both cell lines were integrin positive. Moreover, we showed that the toxicity and the selectivity of the conjugates highly depended on their structure, cellular uptake and propensity to deamidation. The most active conjugate was Dau=Aoa-GFLGK(c[KNGRE]-GG-)-NH₂. In this conjugate, the cyclic NGR peptide was attached through a Gly-Gly dipeptide spacer to the lysine side chain connected to the Cathepsin B labile GFLG spacer that allows lysosomal drug release. Dau was conjugated to the GFLG spacer *via* oxime linkage through an incorporated

aminoxyacetyl (Aoa) moiety. The preparation of the conjugate required a sophisticated synthetic route and the use of orthogonal protecting groups (Figure 1A). Previous studies indicated that the free ϵ -amino group of Lys does not have an impact on biological activity.⁶ To prove our assumption, a set of novel cyclic NGR peptide-Dau conjugates were developed in which the Lys was replaced by different amino acids (Ala, Leu, Nle, Pro and Ser). The main goal of the present study was to investigate whether the exchange of the lysine in the cycle has any influence on the chemostability, selectivity and anti-tumor activity of the conjugates.

Results

Five new conjugates were developed by the replacement of Lys in the cycle in the conjugate $\text{Dau}=\text{Aoa-GFLGK}(\text{c}[\text{KNGRE}]\text{-GG-})\text{-NH}_2$ (**1**) with different amino acids (Nle (**2**), Ala (**3**), Leu (**4**), Pro (**5**) and Ser (**6**)).⁷ These new conjugates could be prepared with better yield in comparison with conjugate **1** because of the simpler synthetic route (Figure 1).



- a) Mtt-cleavage: 2% TFA/DCM; b) Fmoc-Aaa(X)-OH coupling; c) Fmoc-cleavage 2% piperidine/2% DBU/DMF, 0.1 M HOBt; d) cleavage from resin 2.5% TIS/ 2.5% H₂O/ 95% TFA (RT, 3 h); e) salt exchange Pyr.HCl 10 eq/MeOH (1 h); f) cyclization: BOP 3eq/HOBt 3eq/DIPEA 6eq/DMF (c=0.5 mg/mL, RT, 24 h); g) deprotection of aminoxyacetic acid 0.2 M NH₄OAc solution (pH 5.0)/1 M methoxylamine (RT, 1 h); h) daunorubicin conjugation (RT, 24 h) in 0.2 M NH₄OAc solution (pH 5.0); i) Fmoc-cleavage 4% hydrazine/DMF (RT, 2 h).

Figure 2: Schematic representation of the synthesis of cyclic KNGRE (A) and XNGRE (B) drug-conjugates.

Table 1. Stability of cyclic NGR peptide-daunorubicin conjugates

Ratio of Asn-/Asp-/isoAsp-derivatives (DMEM CM, 37 °C)							
Code	Aaa in position X of the conjugates	6 h			72 h		
		NGR	DGR	isoDGR	NGR	DGR	isoDGR
1	Lys	100	0	0	100	0	0
2	Nle	93	1	6	58	9	33
3	Ala	96	0	4	58	11	31
4	Leu	93	0	7	54	11	35
5	Pro	73	14	13	19	46	35
6	Ser	93	0	7	56	12	31

The best yield could be observed in the case of conjugate **2** that was five times higher (overall yield was 10.6%) than in the case of the original compound.

Chemical stability of cyclic NGR bioconjugates was investigated under the treatment conditions used for the *in vitro* cytotoxicity experiments. Deamidation rate was evaluated by HPLC-MS at 0 min, 6 h and 72 h. In contrast to the control conjugate (**1**) that showed high stability in our previous study, the novel conjugates suffered rearrangement in time. The results presented similar *isoAsp/Asp* (~3:1) rates after deamidation of conjugates **2**, **3**, **4** and **6** calculated from the area under the curve. After 6 h, the reasonable rearrangement was observed, which increased over time. Nevertheless, 54-58% of the parent cyclic NGR conjugates was still intact after 72 h (Table 1). Decreased stability was detected in the case of the Pro-containing conjugate (**5**) with faster deamidation and a higher ratio of DGR. Except for deamidation, no other decomposition could be observed during the entire execution of the study.

The antitumor effects of bioconjugates were examined *in vitro* on CD13(+) HT-1080 human fibrosarcoma and on CD13(-) HT-29 human colon adenocarcinoma cells. Both cell types are integrin receptor positive. It seems that the replacement of Lys by the hydrophilic amino acid Ser (**6**) is not favored (Table 2). However, the incorporation of hydrophobic amino acids was well tolerated. The conjugate with a bulky side chain in this position (Leu, **4**) had higher IC₅₀ values that might be explained by steric hindrance. The bioconjugates with Nle (**2**) or Ala (**3**) showed the best antitumor activity on both cell lines. Conjugate **2** showed similar activity on HT-1080 and higher activity on HT-29 cells compared to the control conjugate **1**. To further characterize the biological activity of the conjugates, their lysosomal degradation

and cellular uptake were also investigated. The degradation of the conjugates resulted in Dau=Aoa-Gly-OH in all cases in rat liver lysosomal homogenate and no significant difference in the speed of the metabolite release could be detected. Therefore, this cannot be the reason for the different antitumor activity.

Table 2: *In vitro* cytostatic/cytotoxic effects of compounds on HT-29 and HT-1080 cells

Compounds	HT-1080	HT-29	HT-1080	HT-29
	(6 h)	(6 h)	(72 h)	(72 h)
	IC ₅₀ (μM)	IC ₅₀ (μM)	IC ₅₀ (μM)	IC ₅₀ (μM)
Daunorubicin	1.4 ± 0.6	0.3 ± 0.2	0.5 ± 0.2	0.1 ± 0.1
Dau=Aoa-GFLGK(c[KNGRE]-GG-)-NH₂ (1)	5.7 ± 0.5	8.7 ± 1.2	1.4 ± 0.7	3.0 ± 0.6
Dau=Aoa-GFLGK(c[NleNGRE]-GG-)-NH₂ (2)	5.5 ± 0.3	2.2 ± 0.2	2.3 ± 0.6	1.3 ± 0.2
Dau=Aoa-GFLGK(c[ANGRE]-GG-)-NH₂ (3)	8.9 ± 0.8	4.3 ± 0.5	3.6 ± 0.7	3.2 ± 0.8
Dau=Aoa-GFLGK(c[LNGRE]-GG-)-NH₂ (4)	57.5 ± 6.3	47.0 ± 5.4	20.6 ± 0.4	14.1 ± 0.7
Dau=Aoa-GFLGK(c[PNGRE]-GG-)-NH₂ (5)	9.4 ± 4.0	14.6 ± 4.7	3.5 ± 1.0	3.7 ± 0.8
Dau=Aoa-GFLGK(c[SNGRE]-GG-)-NH₂ (6)	>100	64.7 ± 4.9	63.7 ± 9.5	39.4 ± 2.9

The cellular uptake of Dau containing conjugates can be followed by flow cytometry (Figure 2). The accumulation of conjugates **2**, **4** and **5** increased significantly in HT-29 cells than HT-1080 in comparison with the other conjugates. The low cytostatic/cytotoxic effects of conjugate **6** can be deduced by the results of cellular uptake study. The Ser-containing conjugate did not enter HT-1080 cells, while a slightly higher cellular uptake was detected in HT-29 cells, although the uptake for this conjugate was still much lower than in the case of the other tested bioconjugates.

From these findings, we could conclude that replacement of Lys in the Dau=Aoa-GFLGK(c[KNGRE]-GG-)-NH₂ (**1**) conjugate by different amino acids provides a more convenient and cost-effective synthetic route. Among the new cyclic NGR peptide – daunorubicin conjugates the most effective compound was Dau=Aoa-GFLGK(c[NleNGRE]-GG-)-NH₂ (**2**), which showed similar activity on HT-1080 CD13(+) cells to Dau=Aoa-GFLGK(c[KNGRE]-GG-)-NH₂, and a significantly higher antitumor effect on HT-29 CD13(-) cells. Therefore, these two conjugates were further studied *in vivo*.

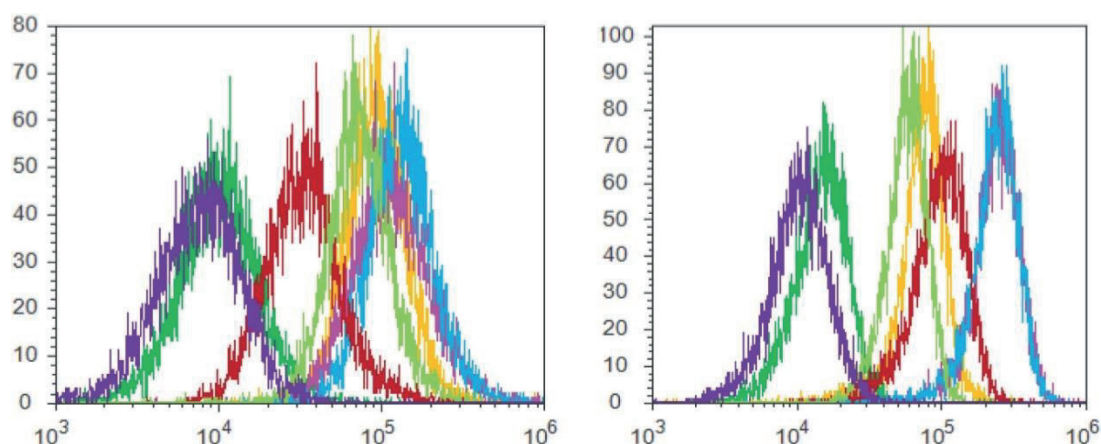


Figure 3: Direct uptake of Dau of conjugate **1** (yellow); **2** (light blue) **3** (light green); **4** (red); **5** (pink); **6** (green) by (left) HT1080 and (right) HT-29 cells, using 10 μ M conjugate for each sample. Untreated control is marked with purple detecting the autofluorescence of the cells.

Kaposi sarcoma (KS) is one of the most deadly and aggressive types of tumors in HIV-1-infected people.⁸ KS tumor cells express a high level of CD13 and this is a key factor for the contribution of increased vascularization of the tumor. Thus, the conjugates were studied on mice with subcutan developed KS tumors. The tumor growth inhibition of conjugate **1** was higher (37.7%) than the observed inhibition in the case of the free drug and conjugate **2**.⁹ In contrast conjugate **2** was more potent on orthotopically developed HT-29 colon carcinoma (low CD13 but high integrin expression) bearing mice (45.7% vs. 16.9%).⁹ The results suggested that conjugate **1** has a significantly higher affinity to CD13 receptors than to integrins because of its stability (no significant rearrangement to *iso*Asp derivative), while conjugate **2** was rather potent on HT-29 tumor that can be explained by the relatively fast Asn/*iso*Asp switch in the sequence.

References

1. Corti A, Curnis F. *Curr Pharm Biotechnol* **12**: 1128-1134 (2011)
2. Geiger T, Clarke S. *J Biol Chem* **262**:785-794 (1987)
3. Spitaleri A, Mari S, Curnis F, Traversari C, Longhi R, Bordignon C, Corti A, Rizzardi G-P, Musco G *J Biol Chem* **283**:19757-19768 (2008)
4. Enyedi KN, Czajlik A, Knapp K, Láng A, Majer Zs, Lajkó E, Kőhifdai L, Perczel A, Mező G. *J Med Chem* **58**:1806-1817 (2015)
5. Enyedi KN, Tóth S, Szakács G, Mező G. *PLoS One* **12**: e0178632 (2017)
6. Negussie AH, Miller JL, Reddy G, Drake SK, Wood BJ, Dreher MR. *J Control Release* **143**: 265-273 (2010)
7. Tripodi AAP, Tóth S, Enyedi KN, Schlosser G, Szakács G, Mező G. *Beilstein J Org Chem* **14**: 911-918 (2018)

8. Browning PJ, Sechler JM, Kaplan M, Washington RH, Gendelman R, Yarchoan R, Ensoli B, Gallo RC. *Blood* **84**: 2711-2720 (1994)
9. Tripodi AAP, Randelović I, Biri-Kovács B, Szeder B, Mező G, Tóvári J. *Pathol Oncol Res* **26**: 1879-1892 (2020)

Design, synthesis and characterization of Pancreatic Ductal Adenocarcinoma (PDAC) targeting antitumor daunomycin-peptide conjugates

Levente E. Dókus^{1,2}, Eszter Lajkó³, Orsolya Láng³, Diána Mező³, Zsófia Szász³, Angéla Takács³, László Kőhidai³, Gitta Schlosser², Ivan Randelović⁴, József Tóvári⁴, Gábor Mező^{1,2}

¹MTA-ELTE Research Group of Peptide Chemistry, Hungarian Academy of Sciences, Eötvös L. University, Budapest, Hungary

²Institute of Chemistry, Eötvös L. University, Budapest, Hungary

³Department of Genetics, Cell- and Immunobiology, Semmelweis University, Budapest, Hungary

⁴Department of Experimental Pharmacology, National Institute of Oncology, Budapest, Hungary

Introduction

Pancreatic Ductal Adenocarcinoma (PDAC) is one of the most aggressive and dangerous cancerous diseases with a high mortality rate.¹ The average 5-year survival rate is less than 5%.² The early diagnosis of PDAC is still difficult, and most patients have already progressed to not operable and incurable statuses at the recognition of the disease.³ In addition, the chemotherapy applied to treat pancreatic cancers is usually ineffective due to the fast development of resistance. Furthermore, chemotherapy causes many side effects because of the low selectivity of the currently used drugs.⁴ Therefore, the design of efficient anticancer agents against PDAC is one of the most challenging tasks for scientists working on cancer research.⁵ Targeted tumor therapy could be a promising strategy to overcome these drawbacks in pancreatic cancer treatment – similarly to other types of cancers.⁶ Targeted tumor therapy is based on targeting tumor-specific or overexpressed receptors or other cell surface compartments on tumor cells that can be recognized selectively by antibodies or small molecules such as folic acid or peptides.^{7,8} Several homing peptides have been described in the literature that recognize pancreatic cancer cells and could be used for drug targeting directly or as part of nanoparticles.⁹⁻¹²

Here we report peptide–drug conjugates in which daunomycin (Dau) as an anticancer agent is linked *via* oxime bond to different types of homing peptides. For this study, two homing peptides were selected. The first one is based on a neurotensin fragment (⁶PRRPYIL¹³) which binds to neurotensin receptors that are overexpressed in numerous tumor types.¹³ The other one is KTLLPTP heptapeptide, which is able to recognize plectin, a protein

spacer did not provide a positive effect on the antitumor activity (conjugate **2**, **5** and **6**). In addition, the elimination of the Pro in position 10 caused the full loss of the antitumor effect (**4**).

In the case of plectin targeting (KTLLPTP) peptide, which was identified by phage-display, a similar effect was detected. Conjugate **7** proved to be one of the most efficient antitumor agents but the GFLG containing analogue (**8**) did not show any activity.

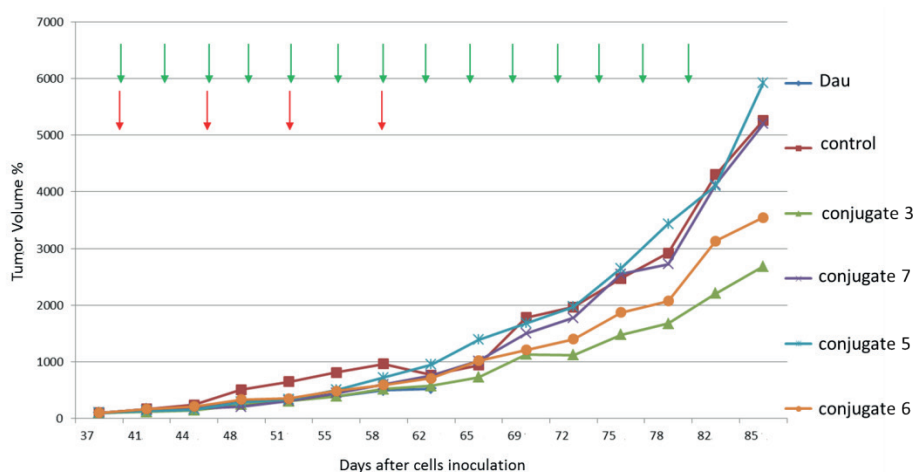
Table 1. Antitumor effect of the conjugates on PANC-1 cell –line

Code	Compounds	Viability ^a (%) at 10 ⁻⁵ M concentration, after 72 h incubation
1	<i>Dau=Aoa-RRPYIL-OH</i>	75.3 ± 9.08
2	<i>Dau=Aoa-KPRRPYIL-OH</i>	>100
3	<i>Dau=Aoa-KRRPYIL-OH</i>	4.7 ± 1.78
4	<i>Dau=Aoa-GFLG-KPRRYIL-OH</i>	>100
5	<i>Dau=Aoa-GFLG-KPRRPYIL-OH</i>	11.0 ± 1.70
6	<i>Dau=Aoa-GFLG-KRRPYIL-OH</i>	13.0 ± 1.47
7	<i>Dau=Aoa-KTLLPTP-NH₂</i>	4.8 ± 1.25
8	<i>Dau=Aoa-GFLG-KTLLPTP-NH₂</i>	>100
9	<i>Dau=Aoa-KTLLPTP-KRRPYIL-OH</i>	69.8 ± 5.7
10	<i>Dau=Aoa-KRRPYIL-KTLLPTP-NH₂</i>	>100
11	<i>Dau=Aoa-GFLG-K(Dau=Aoa)TLLPTP-KRRPYIL-OH</i>	>100
12	<i>Dau=Aoa-GFLG-K(Dau=Aoa)RRPYIL-KTLLPTP-NH₂</i>	>100
13	<i>Dau=Aoa-K(Dau=Aoa)TLLPTP-KRRPYIL-OH</i>	41.3 ± 7.3
14	<i>Dau=Aoa-K(Dau=Aoa)RRPYIL-KTLLPTP-NH₂</i>	95.6 ± 3.3

^a Cell index (CI) values of the treated cells are normalized to the CI values of the control wells and expressed as percentages. Data are given as mean values ± standard deviation (SD), (n=3).

Further derivatives were developed by the combination of the most effective homing sequences: KRRPYIL and KTLLPTP. These constructions were synthesized using the successful linear (9, 10) or branched structure (11-14) which may lead to the design of efficient antitumor agents.¹⁶ Unfortunately, most of these conjugates lost the antitumor effect completely except conjugates 9 and 13 that showed moderate activity.

The four most efficient conjugates (3, 5, 6, 7) identified in the *in vitro* studies were applied in an *in vivo* experiment using *s.c.* developed PANC-1 tumor-bearing SCID mice. Results were compared with free drug administration. It can be observed that the antitumor effect of conjugates is different considering the tumor volume and weight.



Green arrows indicate the days of administration with conjugates
 Red arrows indicate the days of administration with daunomycin

Figure 1. *In vivo* tumor growth inhibition on PANC-1 tumor-bearing mice measured by tumor volume

After the termination of animals (on day 85), it was indicated that the tumor volume decreased by 49% for conjugate 3, 1.2% for conjugate 7 and 32.6% in case of conjugate 6, respectively (Figure 1), but conjugate 5 did not present any effect. In the case of tumor weight measurement, 5 also did not inhibit tumor growth, while conjugates 6 and 3 showed very modest, non-significant tumor growth inhibition (3.3% and 4.6%, respectively). In this case, conjugate 7 induced 15.9% decrease of tumor weight compared to the control animals (Figure 2). Conjugate 3 showed the highest antitumor activity followed by conjugates 6 and 7 (considering the tumor volume). Conjugate 5 showed the lowest antitumor activity. It is worth mentioning that on day 59 when the Dau treated group had to be terminated because of toxic side effects, all conjugates showed a bit lower activity compared with the free Dau. In summary, the results indicated that the two most efficient agents were conjugate 3 that

inhibited better the growth of tumor volume and conjugate 7 that has a higher inhibition effect on the growth of tumor weight.

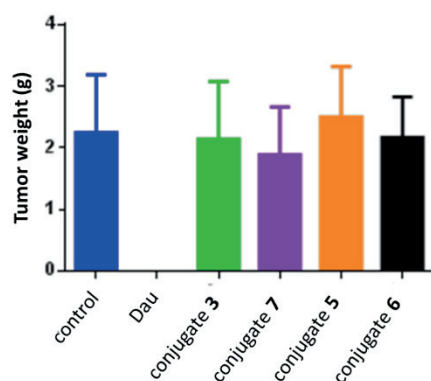


Figure 2. *In vivo* tumor growth inhibition on PANC-1 tumor bearing mice measured by tumor weight

References

1. Vincent A, Herman J, Schulick R, Hruban, RH, Goggins M. *Lancet* **378**: 607-620 (2011)
2. Hidalgo M. *N Engl J Med.* **362**: 1605-1617 (2010)
3. Zhang L, Sanagapalli S, Stoita A, *World J. Gastroenterol* **24**: 2047-2060 (2018)
4. Diab M, Azmi A, Mohammad R, Philip PA. *Expert Opin Pharmacother* **20**: 535-546 (2019)
5. Xie D, Xie K. *Genes Dis.* **2**: 133-143 (2015)
6. Szepeshazi K, Schally AV, Block NL, Halmos G, Nadji M, Szalontay L, Vidaurre I, Abi-Chaker A, Rick FG. *Oncotarget* **4**: 751-760 (2013)
7. Vrettos EI, Mező G, Tzakos AG. *Beilstein J Org Chem* **14**: 930-954 (2018)
8. Kutova OM, Guriyev EL, Sokolova EA, Alzeibak R, Balalaeva IV. *Cancers* **11**: 68 (2019)
9. Matters GL, Harms J. *Biomedicines* **6**: E65. (2018)
10. Sanna V, Nurra S, Pala N, Marceddu S, Pathania D, Neamati N, Sechi M. *J Med Chem* **59**: 5209-5220 (2016)
11. Liu X, Jiang J, Ji Y, Lu J, Chan R, Meng H. *Mol Syst Des Eng* **2**: 370-379 (2017)
12. Nishimoto T, Yamamoto Y, Yoshida K, Goto N, Ohnami S, Aoki K. *PLoS One* **7**: e45550 (2012)
13. Leeman SE, Carraway RE. *Ann N Y Acad Sci* **400**: 1-16. (1982)
14. Kelly KA, Bardeesy N, Anbazhagan R, Gurumurthy S, Berger J, Alencar H, Depinho RA, Mahmood U, Weissleder R. *PloSMed* **5**: e85 (2008)
15. Peterson JJ, Meares CF. *Bioconjugate Chem* **9**: 618-626 (1998)
16. Dókus LE, Lajkó E, Randelović I, Mező D, Schlosser G, Kőhidai L, Tóvári J, Mező G. *Pharmaceutics* **12**: 576 (2020)

Synthesis and *in vitro* evaluation of drug-containing melanoma-specific peptide conjugates

Ildikó Szabó¹, Szilvia Bősze¹, Gábor Mező^{1,2}

¹MTA-ELTE Research Group of Peptide Chemistry, Hungarian Academy of Sciences, Eötvös L. University, Budapest, Hungary

²Institute of Chemistry, Eötvös L. University, Budapest, Hungary

Introduction

Increasing mortality rate of tumorous diseases is reported by the World Health Organization. Skin cancer is the most increasing incidence of cancer diseases especially in the case of young adults. Although melanoma is only about 1% of skin cancers, it causes a large majority of skin cancer derived mortality. However, in the case of melanoma, using chemotherapy, radiotherapy or immunotherapy (the main procedures for the treatment of advanced or metastatic cancers) is recommended due to its localization and rapid progression. Thus, the high and continuously rising rate of death among melanoma patients has encouraged new research focusing on therapies and drugs with increasing efficiency, especially against metastatic melanoma. Selective and targeted approaches might improve the impact of anticancer therapies with fewer side effects.

Melanoma is originated from the malignant transformation of melanocytes which are the melanin-producing cells of the skin, hair and eyes. It is formed either by dysfunction of dysplastic nevi or a single melanocyte.¹ Melanocytes are located with keratinocytes in the basal layer of the epidermis and they form a very stable population, as they proliferate extremely rarely under normal circumstances. Not only the outer layer (epidermis), but also the inner layer (dermis) of the skin, which involves hair roots, blood and lymph-vessels and nerves, includes melanocytes, though they are biologically different population than epidermis located ones. Based on this evidence, cutaneous melanoma is a heterogeneous tumour, which involves the wide population of melanocytes with different origin and differentiation stages (from undifferentiated, cancer stem-like cells with self-renewal capacity and high proliferation and differentiation ability to functional melanocytes). Among all type of skin cancers, melanoma has the highest rate of the metastatic effect. Based on its location, it has a high potential to spread rapidly through other body sites by entering the lymphatic system and bloodstream.

Cell surface receptors with altered expression levels are not the only specific and selective targets for tumor cells. Markedly, modified proteoglycan expression and structure

can also be observed during tumor development and growth.² The melanoma-associated chondroitin sulfate proteoglycan (MCSP, also called NG2) is a type I single-pass transmembrane proteoglycan,³ which is widely expressed in several different tumors, including glioblastomas, chondrosarcomas, melanomas and some leukemias.⁴⁻⁷ Functionally, it promotes tumor vascularization⁸ due to binding to collagen VI and it promotes cell survival and adhesion.⁹ Antibodies against NG2 inhibit melanoma cell growth both *in vitro* and *in vivo*.¹⁰⁻¹² Moreover, targeting NG2 *in vivo* in a highly malignant tumor model reduced tumor growth and angiogenesis was determined.¹³ Burg *et al.* identified two novel decapeptide ligands for the NG2 proteoglycan using phage display. Based on the structure, the two sequences are clearly different (Peptide1: TAASGVRSMH; Peptide2: LTLRWVGLMS), but they may act as mimotopes of each other on the basis of small areas of similarity (ASG vs LTL; VR vs VG). Both peptides have high affinity and specificity to NG2 proteoglycan, and they can bind to similar sites on NG2.¹⁴ Guan *et al.* developed Peptide1 conjugated biodegradable nanoparticles loaded with docetaxel, as a new nanomedicine. The construct achieved controlled drug release, and it had significant *in vitro* and *in vivo* antitumor effect which was mediated *via* NG2 receptor.¹⁵

Based on the above-mentioned facts, drug-containing melanoma-targeting peptide conjugates were designed, synthesized and their *in vitro* evaluation was performed in order to establish structure-activity relationships and to find the most promising construct for melanoma targeting.

Results

Melanoma targeting phage display peptides (Peptide1 and Peptide2) were synthesized by solid-phase peptide synthesis using Fmoc/^tBu strategy. For both peptides, the native sequence and their modified versions were also synthesized. The following modifications were performed; i) methionine was replaced by norleucine to avoid the unwanted oxidation; ii) enzyme labile GFLG spacer was used to elongate the peptides at the N-terminus to enhance the release of the drug from the construct; and iii) scrambled and truncated peptide sequences were synthesized to establish the optimal effective sequence. The peptides were built up on Rink Amide MBHA resin using Fmoc protected amino acid derivatives. At the end of the synthesis, Boc protected aminoxyacetic acid was coupled to the N-terminus in order to functionalize the peptides for drug conjugation. Unfortunately, synthesis of GFLG spacer containing Peptide1 was unsuccessful, due to its hydrophobic feature; it forms aggregates immediately after the cleavage. Therefore, its daunomycin conjugate cannot be prepared. But

in the case of truncated Peptide1 analogs, this aggregation was not observed. Before the conjugation, peptides were cleaved from the resin and purified by preparative RP-HPLC and characterized by analytical RP-HPLC and ESI-MS (data not shown). Daunomycin as a drug was coupled to the aminoxy acetylated peptides *via* oxime bond. Conjugation was carried out in slightly acidic condition (250 mM NaOAc buffer, pH 5.2). The conjugates were purified by preparative RP-HPLC and characterized by analytical RP-HPLC and ESI-MS (Table 1). The yield of conjugation was strongly dependent on the peptide sequence. In the case of Peptide1 based conjugates due to their poor solubility and high aggregation ability, the yield was only 10-15%. In case of Peptide2, conjugates were formed almost quantitatively.

In the first step, the *in vitro* cytostatic effect of the conjugates was determined on A2058 (ATCC[®] CRL-11147) human melanoma cell culture. The most effective conjugates were also tested on A431 (ATCC[®] CRL-1555) human epithelial (but not melanoma originated) cell culture in order to investigate the selectivity of these conjugates. In case of Peptide1 conjugates, replacement of Met to Nle (**Conj3**) has no significant effect on the activity; both conjugates have moderate *in vitro* cytostatic effect (62.8 ± 22.1 μ M and 22.1 ± 12.1 μ M, respectively) on A2058 cells. Incorporation of GFLG enzyme labile spacer in both cases – native (**Conj2**) and Nle substituted (**Conj4**) ones – significantly increases the *in vitro* efficacy (5.2 ± 2.4 μ M and 2.3 ± 1.3 μ M, respectively). Truncation of Peptide1 sequence is allowed; not only the first two (**Conj5**), but the first four (**Conj6**) N-terminal amino acids can also be eliminated without reduction of activity (1.3 ± 0.6 μ M and 3.1 ± 1.1 μ M, respectively) on A2058 cells. Interestingly, the scrambling of the targeting Peptide1 sequence (**Conj5**) has not influenced the *in vitro* activity compared to Nle-substituted one (**Conj4**) on A2058 cells (2.3 ± 1.3 μ M and 1.3 ± 0.6 μ M, respectively).

In case of Peptide2, not only the replacement of Met by Nle (**Conj9**), but also the incorporation of GFLG spacer (**Conj10**) decreased the *in vitro* cytostatic effect (17.5 ± 3.3 μ M and 26.5 ± 17.6 μ M, respectively) on A2058 cells. Scrambling of the targeting Peptide2 sequence (**Conj11**) does not influence the *in vitro* activity compared to the native sequence (**Conj8**) on A2058 cells (4.3 ± 1.9 μ M and 2.5 ± 0.6 μ M, respectively). Truncation of Peptide2 sequence is moderately allowed; the first two N-terminal amino acids (LT, **Conj12**) can be eliminated without reduction of cytostatic effect. However, further elimination of additional two amino acids, LR (**Conj13**) is not allowed, it can significantly decrease the *in vitro* activity. These modifications do not only influence the *in vitro* cytostatic activity, but they have also effect on the selectivity. While the native sequence (**Conj8**) proves to be melanoma

specific ($4.3 \pm 1.9 \mu\text{M}$ on A2058 and $14.0 \pm 0.09 \mu\text{M}$ on A431), this selectivity is absent in case of the scrambled one (**Conj11**; $2.5 \pm 0.6 \mu\text{M}$ on A2058 and $2.6 \pm 0.9 \mu\text{M}$ on A431).

Compared to Peptide2 conjugates, unfortunately, none of the Peptide1 conjugates showed melanoma specificity, all of the Peptide1 conjugates have similar IC_{50} values on A2058 and A431 cells.

Table 1. Chemical characterization of melanoma-specific conjugates and their IC_{50} values on A2058 and A431 cells

Code	Conjugates	t_R (min) ^a	M_{av} (Da) ^b		IC_{50} (μM) ^c	
			calc	meas	A2058	A431
Conj1	Dau=Aoa-TAASGVRSMH-NH ₂	10.6	1596.6	1596.5	62.8 ± 22.1	n.t*
Conj2	Dau=Aoa-GFLG-TAASGVRSMH-NH ₂	13.5	1970.5	1970.9	5.2 ± 2.4	n.t*
Conj3	Dau=Aoa-TAASGVRSNleH-NH ₂	13.9	1578.1	1578.8	22.1 ± 12.1	n.t*
Conj4	Dau=Aoa-GFLG-TAASGVRSNleH-NH ₂	13.7	1952.5	1953.1	2.3 ± 1.3	1.2 ± 0.5
Conj5	Dau=Aoa-GFLG-ARASNleHSTGV-NH ₂	13.7	1952.5	1952.2	1.3 ± 0.6	2.2 ± 2.1
Conj6	Dau=Aoa-GFLG-ASGVRSNleH-NH ₂	13.9	1780.4	1780.5	3.1 ± 1.1	1.9 ± 1.4
Conj7	Dau=Aoa-GFLG-GVRSNleH-NH ₂	14.1	1622.2	1622.3	2.5 ± 1.1	1.2 ± 0.5
Conj8	Dau=Aoa-LTLRWVGLMS-NH ₂	14.4	1756.1	1756.2	4.3 ± 1.9	14.0 ± 0.0
Conj9	Dau=Aoa-LTLRWVGLNleS-NH ₂	15.1	1737.5	1737.2	17.5 ± 3.3	n.t*
Conj10	Dau=Aoa-GFLG-LTLRWVGLNleS-NH ₂	18.1	2112.3	2112.4	26.5 ± 17.6	n.t*
Conj11	Dau=Aoa-VGLMWSLTRL-NH ₂	17.1	1756.3	1756.5	2.5 ± 0.6	2.6 ± 0.9
Conj12	Dau=Aoa-GFLG-LRWVGLMS-NH ₂	16.1	1933.6	1933.4	4.6 ± 2.5	4.3 ± 0.7
Conj13	Dau=Aoa-GFLG-WVGLMS-NH ₂	17.4	1663.9	1663.8	10.3 ± 7.1	16.7 ± 1.3
Dau	Daunomycin·HCl				<0.16	<0.16

^aAnalytical RP-HPLC, Agilent Eclipse XDB C8, 5 μm , 80Å, 4.6 x 150 mm, HPLC column, gradient: 5% B, 2 min; 5-100% B, 20 min.

^bBruker Daltonics Esquire 3000plus (Bremen, Germany) ion trap mass spectrometer. Spectra were acquired in the 50–2000 m/z range

^c IC_{50} values were determined by a computerized curve-fitting program (Origin 7.5). Values shown are mean \pm SE of four independent experiments, each performed in four parallels.

*n.t.: not tested

Cellular uptake profile was determined by flow cytometry using A2058 human melanoma and A431 human epithelial cells. Based on the IC_{50} values, Peptide1 originated conjugates do not seem to be melanoma-cell specific *in vitro*. Therefore, **Conj4**; **5**; **6**; **7** were selected for cellular uptake studies to confirm this hypothesis. These conjugates have the same structure; the GFLG enzyme labile linker is located between the drug and the targeting unit. In these cases, the release of the drug might occur in a similar manner (the same

metabolite can be formed), suggesting that only the targeting unit is responsible for the *in vitro* efficacy.

In all cases, the concentration-dependent cellular uptake profile was detected. Although the detected fluorescence intensity of A2058 cells was approx. twice as high as that of A431, the cellular uptake profile of the conjugates is similar. **Conj4** can be taken up the most effectively and **Conj7**, with the shortest targeting sequence, is the least internalized one. The scrambled sequence containing **Conj5** and the two amino acids truncated one (**Conj6**) have similar internalization ability on both cell cultures (Figure 1).

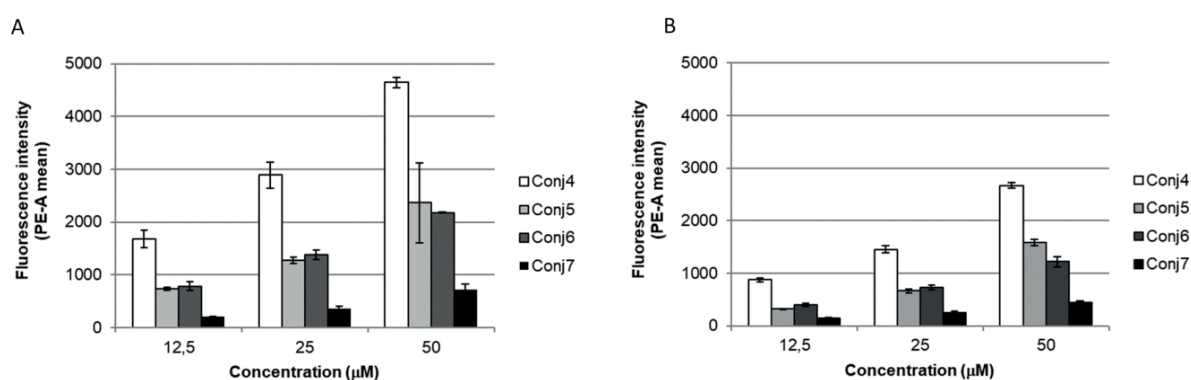


Figure 1. Cellular uptake profile of **Conj4**, **Conj5**, **Conj6** and **Conj7** on A2058 (A) and on A431 (B) cell cultures. The intracellular fluorescence intensity of A2058 or A431 cells was monitored by flow cytometer (BD LSR II) which is proportional to the cellular uptake. Data were analyzed with FACSDiVa 5.0 software.

In conclusion, drug-containing melanoma-specific peptide-based conjugates were designed, synthesized and investigated *in vitro*. Although most of the conjugates were very promising based on their *in vitro* cytostatic activity; the *in vivo* and further therapeutic application of these targeting peptides themselves might be very limited due to their poor solubility and decreased melanoma specificity. However, their application as targeting units for nanoparticles appears to be promising.

References

1. Eggermont AM, Spatz A, Robert C. *Lancet* **383**: 816-27 (2014)
2. Nikitovic D, Berdiaki A, Spyridaki I, Krasanakis T, Tsatsakis A, Tzanakakis GN. *Front Endocrinol (Lausanne)* **9**:69 (2018)
3. Price MA, Colvin Wanshura LE, Yang J, Carlson J, Xiang B, Li G, Ferrone S, Dudek AZ, Turley EA, McCarthy JB. *Pigment Cell Melanoma Res* **24**: 1148-57 (2011)
4. Behm FG, Smith FO, Raimondi SC, Pui CH, Bernstein ID. *Blood* **87**:1134-1139 (1996)

5. Real FX, Houghton AN, Albino AP, Cordon-Cardo C, Melamed MR, Oettgen HF, Old LJ. *Cancer Res* **45**: 4401-4411 (1985)
6. Schrappe M, Klier FG, Spiro RC, Waltz TA, Reisfeld RA, Gladson CL. *Cancer Res* **51**: 4986-4993 (1991)
7. Léger O, Johnson-Léger C, Jackson E, Coles B, Dean C. *Int J Cancer* **58**: 700-705 (1994)
8. You WK, Yotsumoto F, Sakimura K, Adams RH, Stallcup WB. *Angiogenesis* **17**:61-76 (2014)
9. Cattaruzza S, Nicolosi PA, Braghetta P, Pazzaglia L, Benassi MS, Picci P, Lacrima K, Zanooco D, Rizzo E, Stallcup WB, Colombatti A, Perris R. *J Mol Cell Biol* **5**: 176-193 (2013)
10. Harper JR, Reisfeld RA. *J Natl Cancer Inst* **71**: 259-263 (1983)
11. Bumol TF, Wang QC, Reisfeld RA, Kaplan NO. *Proc Natl Acad Sci U S A* **80**: 529-533 (1983)
12. Harper J, RA R. In *Biology of Proteoglycans*, Mecham TW. a. R., Ed. 345–366 (1987)
13. Wang J, Svendsen A, Kmiecik J, Immervoll H, Skaftnesmo KO, Planagumà J, Reed RK, Bjerkvig R, Miletic H, Enger P, Rygh CB, Chekenya M. *PLoS One* **6**: e23062 (2011)
14. Burg MA, Pasqualini R, Arap W, Ruoslahti E, Stallcup WB. *Cancer Res* **59**: 2869-2874 (1999)
15. Guan YY, Luan X, Xu JR, Liu YR, Lu Q, Wang C, Liu HJ, Gao YG, Chen HZ, Fang C. *Biomaterials* **35**: 3060-3070 (2014)

Optimization of the structure of targeted Daunomycin conjugates against non-small cell lung cancer

Zoltán Bánóczy¹, Ildikó Szabó², Gábor Mező^{1,2}

¹Institute of Chemistry, Eötvös L. University, Budapest, Hungary

²MTA-ELTE Research Group of Peptide Chemistry, Hungarian Academy of Sciences, Eötvös L. University, Budapest, Hungary

Introduction

Cancer is one of the leading causes of death in the World and in the EU too.^{1,2} Lung cancer alone was responsible for 1.7 million deaths worldwide in 2016. As tumor cells are originated from normal cells they are very similar to those. This makes it highly challenging to eliminate them without the destruction of healthy tissues. In spite of the common origin, small differences can be found in their receptors or enzyme sets. These little differences may allow a valuable increase in the selectivity of therapy and may enhance the rate of success during treatment. Thus, identification of new therapeutically useful targeting units is a hot topic.

An often used promising tool to identify tumor homing peptides is the technique of phage display.³ These are mostly short, tumor specific peptides and can specifically accumulate into tumors. One drawback of this technique is that there is no optimization of the identified peptides. However, sometimes the optimized sequences may have more therapeutic values compared to the original ones. The chemical modification may increase both the stability and the specificity of these peptides.⁴ Phage display technique was carried out to identify tumor homing peptides against non-small cell lung cancer as well.⁵⁻⁷

Tumor homing peptides can be applied to deliver antitumor drugs into tumor tissues to decrease the side effect and thus increase the efficacy. The covalent linkage, the number of drugs and the structure of conjugates may affect the efficiency.

Results

Based on the literature, two tumor homing peptides were selected for further optimization. One of them was the ARRPKLD peptide that was selected based on a selective peptide motif A(S)RXPXXX.⁶ We used this peptide and motif to develop tumor-targeting drug conjugates (Table 1, conjugate 1-14). Unfortunately, the identification of a tumor homing peptide does not give any information about the mechanism and selectivity of their cellular uptake. It is unclear, what is the main target of these peptides that causes their tumor

cell specificity. If these peptides and their conjugates can be internalized into the tumor cells by endocytosis, the conjugates can be degraded in the lysosomes. In that case an enzyme labile spacer can be used to increase the effect of conjugates. In our constructs, two different spacers – GFLG and LRRY that can be cleaved by lysosomal Cathepsin B were compared. Although the authors selected the ARRPKLD sequence, we were interested in comparing it with a peptide containing serine at the N-terminus. These kinds of peptides were the second in the enrichment assays. Furthermore, as the motif allows all amino acids in position 5 (A(S)RXPXXX), conjugates with Gly at this position were synthesized too. The linkage between the drug and the transporter unit may have a high influence on biological activity. Thus, the effect of two different kinds of covalent bond was studied. The Dau was coupled in some of our conjugates *via* an oxime bond while in the other *via* an amide bond (Figure 1). The latter one is stable in physiological conditions, thus the drug is not released from these constructs, while in case of oxime bond some release may happen inside the cells.

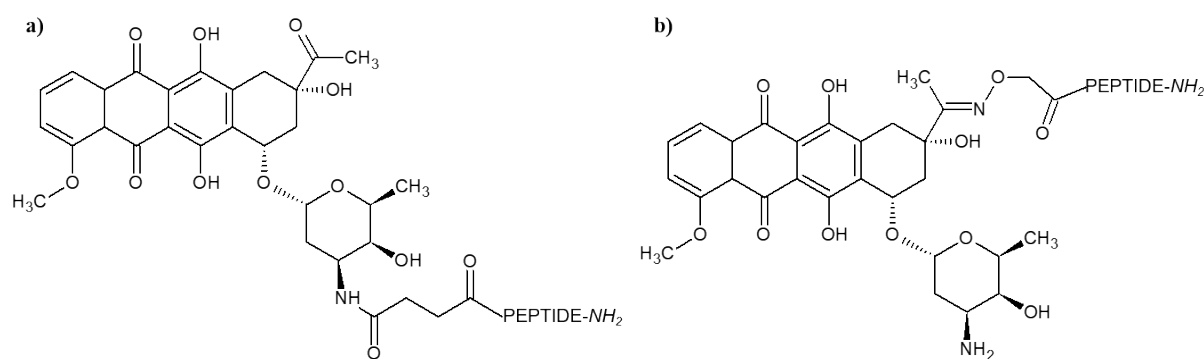


Figure 1. The structure of a) Dau-Suc conjugates and b) Dau=Aoa conjugates

The cytostatic effect of these conjugates was studied on EBC-1 cells, a human lung squamous cell carcinoma line, as a model.⁸ The cells were treated with the solution of conjugates (0.83-100 μ M concentration range) for 24 h. Then the cells were washed and were cultured for 48 h in serum-containing medium. The *in vitro* cytostatic effect was determined using MTT assay and IC₅₀ values were determined from the viability vs lg(c) curve (Table 1). Among the best conjugates – their IC₅₀ values are less than 10 μ M – two contained Ala (conjugates **1** and **11**) while three conjugates contained Ser at the N-terminus (conjugates **2**, **4** and **6**). Three conjugates (**7**, **10** and **13**) had no or moderate cytostatic activity. All effective conjugates contained spacer, four of them (**1**, **2**, **6** and **11**) had the GFLG one. The comparison of the effect of conjugates with Lys or Gly showed that Lys is preferable at this position.

Based on the above mentioned structure–activity relationship we can conclude that Ser at the N-terminus and GFLG spacer are better choices in case of this set of conjugates.

Table 1. The *in vitro* cytostatic activity of conjugates

Code	Peptide	IC ₅₀ (μM)		
		EBC-1	A2058	A431
1	Dau=Aoa-GFLG-ARRPKLD-NH ₂	3.1±0.4	8.1±0.5	12.2±1.0
2	Dau=Aoa-GFLG-SRRPKLD-NH ₂	6.7±1.1	8.9±0.4	14.4±2.6
3	Dau=Aoa-LRRY-ARRPKLD-NH ₂	50.8±36.2	n.d.	n.d.
4	Dau=Aoa-LRRY-SRRPKLD-NH ₂	6.4±3.9	53.2±11.7	89.7±14.6
5	Dau=Aoa-GFLG-ARRPGLD-NH ₂	40.8±27.2	n.d.	n.d.
6	Dau=Aoa-GFLG-SRRPGLD-NH ₂	4.5±1.8	2.0±0.5	3.9±1.8
7	Dau=Aoa-LRRY-ARRPGLD-NH ₂	100	n.d.	n.d.
8	Dau=Aoa-LRRY-SRRPGLD-NH ₂	13.3±4.5	n.d.	n.d.
9	Dau-Suc-ARRPGLD-NH ₂	53.8±8.8	n.d.	n.d.
10	Dau-Suc-SRRPGLD-NH ₂	>100	n.d.	n.d.
11	Dau-Suc-GFLG-ARRPGLD-NH ₂	4.4±2.6	>100	>100
12	Dau-Suc-GFLG-SRRPGLD-NH ₂	10.2±9.8	n.d.	n.d.
13	Dau-Suc-GFLG-ARRPKLD-NH ₂	>100	n.d.	n.d.
14	Dau-Suc-GFLG-SRRPKLD-NH ₂	57.4±5.8	n.d.	n.d.
15	Dau=Aoa-LRRY-DWTY-NH ₂	20.8±15.1	n.d.	n.d.
16	Dau=Aoa-LRRY-SYDWTY-NH ₂	7.4±5.4	n.d.	n.d.
17	Dau=Aoa-LRRY-LRSYDWTY-NH ₂	10.3±5.7	n.d.	n.d.
18	Dau=Aoa-LRRY-TDSILRSYDWTY-NH ₂	20.7±1.2	n.d.	n.d.
Dau	Daunomycin	0.05±0.03	n.d.	n.d.

n.d no data

For studying the tumor selectivity of the best five conjugates, A2058 malignant melanoma⁹ and A431 human squamous carcinoma¹⁰ cells were treated with these conjugates as well. The cytostatic activity of conjugate **1**, **2** and **6** was very similar on these cells compared to their activity on EBC-1. On the other hand, conjugate **4** and **11** showed lower or no cytostatic activity, respectively. They differ from each other only in the presence (**4**) or absence (conjugate **1**, **2** and **6**) of LRRY spacer. Based on these results, it seems that this spacer is not appropriate in case of these two cell lines.

The three best (**1**, **2** and **6**) and one ineffective (**7**) conjugates were selected to study their cellular uptake on EBC-1 cells. The cells were treated for 3 h then were washed and their fluorescence intensity was measured by flow cytometry (Figure 2). Although conjugates **1**, **2** and **6** have very similar *in vitro* cytostatic activity, they showed different internalization. Conjugates **2** and **6** have lower cellular uptake compared to conjugate **1** (Figure 2). On the other hand, all have more pronounced internalization than that of the ineffective conjugate **6** (Figure 2), which is in accordance with the IC₅₀ values. Although in case of the cytostatic effect the Ser is better, it is not preferable in the sequence if cellular uptakes are compared (at least in case of the studied conjugates). These cellular uptake results gave back clearly the

noticed success of sequences in accumulation in tumors.⁶ The identified best sequence showed the highest internalization in our experiments and alteration of this “preferred” sequence by double substitution (Lys⁵→Gly⁵ and Ala¹→Ser¹) decreased dramatically the cellular uptake. Although only one conjugate with LRRY spacer was studied, the results may indicate that this tetrapeptide reduced the internalization to a great extent.

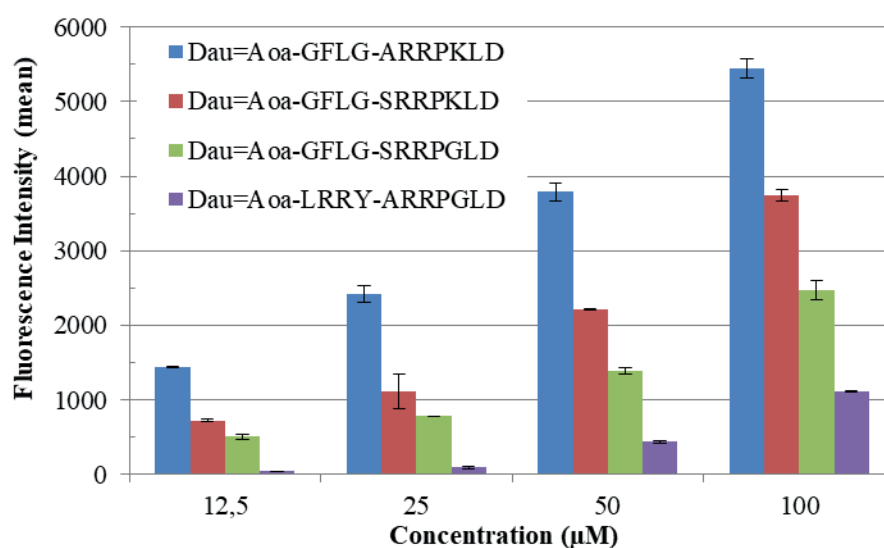


Figure 2. Cellular uptake of conjugates containing XRRPYLD peptides on EBC-1 cells (where X is Ala or Ser and Y is Gly or Lys).

The other tumor homing peptide that was used in our study was the TDSILRSYDWTY sequence. It was also determined that the WTY region is important for cell binding.⁵ In our study truncated peptides were used to identify the minimal sequence which is necessary for the tumor targeting. For this purpose, four conjugates were synthesized (Table 1, conjugates **15-18**), the original peptide with LRRY as enzyme labile spacer and its shorter derivatives. In all conjugates Dau was coupled to the peptide via oxime bond. Two of them were very promising based on their *in vitro* cytostatic activity (Table 1). The longest and the shortest ones (conjugate **15** and **18**) have the same activity, suggesting that one of them is too short while the other is too long that might not have a favorable structure for receptor binding. The most effective conjugate was the Dau-Aoa-LRRY-SYDWTY, while increasing the length of the peptide (Dau-Aoa-LRRY-LRSYDWTY) resulted in a slight decrease in the cytostatic activity.

The internalization of conjugates was measured by flow cytometry on EBC-1 cells. The cells were treated for 3 h then were washed and their fluorescence intensity was measured by flow cytometry (Figure 3). Conjugate **17** showed the highest cellular-uptake ability, although it did not have the highest cytostatic activity. The internalization of the most

cytostatic conjugate (17) was not so outstanding. These findings suggest that not only the internalization, but other factors (e.g. stability, the intracellular fate) could be important in the biological activity.

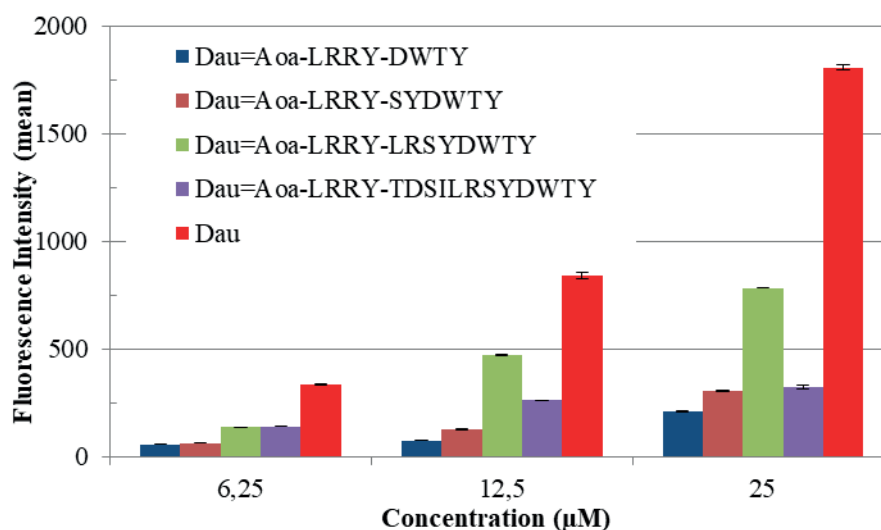


Figure 3. Cellular uptake of conjugates containing TDSILRSYDWTY sequence and its truncated derivatives on EBC-1 cells.

Our results proved that the tumor homing peptides may be suitable for the synthesis of conjugates with antitumor activity, but their structure can be further optimized to increase their effect. Our optimized conjugates showed improved antitumor activity and may be used in tumor therapy.

References

1. <https://www.who.int/news-room/fact-sheets/detail/the-top-10-causes-of-death>, (n.d.)
2. https://ec.europa.eu/eurostat/statistics-explained/index.php?title=Causes_of_death_statistics#Main_findings, (n.d.)
3. Saw PE, Song EW. *Protein Cell* **10**: 787-807 (2019)
4. Kiss K, Biri-Kovács B, Szabó R, Randelović I, Enyedi KN, Schlosser G, Orosz Á, Kapuvári B, Tóvári J, Mező G. *Eur J Med Chem* **176**: 105-116 (2019)
5. Chang D-K, Lin C-T, Wu C-H, Wu H-C. *PLoS One* **4**: e4171 (2009)
6. [6] Koivistoinen A, Ilonen IIK, Punakivi K, Räsänen JV, Helin H, Sihvo EI, Bergman M, Salo JA. *Clin Transl Oncol* **15**: 492-498 (2013)
7. Chi Y-H, Hsiao J-K, Lin M-H, Chang C, Lan C-H, Wu H-C. *Theranostics* **7**: 1612–1632 (2017)
8. Hiraki S, Miyai M, Seto T, Tamura T, Watanabe Y, Ozawa S, Ikeda H, Nakata Y, Ohnoshi T, Kimura I. *Hagan* **22**: 53-58 (1982)
9. Fabricant RN, De Larco JE, Todaro GJ. *Proc Natl Acad Sci USA* **74**: 565-569 (1977)
10. Giard DJ, Aaronson SA, Todaro GJ, Arnstein P, Kersey JH, Dosik H, Parks WP. *J Natl Cancer Inst* **51**: 1417-1423 (1973)

Peptide-based delivery vehicles for tumor tissue targeting

Zsuzsa Baranyai¹, Katalin Uray¹, Beáta Biri-Kovács^{1,2}, Lilla Horváth^{1,2}, Szilvia Bősze¹

¹MTA-ELTE Research Group of Peptide Chemistry, Hungarian Academy of Sciences, Eötvös L. University, Budapest, Hungary

²Eötvös Loránd University (ELTE), Faculty of Science, Institute of Chemistry, Budapest, Hungary

Introduction

Conjugating antitumor compounds with peptide-based delivery vehicles, particularly cell-penetrating or cell surface protein (receptor/adhesion protein etc.) specific peptides could enhance their cellular internalization rate and efficacy. Cell membranes and other tissue barriers hamper drug candidates' distribution and cellular uptake; therefore, most of the active compounds are of limited therapeutic value. Targeted tumor therapy is based on anticancer drugs being delivered to tumor cells by specific carrier molecules, with the result of lowering side effects of the chemotherapeutic agent. Different peptide-based delivery vehicles can be applied. (1) One of these approaches is using cell-penetrating peptides such as SynB3 or others conjugated not only to the drug molecule but to a targeting moiety. (2) Another approach is the use of peptides targeting cell surface proteins, which can be (a) ligands of cell surface receptors expressed exclusively or in highly elevated level on cancer cells, (b) or other cell surface structures, *e.g.* adhesion molecules such as nectin-1, characteristic for certain cell types (Figure 1).

SynB3 peptide (RRLSYSRRRF) is a cell-penetrating peptide that is reported to be able to cross the blood-brain barrier with high efficiency.¹⁻³ It is a derivative of a natural antimicrobial peptide called protegrin-1. The transport mechanism of SynB3 has been identified as temperature and energy-dependent adsorptive-mediated transcytosis. It is also suggested that SynB3 is sequestered within endocytotic vesicles and might be degraded within lysosomal compartments.⁴

Tuftsins are naturally occurring tetrapeptides produced by enzymatic cleavage from immunoglobulin G. Tuftsins have immunostimulatory effect and antitumor activity through the activation of immunologic effector cells. Moreover, tuftsins can bind to the neuropilin-1 receptor (NRP-1) and can be transported by the CendR pathway, which is an endocytotic/exocytotic transport.⁵ NRP-1 is upregulated in angiogenic tumor blood vessels and in tumor cells and its ligands often have CendR motif (R/KXXR/K, C-end rule) with the ability of tumor and tissue penetration through the CendR pathway.^{6,7} A tuftsins analogue with the sequence of TKPPR possesses the CendR motif and has a high affinity to NRP-1.

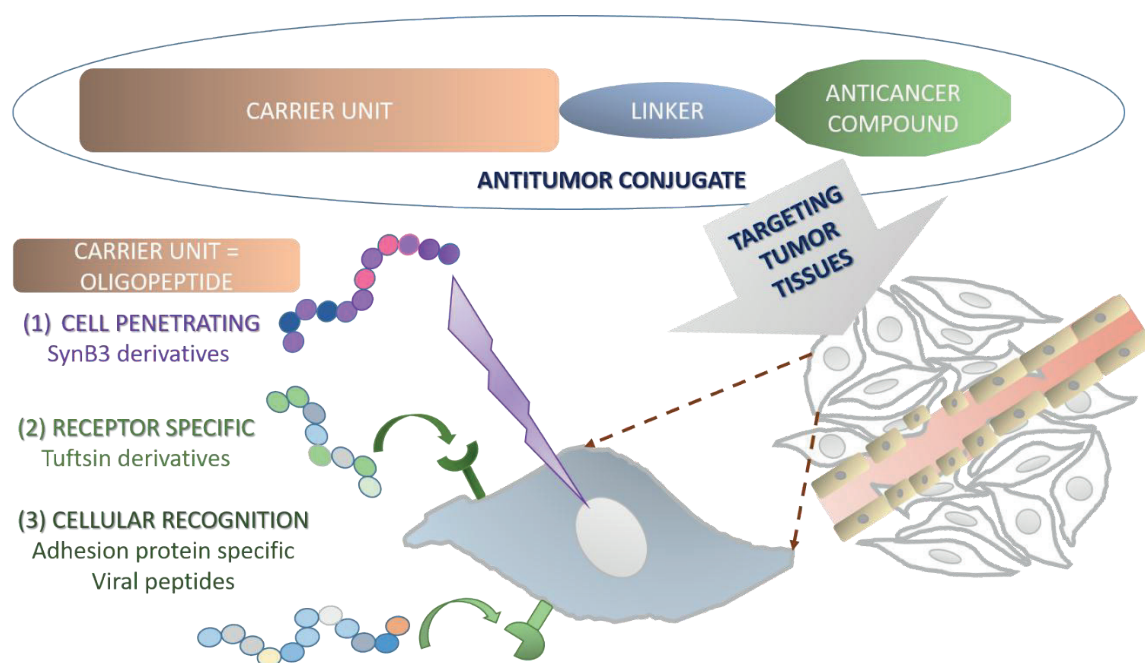


Figure 1. Targeting tumor tissue with antitumor conjugates containing peptide-based carriers bearing different features as (1) cell-penetrating, (2) tumor cell receptor-specific and (3) adhesion protein-specific peptides.

Herpes simplex viruses (HSV-1 and HSV-2 of *Alphaherpesvirinae*) show unique entry mechanism into the host cells using their gD envelop glycoprotein as well as gB, gC and gH/gL, as it is usual in case of other herpes viruses. gD glycoprotein selectively binds the nectin-1 adhesion protein on the surface of the host cells, then the glycoprotein undergoes major conformational changes resulting in the triggering of the other viral proteins to effect the fusion.⁸ According to the known 3D structure of the HSV-1 gD – nectin-1 three regions are in close contact with each other.^{9,10} We hypothesized that parts of these regions may internalize into nectin-1 bearing cells and can also be used as delivery vehicles.

Results

We have designed and synthesized different SynB3 and tuftsin derivatives and a combined peptide composed of SynB3 and tuftsin. The SynB3 peptide was decanoylated in order to modify the lipophilicity, penetration ability and membrane interaction of the original peptide. The intracellular localization of selected, fluorescently labeled peptides was investigated on HUVECs (human umbilical vein endothelial cells), these cells were used to model tumor-related vascular endothelial cells that have NRP-1 on their surface (Figure 2). The intracellular localization was also studied on U87 human glioblastoma cell line as a model cell for gliomas (Figure 2). The localization patterns of the fluorescently labeled

peptides were similar in case of the two different cell types. The SynB3 peptide (Cf-S) can be found in the cytosol, in the nucleus and in a small amount of lysosomal localization was also detected. In contrast, the tuftsin analogue Cf-T showed high lysosomal localization but no co-localization with the nucleus. The combined peptide (Cf-ST) had the intracellular distribution characteristics of the parent Cf-S and Cf-T peptides. It could be detected in both the lysosomes and in the nucleus. The decanoyl side chain containing peptide (Cf-SD) was cytotoxic on the cells, probably it has a membrane damaging effect, it can be seen in the cytosol and in the nucleus with a highly homogeneous distribution. These findings suggest that the uptake of the cell-penetrating Cf-S peptide is a complex process; probably direct penetration and vesicular transport are also present. As expected, the tuftsin analogue mainly can enter the cells by receptor-mediated endocytosis. The combined peptide follows both internalization mechanisms of its parent peptides. Modification of a cationic cell-penetrating peptide with a hydrophobic fatty acid chain leads to higher cellular uptake and at the same time it has cytotoxic effect probably due to its highly amphiphilic characteristic.

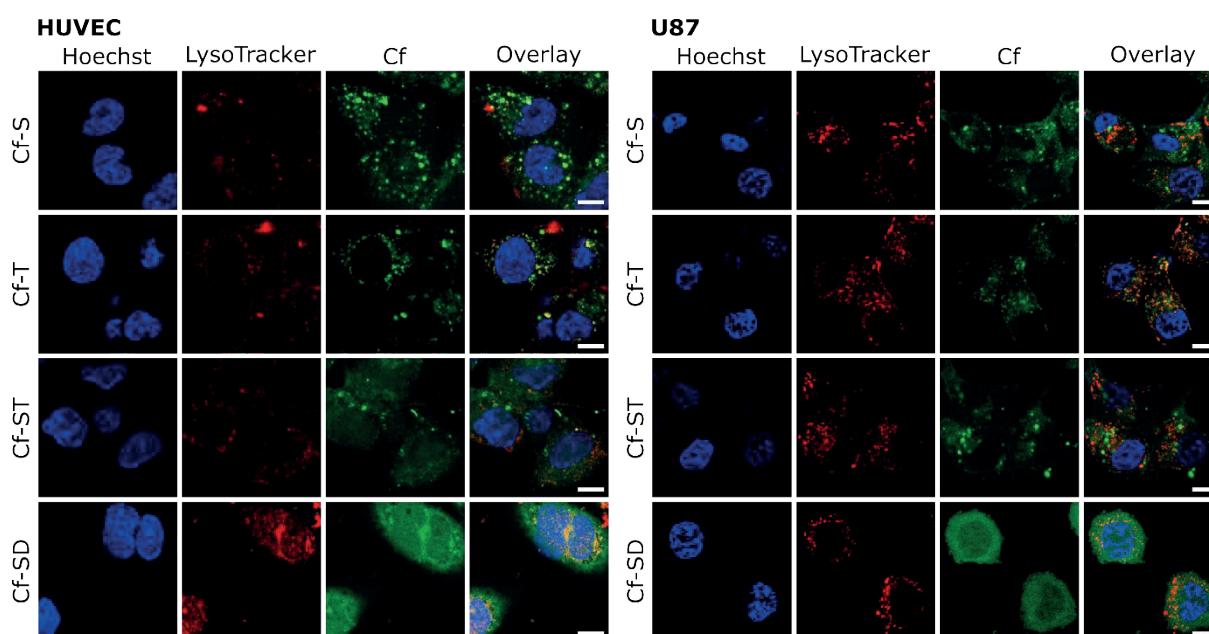


Figure 2. Localization of Cf-peptides in HUVEC and U87 cells by confocal microscopy. Nuclei were stained with Hoechst 33342 (blue), lysosomes were stained with LysoTracker Deep Red (red), cells were incubated with Cf-peptides (green, 25 μ M, 30 min except for Cf-SD where 12.5 μ M was used). Scale bar represents 10 μ m.

Based on the known 3D structure of the HSV1 gD – nectin-1 complex (PDB ID: 3U82)^{9,10}, we have selected three regions of gD making contact with nectin-1 (Figure 3A), and carboxyfluorescein labeled overlapping peptides were designed and synthesized representing these regions. The cellular internalization of these peptides into SH-SY5Y

neuroblastoma cells (as a model of neuroblastomas) has been determined by flow cytometry and is depicted in Figure 3B for representative peptides. Region II peptides showed negligible internalization. Some Region I peptides showed cellular entry at higher concentrations, but Cf-HSV 228-247 ($^{228}\text{QRTVAVYSLKIAGWHGKPAP}^{247}$) peptide showed the most efficient cellular entry, with Cf-HSV-219-238 ($^{219}\text{NleLPRFIPENQRTVAVYSLKI}^{238}$ where *Nle* represents norleucine substituting the native methionine) also showing significant entry in lower (10 μM) concentration. Certain C- and N-terminal truncation of 228-247 and the substitution of Lys²³⁷ Arg and Trp²⁴¹ Phe were well tolerated.¹¹ The propensity of the peptides to adopt helical conformation in the lipomimetic solvent trifluoroethanol showed a strong correlation with their ability to internalize into the neuroblastoma cells.¹¹

Parallel with flow cytometry measurements, to assess qualitative information regarding the subcellular localization, internalized peptides were imaged by confocal laser scanning microscopy. Peptides with high ability to internalize (as positive and negative examples, see Cf-HSV-219-238 and Cf-HSV-236-255, respectively, in Figure 3C) could be imaged in the cytosol and the nucleus, but there is no direct co-localization with lysosomal staining. This suggests that there is no vesicular transport involved in the uptake of the Cf-peptide.

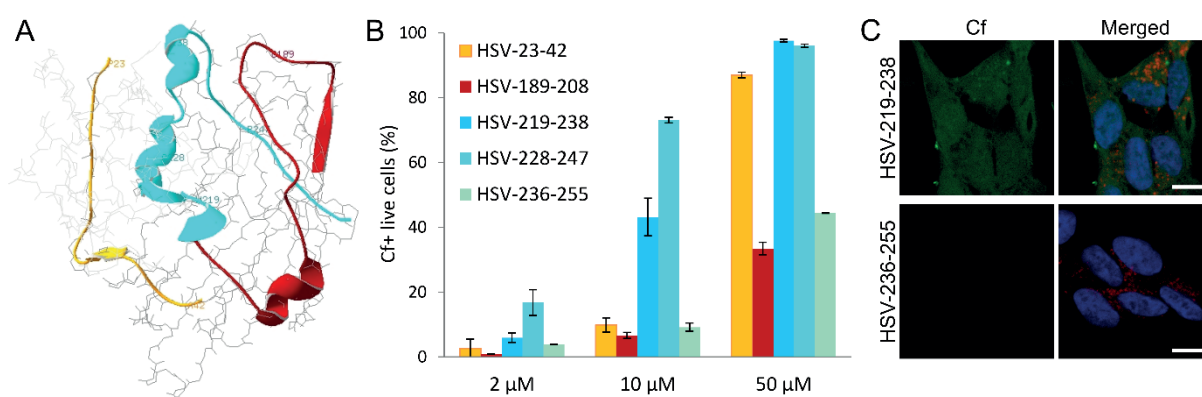


Figure 3. (A) Structure of the HSV1 gD (dark grey) –nectin-1 (light grey) complex (PDB ID: 3U82), the selected regions of the HSV1 gD (region I: yellow, region II: red, region III: cyan), (B) internalization of Cf-HSV1 gD peptides into SH-SY5Y cells at $c = 2, 10$ and $50 \mu\text{M}$, percentage of Cf-positive live cells, (C) internalization of Cf-HSV1 gD peptides visualized by confocal microscopy (green), nuclei and lysosomes are stained with Hoechst 33342 (blue) and LysoTracker (red), respectively, scale bar represents $10 \mu\text{m}$.

Conclusion

In the framework of grant NVKP_16-1-2016-0036 we have identified potential new carrier peptides of different origin as delivery vehicles. They can improve the cellular uptake

of different cargoes (*i.e.*, drugs or drug candidates). These peptide carriers possess favorable internalization properties and they have different intracellular routes. The localization of the cell-penetrating type peptide was mainly cytosolic, while that of the receptor-specific tuftsin carrier was rather lysosomal. The viral carriers after internalization displayed ubiquitous distribution in the cytosol and in the nucleus as well.

Acknowledgements

These studies were also supported by ELTE Thematic Excellence Programme 2020 (National Research, Development and Innovation Office: TKP2020-IKA-05, NKFIH-1157-8/2019-DT) and by grant VEKOP-2.3.3-15-2017-00020 from the European Union and the State of Hungary, co-financed by the European Regional Development Fund.

References

1. Rousselle C, Clair P, Lefauconnier JM, Kaczorek M, Scherrmann JM, Tamsamani J. *Mol Pharmacol* **57**: 679-686 (2000)
2. Stalmans S, Bracke N, Wynendaele E, Gevaert B, Peremans K, Burvenich C, Polis I, De Spiegeleer B. *PLoS One* **10**: e0139652 (2015)
3. Oller-Salvia B, Sanchez-Navarro M, Giralt E, Teixido M. *Chem Soc Rev* **45**: 4690-4707 (2016)
4. Drin G, Rousselle C, Scherrmann JM, Rees AR, Tamsamani J. *AAPS PharmSci* **4**: E26 (2002)
5. Nissen JC, Selwood DL, Tsirka SE. *J Neurochem* **127**: 394-402 (2013)
6. Leng Q, Woodle, MC, Mixson AJ. *Drugs Future* **42**: 95-104 (2017)
7. Ruoslahti E. *Adv Drug Deliv Rev* **110-111**: 3-12 (2017)
8. Lazear E, Whitbeck JC, Zuo Y, Carfi A, Cohen GH, Eisenberg RJ, Krummenacher C. *Virology* **448**: 185-195 (2014)
9. Zhang N, Yan J, Lu G, Guo Z, Fan Z, Wang J, Shi Y, Qi J, Gao GF. *Nat Commun* **2**: 577 (2011)
10. Di Giovine P, Settembre EC, Bhargava AK, Luftig MA, Lou H, Cohen GH, Eisenberg RJ, Krummenacher C, Carfi A. *PLoS Pathog* **7**: e1002277 (2011)
11. Bősze Sz, Zsila F, Biri-Kovács B, Szeder B, Majer Zs, Hudecz F, Uray K. *Biomolecules* **10**: 721 (2020)

Tandem mass spectrometry of daunorubicin-containing peptide conjugates

Gitta Schlosser¹, Mohammed Al-Majidi^{1,2}, Adina Borbély¹, Lilla Pethő³, Dániel Szabó^{1,2,4}, Levente Dókus^{3,5}, Gábor Mező^{3,5}

¹MTA-ELTE Lendület Ion Mobility Mass Spectrometry Research Group, Institute of Chemistry, Eötvös L. University, Budapest, Hungary

²Hevesy György PhD School of Chemistry, Institute of Chemistry, Eötvös L. University, Budapest, Hungary

³MTA-ELTE Research Group of Peptide Chemistry, Hungarian Academy of Sciences, Eötvös L. University, Budapest, Hungary

⁴MS Proteomics Research Group, Research Centre for Natural Sciences, Hungarian Academy of Sciences, Budapest, Hungary

⁵Institute of Chemistry, Eötvös L. University, Budapest, Hungary

Introduction

Daunomycin (Dau) is an anthracycline anticancer drug, commonly used for the treatment of several types of leukemia.¹ It consists of an anthraquinone aglycon moiety and a daunosamine sugar linked to the tetracycline by an *O*-glycosidic bond. Daunorubicin is used in our laboratory for the development of anticancer peptide-drug conjugates.²⁻⁶ These constructs showed efficient antitumor activity; therefore, these are promising candidates for targeted cancer therapy. Peptide-drug conjugates have complex structures, and for this reason mass spectrometry is generally used for verification of the composition, as well as for analytical characterization. However, mass spectrometric analysis of anthracycline-containing peptide-drug conjugates is still challenging.^{7,8} Electrospray ionization (ESI) is the most widely used ionization method for peptides and proteins. This is a soft ionization technique that produces intact, singly or multiply protonated species from peptides. Besides the determination of molecular mass and verification of elemental composition, tandem mass spectrometry (MS/MS) can also be used to sequence peptides and verify modification sites. However, mass spectrometric analysis of daunomycin-containing peptide conjugates is hindered by the degradation of the compounds during electrospray ionization (ESI). Daunomycin-containing bioconjugates show significant in-source fragmentation.⁷ This process results in the spontaneous dissociation of the glycosidic bond before the high vacuum region of the mass spectrometer and leads to the appearance of conjugate fragments with sugar loss. These fragment ions are usually detected in the full scan ESI-MS mass spectra as base peaks. Therefore, the aim of our work was to investigate the mass spectrometric behavior of daunomycin-containing peptide conjugates in details. MS/MS fragmentation properties

were studied by higher-energy collision-induced dissociation (higher-energy C-trap dissociation, HCD) in energy-resolved tandem mass spectrometric experiments.

Results

Daunomycin-containing peptide conjugates were studied by HCD fragmentation using a Thermo Scientific Q Exactive Focus (Bremen, Germany) mass spectrometer equipped with a heated electrospray ionization source (HESI). MS/MS breakdown graphs were recorded to explore the energy evolution of the fragmentation pathways which lead to the appearance of conjugate ions that have lost the sugar moiety.⁸ For this study, linear peptide conjugates were selected in which a drug molecule is attached to an aminooxyacetic acid (Aoa) linker at the *N*-terminus of the peptides using oxime bond.² MS/MS spectra of various protonated peptide ions were recorded as a function of the HCD collision energy (CE) over the range from 10-100 eV.⁸ Under our experimental conditions, all studied peptide conjugates showed an intensive in-source fragmentation, resulting in the loss of the sugar moiety. Intact singly or multiply protonated molecules were also detected, however, these fragment ions appear as the most intense signals in the mass spectra.

To demonstrate the extent of the in-source fragmentation for these compounds and the facile loss of the sugar moiety, Figure 1 shows the full scan ESI-MS spectra of two different peptide conjugates using direct sample infusion. Peptides were dissolved in a solvent mixture composed of acetonitrile and water (1:1, v/v) and 0.1% acetic acid. In the case of these linear constructs, singly and multiply protonated molecules can be identified in the full scan ESI-MS spectra (Figure 1). Ion ratios of the protonated molecules depend on the molecular weight of the constructs and the sequence of the peptide.⁸ As shown in Figure 1, beside the intact protonated molecules, additional intense signals can be detected in the mass spectra. These peaks belong to fragment ions formed by the loss of the daunosamine sugar molecule (129 Da mass decrease). The glycosidic bond between the daunosamine sugar and the tetracycline aglycone moiety can be cleaved under acidic conditions during the synthesis of the conjugates as well. This side reaction results in significantly decreased biological effects. Therefore, it is crucial that the homogeneity and the structure of the synthesized compounds are verified using suitable mass spectrometric techniques.

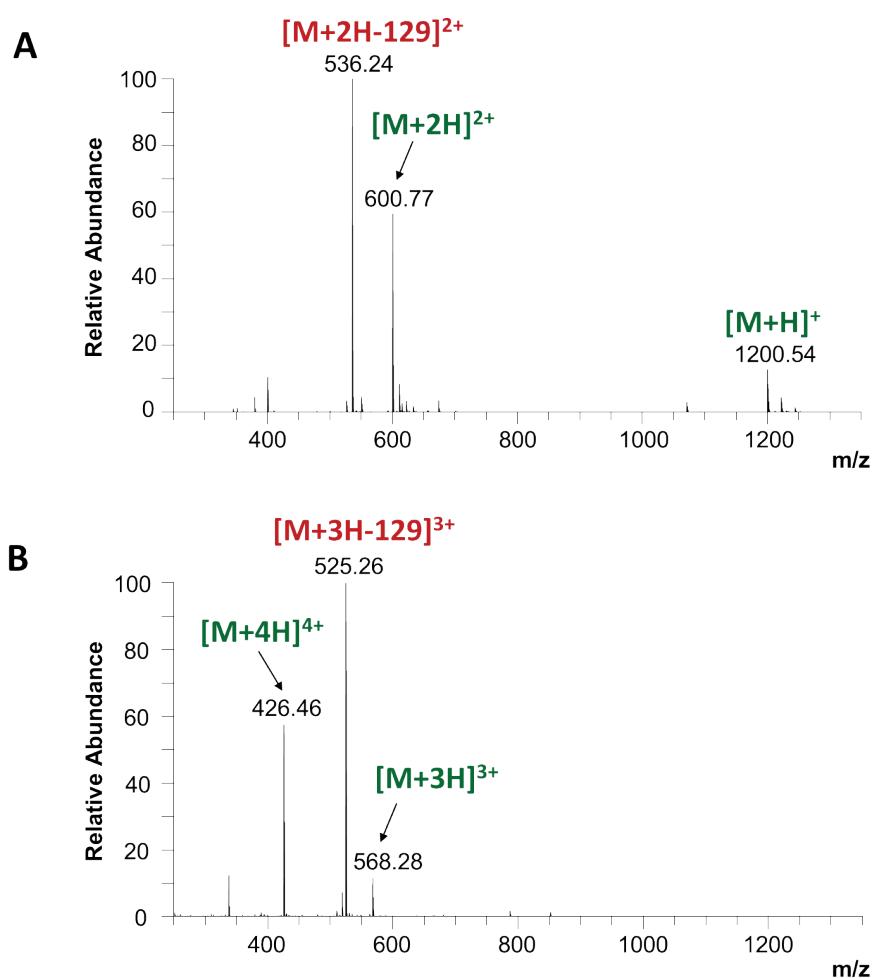


Figure 1. Full scan ESI-MS spectra of daunomycin-containing peptide conjugates. A) *Dau=Aoa-SKAAKN-OH*; B) *Dau=Aoa-GFLGKSAAKN-OH*.

To investigate the formation of fragments with sugar loss in detail, energy-dependent fragmentation experiments were performed for various peptide conjugates. In these studies, MS/MS data of different precursor charge states (+1, +2, +3) were acquired in a wide collision energy range. Survival yield curves were calculated for the precursor ions, as well as ion intensity changes for the most important fragment ions.⁸

Energy-dependent experiments showed that the HCD collision energy required to induce the fragmentation of the conjugates greatly depended on the molecular weight of the peptides as well as the charge state of the selected precursor ions. Peptide conjugates with a lower molecular weight and of a higher charge state were much more prone to fragmentation at lower collision energy values. Loss of the sugar is the leading fragmentation pathway, after which the charge can be located on the remaining peptide ion or on the sugar. In the latter case, the protonated sugar molecule can be detected at *m/z* 130, together with the charge-reduced counterpart peptide ion which has lost the protonated sugar. An example of such an MS/MS spectrum is shown in Figure 2.

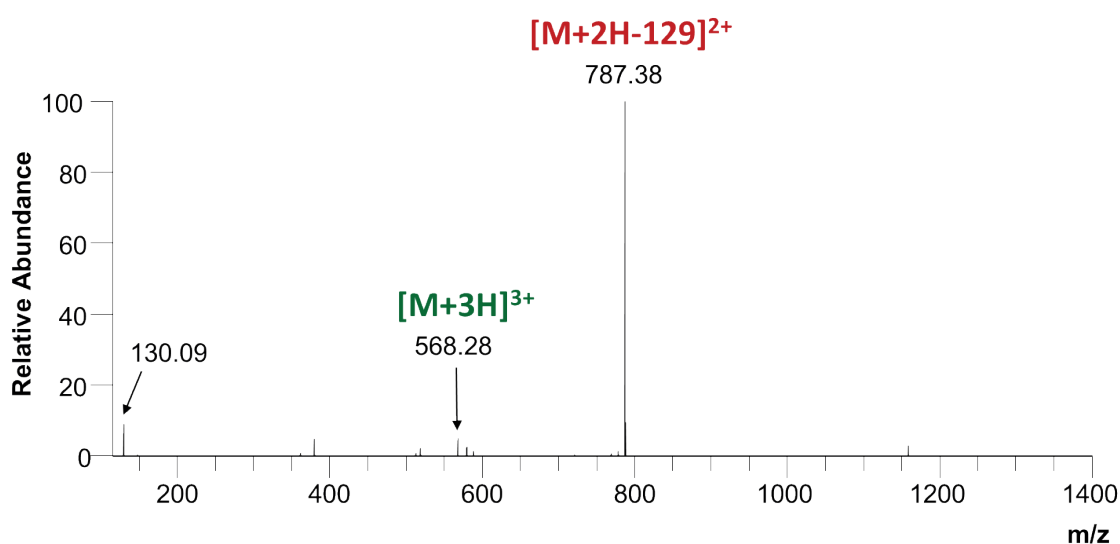


Figure 2. MS/MS spectrum of the triply protonated *Dau=Aoa-GFLGKSKAAKN-OH* (green) conjugate at 10 eV HCD collision energy. Charge-reduced fragment ion with sugar loss is detected as a base peak (red) together with the lower intensity protonated sugar.

Figure 2. demonstrates the HCD MS/MS spectrum of a triply charged peptide conjugate. This ion exhibits very low stability, and it is almost completely decomposed even under the lowest possible fragmentation energy of the instrument that was used for the experiments (10 eV). Interestingly, the fragment ion lacking the sugar moiety but bearing two charges only is dominant in this MS/MS spectrum. Our results point at an unusual instability of these multiply charged peptide conjugate ions in general. We observed that the charge separation process, in which a protonated sugar is eliminated from the ions, resulting in the appearance of the charge-reduced fragment ions is a key fragmentation pathway in the case of daunomycin-containing peptide conjugates. This process is demonstrated in Figure 3. Figure 3 shows the plots of normalized intensities of a fragment ion with sugar loss in the function of the collision energy in the case of different multiply charged precursor ions. The results demonstrate that the charge separation process, which leads to the formation of a fragment ion with a lower charge state (green line), is dominant for this compound (Figure 3.). MS/MS fragmentation of the precursor ion with charge state +3 leads to the dominant formation of the charge-reduced fragment (+2), even at very low collision energies (green line). MS/MS fragmentation of the doubly-charged precursor ion with +2 charges produces the same species at higher collision energies, and in this case other fragment ion types can also be observed (blue line).

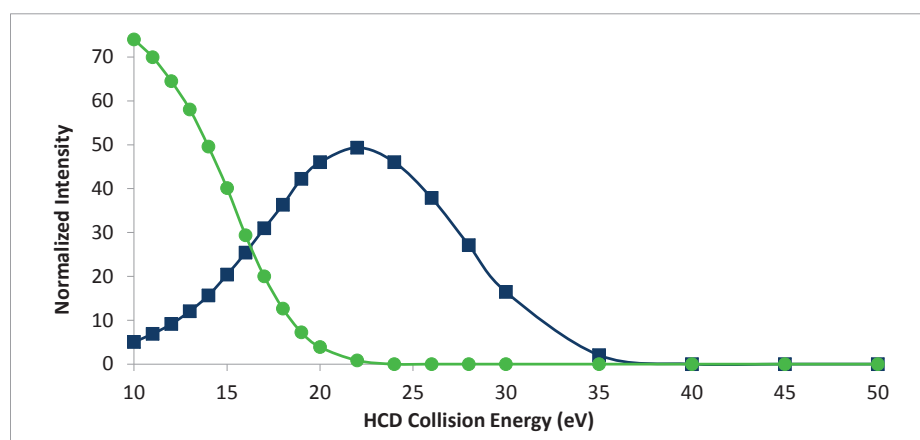


Figure 3. Intensity of the doubly charged fragment ion with sugar loss, $[M+2H-129]^{2+}$, in the function of the HCD collision energy for *Dau=Aoa-GFLGKSKAAKN-OH*. Precursor ions: doubly protonated molecule, $[M+2H]^{2+}$ (blue), and triply protonated molecule, $[M+3H]^{3+}$ (green). Intensity values are normalized to the sum of all peak intensities in the respective spectrum.

In conclusion, our research was focused on the MS/MS fragmentation of daunorubicin-containing peptide conjugates, which results predominantly in fragment ions with the loss of the daunosamine sugar. Charge separation is a key fragmentation pathway for these multiply protonated ions. This process can also occur during the ionization, and results in complex mass spectra. Tune parameters of the mass spectrometer can slightly influence the in-source fragmentation, but we suggest the use of appropriate neutral buffers to decrease the charge state of the ions and thereby to prevent the dissociation of the highly charged species. These results could be used to predict the mass spectrometric behavior of these PDCs and could help in the evaluation of the mass spectrometric results as well as in the optimization of their MS detection.

References

1. Gewirtz DA. *Biochem Pharmacol* **57**: 727–741 (1999)
2. Szabó I, Manea M, Orbán E, Csámpai A, Bosze Sz, Szabó R, Tejada M, Gaál D, Kapuvári B, Przybylski M, Hudecz F, Mező G. *Bioconjugate Chem*, **20**: 656 (2009)
3. Kapuvári B, Hegedüs R, Schulcz Á, Manea M, Tóvári J, Gacs A, Vincze B, Mező G. *Invest New Drugs* **34**: 416–423 (2016)
4. Enyedi KN, Tóth Sz, Szakács G, Mező G. *PLoS ONE* **12**: e0178632 (2017).
5. Mező G, Dókus L, Schlosser G, Lajkó E, Szász Z, Randelovich I, Biri-Kovács B, Tóvári J, Kőhidai L. *Magyar Onkológia*, **63**: 301 (2019)
6. Dókus LE, Lajkó E, Randelović I, Mező D, Schlosser G, Kőhidai L, Tóvári J, Mező G. *Pharmaceutics*, **12**: 576 (2020)
7. Pethő L, Mező G, Schlosser G. *Molecules*, **24**: 2981 (2019)
8. Al-Majidi M, Szabó D, Dókus L, Steckel A, Mező G, Schlosser G. *J Mass Spectrom* **55**: e4641 (2020)

Effect of ionization conditions in electrospray ionization mass spectrometry of daunorubicin-tuftsins peptide conjugates

Lilla Pethő¹, Gábor Mező^{1,2}, Gitta Schlosser³

¹MTA-ELTE Research Group of Peptide Chemistry, Hungarian Academy of Sciences, Eötvös L. University, Budapest, Hungary

²Institute of Chemistry, Eötvös L. University, Budapest, Hungary

³MTA-ELTE Lendület Ion Mobility Mass Spectrometry Research Group, Institute of Chemistry, Eötvös L. University, Budapest, Hungary

Introduction

Daunomycin (Dau) is an anthracycline anticancer antibiotic that can bind to the DNA in the nucleus and can inhibit the topoisomerase II α enzyme.¹ The use of daunorubicin in clinical treatments is, however, limited by cardiotoxicity and other severe side-effects. Peptide-drug conjugates (PDCs) containing daunomycin for targeted therapy have been in the focus of intensive interest since years. These constructs are promising candidates to overcome clinical drawbacks. In PDCs, the drug moiety is attached to a targeting peptide, which can bind specifically to a receptor overexpressed on tumor cells, resulting in specific antitumor effect. Tuftsins derivatives have already been successfully applied in the development of drug delivery systems.^{2,3} Tuftsins (TKPR) is a natural tetrapeptide, which is a proteolytic fragment of the IgG Fc heavy chain.⁴ In this molecule, the lysine side chain provides an optimal coupling site for conjugation of drug molecules.

Mass spectrometry is a key technique for the fast and reliable identification of the products during the chemical synthesis of PDCs. However, in the case of anthracyclines and anthracycline derivatives, it is difficult to estimate the purity of the compounds due to an unusual fragmentation during MS analysis. Mass spectra of daunomycin containing bioconjugates show significant in-source fragmentation under the commonly used electrospray ionization mass spectrometry (ESI-MS). The main fragmentation pathway is the cleavage of the glycosidic bond. Emerging number of research papers are published in the field of novel anthracycline-containing PDCs.⁵⁻⁸ However, analytical data report complex mass spectra showing a mixture of protonated molecules, adduct ions and various fragment ions, and publications lack proper assignment and discussion of the detected peaks.

Our research was focused on the analysis of daunorubicin-containing PDCs using ESI-MS and on the determination of appropriate circumstances for the characterization of these complex molecules.⁹ Novel tuftsins-based bioconjugates were synthesized (Figure 1) to

investigate the quality of the mass spectra. The influence of the structure was studied, including the i) number of drug molecules; ii) number of basic functional groups; iii) presence or absence of an enzyme-labile spacer (GFLG) between the targeting peptide and the drug molecule.

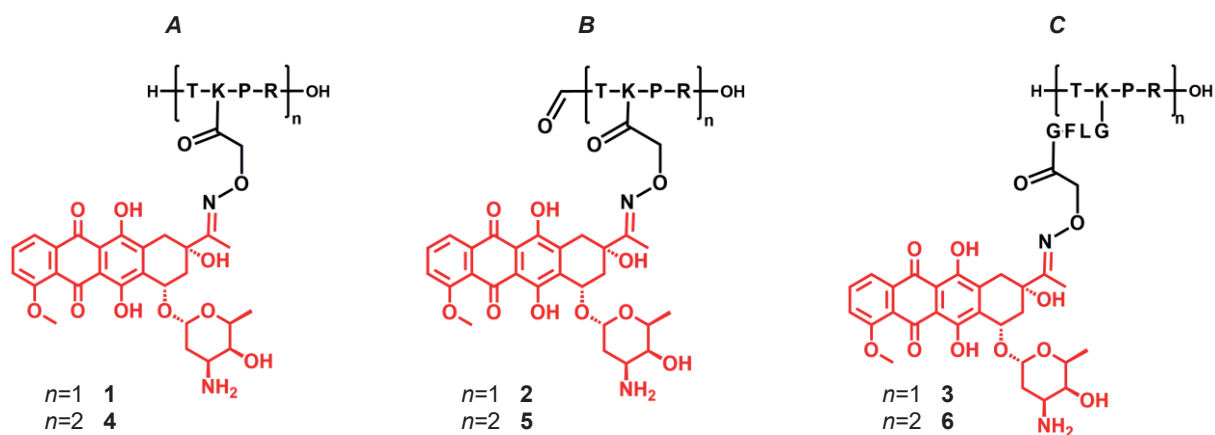


Figure 1. Schematic structure of novel tuftsin bioconjugates containing one or two daunomycin molecules with A.) free *N*-terminal amino group, B.) formylated *N*-terminus, C.) bearing a GFLG spacer.

Results

All peptides were synthesized by solid-phase methodology using Fmoc/tBu strategy. Daunomycin was conjugated to purified aminooxyacetylated peptides by oxime linkage. Tuftsin-daunorubicin bioconjugates and their dimer derivatives (containing two tuftsin units and thereby two daunomycin moieties (Figure 1) were synthesized and purified. Mass spectrometric experiments were performed on a Bruker Daltonics Esquire 3000+ ion trap mass spectrometer equipped with electrospray ionization source, operating with continuous sample injection.

Commonly used ESI-MS experimental conditions for peptides is based on a solvent mixture composed of acetonitrile and water containing 0.1% acetic acid or formic acid. However, the mass spectra of these PDCs showed several peaks under these conditions. Fragment ions can be identified with high intensity, while intact protonated ions have lower abundance. Especially bioconjugates containing two daunomycin molecules (**4**, **5**, **6**) produced highly complex mass spectra showing a combination of sugar losses. We observed that a free *N*-terminal amino group facilitates the cleavage of the glycosidic bond, while blocking the *N*-terminal by formylation (**2**, **5**) results in lower fragmentation. Results indicate that incorporation of a neutral spacer (GFLG) between the peptide and the drug moiety (**3**, **6**), hereby moving the sugar moiety away from the basic tuftsin peptide backbone, slightly decreases the in-source fragmentation of the compounds.

We investigated the effect of the ion source tune parameters and the composition of the solvents used for the ionization of the samples as well. The results showed that significant reduction of the capillary exit potential (to 5 V) could slightly lower the fragmentation and increase the intensity of the intact protonated molecules. Other ion source parameters did not affect the ion ratios significantly.

Furthermore, we studied the effect of solvent mixtures while keeping the reduced capillary exit potential. Besides the commonly used acidic solvent, we used, for example, acetonitrile-water (50:50%, v/v) mixture and solutions containing ammonium bicarbonate (NH_4HCO_3 , 50 mM, pH 7.8) or ammonium acetate buffers (NH_4OAc , 50 mM, pH 6.7) and acetonitrile (50:50%, v/v). These neutral buffers can reduce the charge state of the ions. Our results show that the decrease in the number of charges on the protonated molecules formed during ESI ionization reduced the spontaneous dissociation of the glycosidic bond significantly.

The non-acidic acetonitrile-water mixture could decrease the amount of the fragment ions in case of conjugates **1**, **2**, **3** and **5**, while it was not effective for compounds **4** and **6**. However, in the case of the volatile buffers, intact protonated molecules of all bioconjugates were dominant. NH_4OAc buffer provided clearer ESI-MS spectra and over 95% intact protonated molecules (Figure 2). The best quality spectra could be achieved with a combination of low capillary exit potential (5 V) and NH_4OAc buffer (50 mM, pH 6.7).

Our results show that a higher number of positively charged functional groups in the PDC molecule indicated higher in-source fragmentation. Consequently, structural modifications, such as formylation can influence (enhance or decrease) the gas-phase stability of the molecules. We also found that enhanced distance between the sugar moiety and the positively charged peptide backbone decreases the fragmentation. The spontaneous dissociation of the glycosidic bond is facilitated by the highly charged peptide chain, therefore, shifting the charge states to lower charges can help to keep ions intact. Hence, application of neutral or slightly basic volatile buffers can significantly reduce the fragmentation of the analyte. In our experiments, the most appropriate buffer for suppressed fragmentation was ammonium acetate.

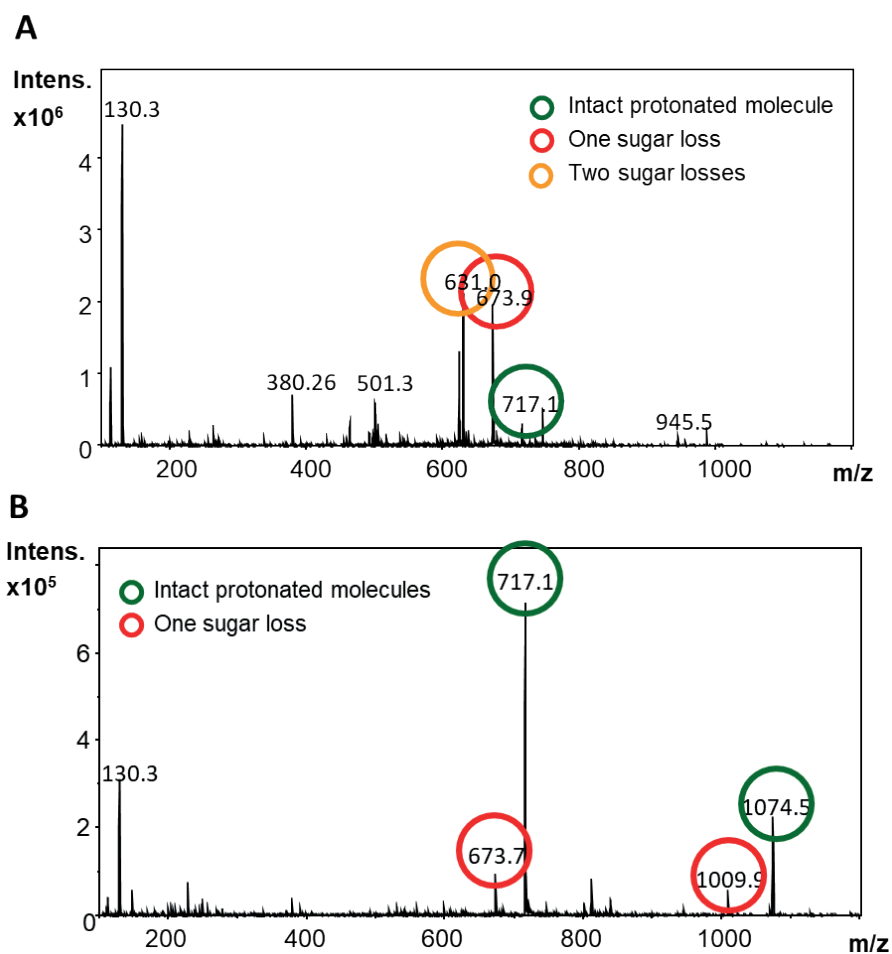


Figure 2. ESI-MS spectra of conjugate 4 in solvent mixtures containing *A.*) 0.1% acetic acid and *B.*) 50 mM NH_4OAc buffer, and acetonitrile (50:50, v/v). Capillary exit potential was set to 5 V in the case of spectrum *B.*

In conclusion, not only the settings of the mass spectrometer but also the structure of the daunorubicin-tuftsins conjugates had a high impact on the ESI-MS spectra. Conditions suggested here can be useful in the analysis of anthracycline-containing bioconjugates, to obtain mass spectra comprising intact protonated molecules.

References

1. Gewirtz DA. *Biochem Pharmacol* **57**: 727–741 (1999)
2. Mező G, Láng O, Jakab A, Bai KB, Szabó I, Schlosser G, Láng J, Köhidai L, Hudecz F. *Peptide Sci* **12**: 328–336 (2006)
3. Bai KB, Láng O, Orbán E, Szabó R, Köhidai L, Hudecz F, Mező G. *Bioconjug Chem* **19**: 2260–2269 (2008)
4. Najjar VA, Nishioka K. *Nature* **228**: 672–673 (1970)
5. Ryppa C, Mann-Steinberg H, Fichtner I, Weber H, Satchi-Fainaro R, Biniossek ML, Kratz F. *Bioconjug Chem* **19**: 1414–1422 (2008)

6. Schreier VN, Pethő L, Orbán E, Marquardt A, Petre BA, Mező G, Manea M. *PLoS ONE* **9**: e94041 (2014)
7. Mező G, Szabó I, Kertész I, Hegedüs R, Orbán E, Leurs U, Bősze S, Halmos G, Manea M. *J Pept Sci* **17**: 39–46 (2011)
8. Krauss U, Kratz F, Beck-Sickinger AG. *J Mol Recognit* **16**: 280–287 (2003)
9. Pethő L, Mező G, Schlosser G. *Molecules* **24**: 2981 (2019)

Synthesis of drug-peptide conjugates using bifunctional spacers

Lea Várhegyi¹, Lilla Pethő^{1,2}, Kata Nóra Enyedi¹

¹Institute of Chemistry, Eötvös L. University, Budapest, Hungary

²MTA-ELTE Research Group of Peptide Chemistry, Hungarian Academy of Sciences, Eötvös L. University, Budapest, Hungary

Introduction

The main challenge of the drug delivery concept in cancer therapy is to transport a sufficient amount of the cytotoxic agent to the diseased site(s) while minimizing their exposure to healthy tissues. To achieve this, one main strategy is the application of peptide – drug conjugates (PDCs).¹

PDCs are nowadays an emerging class of prodrugs, formed through the covalent attachment of a specific peptide sequence to a drug *via* linker(s). PDCs usually consist of a

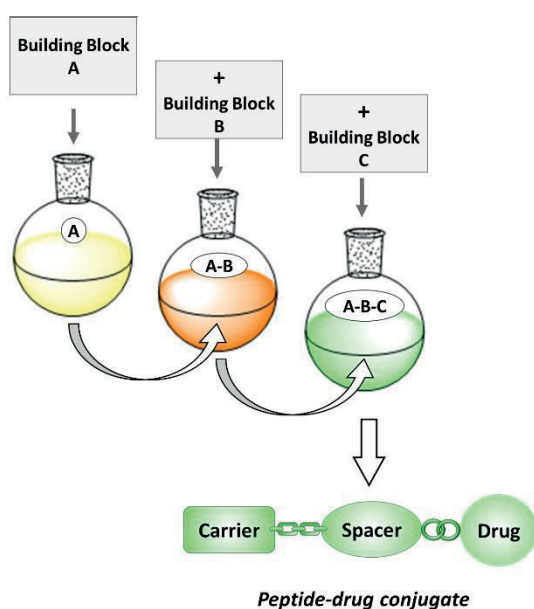


Figure 1. Sequential one-pot reaction

tumor homing peptide that will be most appropriate for the type of cancer needed.² In addition, peptide sequences can be selected according to the required physicochemical properties or the characteristic groups necessary for the conjugation with the therapeutic payload. It follows, however, that the different conjugation methods and functional groups used to form PDCs from the three building blocks (carrier, linker and drug), needs to be compatible with each other.

To this end, we set up a model system in which the side-by-side applicability of the most commonly used conjugation reactions can be investigated. Our main focus was to develop so-

called “sequential one-pot” combinations, as this would be the most efficient way to build PDC libraries (Figure 1).

Our model carrier was GnRH-III (<EHWSHDWKPG-NH₂), a well-known tumor homing peptide.³ GnRH-III also gave us the advantage of examining the conjugation steps in the presence of delicate amino acids, as the peptide contains oxidation and alkylation sensitive histidine and tryptophan. For linker, the GFLG tetrapeptide has been chosen, as a widely used Cathepsin B sensitive spacer,⁴ which is also poorly water soluble, thus, the problem of sparingly soluble sequences also had to be addressed. Two clinically used chemotherapeutic drugs were selected as our model drug molecules: daunomycin (Dau) and methotrexate (Mtx) as they allow a different kind of conjugation.^{5,6}

For the selection of the conjugation techniques, three aspects were considered: it must occur frequently in the literature, must be compatible with each other and should be easily performed with minimal laboratory background. Thus, the oxime-ligation, thioether- and peptide-bond formations were chosen.

Results

Two different derivatives of GnRH-III were prepared, modified on ε-amino group of ³Lys with chloroacetic acid or acetylcysteine (Figure 2, *C1* and *C2*), which allowed the formation of thioether bond with the spacers containing maleimidohexanoic acid (Mal-Hx) (*S5*, *S7*), chloroacetyl (Cl-Ac) group (*S4*, *S6*) or cysteine (*S1*, *S2*, *S3*), accordingly.

The conjugation to the drug molecules could happen *via* amide (*Mtx* and *Dau1*) or oxime bond formation (*Dau2*), therefore the spacer sequences contained a free amine (³Lys side chain: *S4*, *S5*) or succinic acid (Suc) (*S1*) or aminooxyacetic acid (Aoa) (*S4*, *S5*, *S6*, *S7*). This palette of compounds allowed us to study and optimize the sequential one-pot formation of PDCs not only in the order of carrier + spacer → carrier-spacer+ drug, but also the other way around, spacer + drug → spacer-drug + carrier. As the aminooxy-functional group is sensitive to acylation, the combination of oxime and amide conjugation methods were not studied. Therefore, two other combinations were investigated in depth.

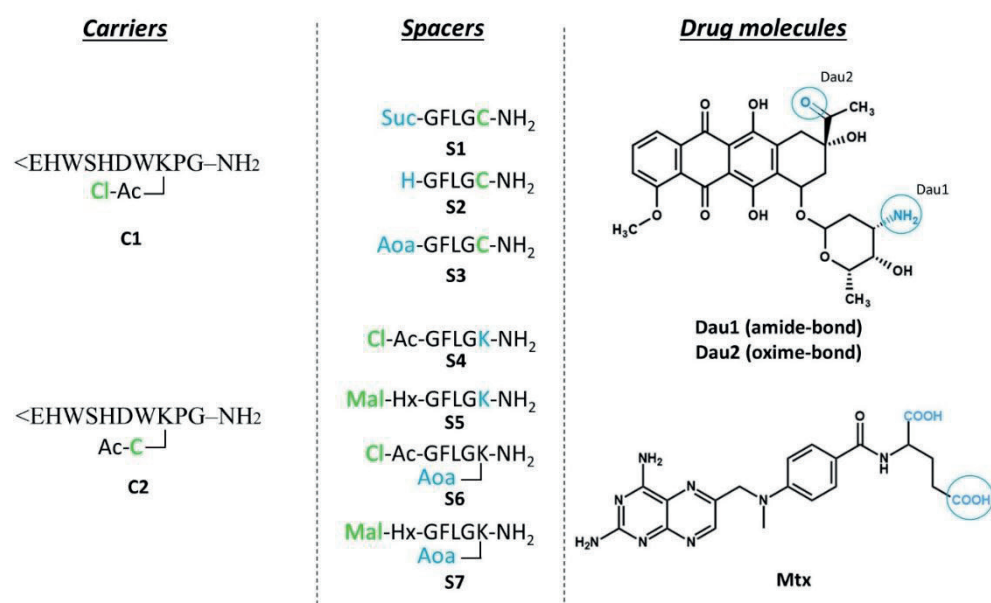


Figure 2. Prepared carrier and spacer molecules and the conjugated chemotherapeutic drugs

Compatibility of amide- and thioether-bond

The peptide-bond formation between the drugs and spacers were carried out in solution, in the presence of PyBOP and DIPEA. Under this alkaline conditions maleimido and chloroacetyl groups, and also daunomycin quickly degraded, therefore it was concluded that *S1-Dau1*, *S4-Mtx*, *S5-Mtx* cannot be synthesised.

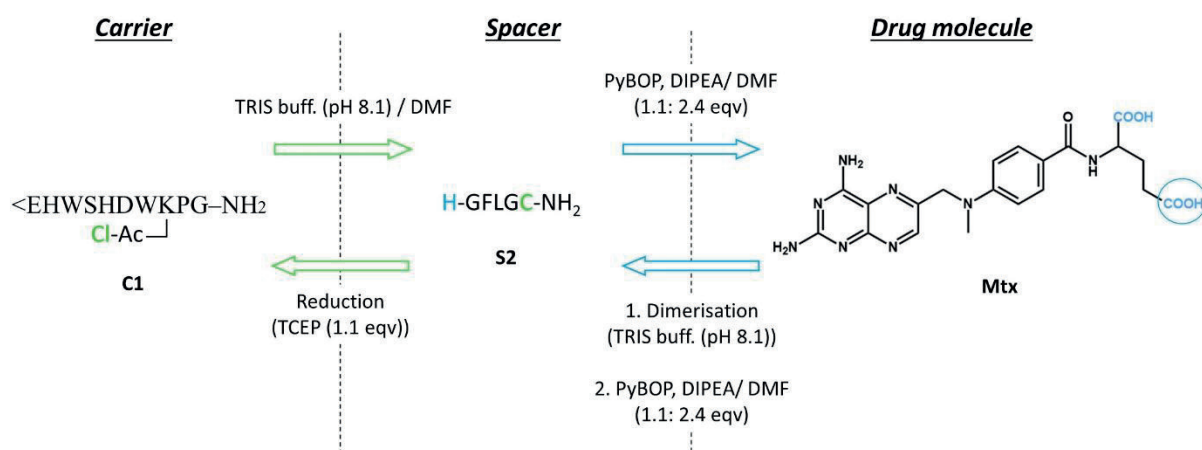


Figure 3. Sequential amide and thioether bond formation

Nevertheless, the two conjugation types could be compatible with each other, even as the first step is the amide bond formation (*Figure 3*). As *S*-acylation is a more reactive pathway compared to *N*-acylation the free thiol group of the *S2* spacer had to be masked

temporarily by dimerization through a disulfide bridge. This was followed by the peptide bond formation with Mtx (*Mtx-S2-S2-Mtx*) and after the reduction of the disulfide bridge with TCEP, the thioether bonded product could be readily synthesised (*C1-S2-Mtx*). Our experimental results also confirmed that a less complicated pathway is when the first conjugation step is the thioether formation, followed by the peptide bond (*C1+S2* → *C1-S2* → *C1-S2+Mtx* → *C1-S2-Mtx*; Figure 3).

Compatibility of oxime and thioether bond

It can be said that the two types of conjugation (oxime and thioether) methods are compatible, unfortunately, as it turned out, our model system was not entirely suitable to investigate it in depth. Thioether formation requires alkaline media and the reaction usually takes 16 h to be totally completed.

Under these conditions, as it was earlier already mentioned, daunomycin quickly decomposes in minutes. Therefore, in our case, sequential one-pot reactions could be carried out only if the first conjugation step is the thioether-bond formation. Under such circumstances **C1-S3-Dau2**, **C2-S6-Dau2** and **C2-S7-Dau2** were effortlessly synthesised in aqueous media only by setting the pH (Figure 4).

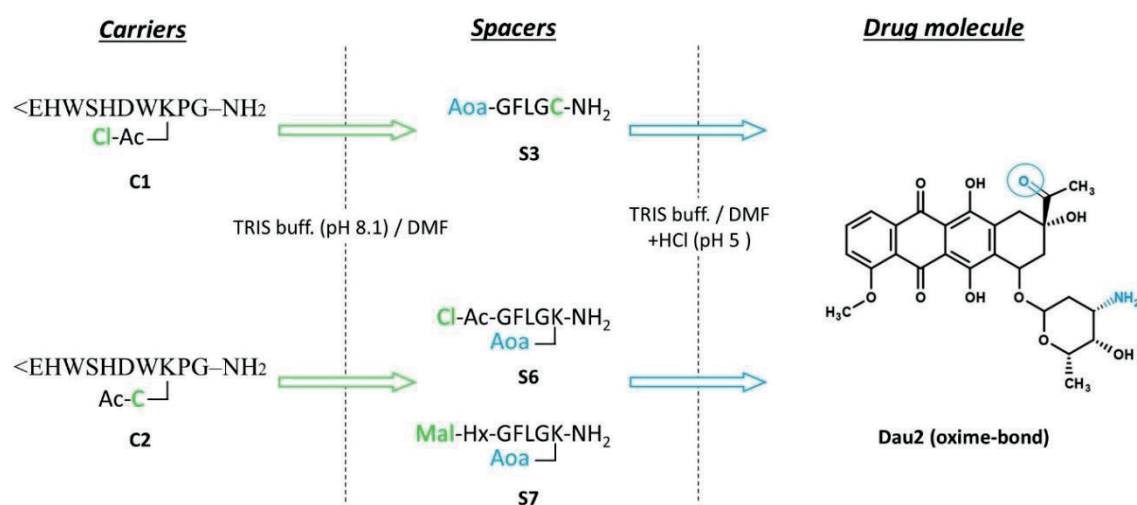


Figure 4. Sequential oxime and thioether bond formation

In summary, our investigation showed that oxime-thioether and amide-thioether conjugations can be used effectively and easily in sequential order for the development of PDC libraries. Further plans include the investigation of other conjugation methods (*e.g.* click-reaction) and their compatibility with each other.

References

1. Vrettos E, Mező G, Tzakos A G. *Beilstein J Org Chem* **14**: 930-954 (2018)
2. Wang Y, Andrew G Cheetham A G, Angacian G, Hao Su , Xie L, Cui H. *Adv Drug Deliv Rev* **111**: 112-126 (2017)
3. Leurs U, Lajkó E, Mező G, Orbán E, Öhlschläger P, Marquardt A, Kőhidai L, Manea M. *Eur J Med Chem* **52**: 173-183 (2012)
4. Poreba M. *The FEBS Journal* **287**: 1936-1969 (2020)
5. Chaires J B. *Biophys Chem* **35**: 191-202 (1990)
6. Puig L. *Actas Dermosifiliogr* **105**: 583-589 (2014)

***In vitro* anti-tumor effect of cinchona-chalcone hybrids with 1,4- or 1,5-disubstituted 1,2,3-triazole linker**

Rita Oláh-Szabó¹, Tamás Jernei², Ildikó Szabó¹, Gábor Mező^{1,2}, Antal Csámpai²

¹MTA-ELTE Research Group of Peptide Chemistry, Hungarian Academy of Sciences, Eötvös L. University, Budapest, Hungary

²Institute of Chemistry, Eötvös L. University, Budapest, Hungary

Introduction

Combining different compounds with antitumor activity can enhance the effect of the hybrid compounds on tumor cells.

Quinine derivatives have several advantageous biological effects: it has been known for a long time as antimalarial agent.¹ Direct antitumor activity of these molecules was also described^{2,3} and they can be applied in combination therapy as well.⁴

Former studies proved the cytotoxic effect of cinchona hybrids on several tumor cell lines like PANC-1 human pancreatic carcinoma, COLO-205 human colon adenocarcinoma, A2058 human melanoma and EBC-1 lung carcinoma.^{5,6} Ferrocene–cinchona hybrids with triazolyl-chalcone linkers showed a marked anti-tumor effect on HT-29 human colon carcinoma and HepG2 human hepatocellular carcinoma⁶ and MCF-7 human breast cancer, SH-SY5Y human neuroblastoma and HL-60 human leukemia cell lines³ and they enhanced the production of reactive oxygen species, inhibited autophagy and increased paclitaxel sensitivity in MDR tumor cell lines as well.⁷

Chalcones are also a well-known group of molecules inducing antitumor activity. Antiproliferative effect elicited by isoliquiritigenin (4,2,4'-trihydroxychalcone) was reported on HeLa and MCF-7 human breast cancer cell lines, whereas other chalcones caused apoptosis *via* inhibition of p53 suppressor protein on tumor cells.⁸ In our research group, the cytotoxicity of 1,3-diphenylchalcone ($IC_{50} = 10.19 \mu\text{M}$) and 1-(*p*-methoxyphenyl)-3-phenyl chalcone ($IC_{50} = 12.43 \mu\text{M}$) was described on HL-60 human leukemia cell line.⁹ In the present study we investigated the *in vitro* cytostatic effect of novel cinchona-chalcone hybrids with 1,4- or 1,5-disubstituted 1,2,3-triazole linker (Figure 1).

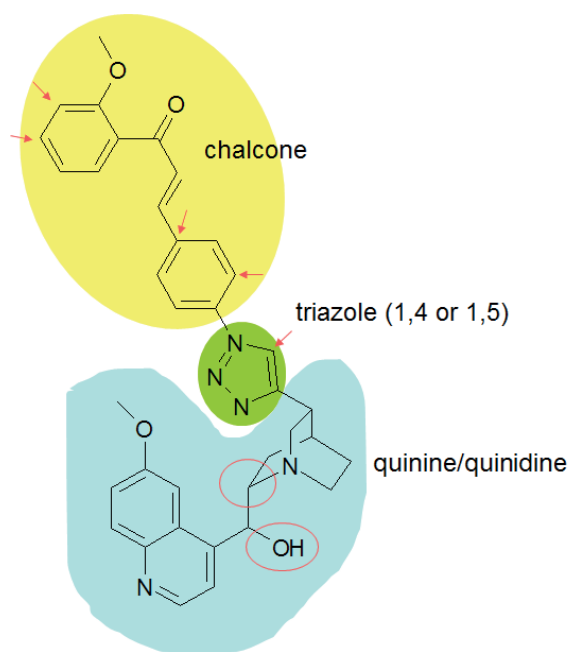


Figure 1. Structure of cinchona-chalcone hybrid molecules with a 1,2,3-triazole linker

Results

Synthesis of the compounds was performed by copper(I)- and ruthenium(II)-catalyzed click reactions according to Károlyi *et al.*³, in some cases modified by Jernei *et al.*⁵

In vitro cytostatic activity of the compounds were tested by MTT assay¹⁰ on tumor cell lines of different origin, including A2058 human melanoma, A431 human epithelial skin carcinoma, HT-29 human colon carcinoma, MDA-MB-231 and MCF-7 human breast carcinoma and HepG2 human hepatocellular carcinoma cell lines. Cells were treated with the compounds at 0.4-50 μM or 0.2-25 μM concentrations. Highest concentration for the treatment was determined with a preliminary solubility probe in serum-free medium (RPMI-1640 or DMEM). Treatment was taken place overnight, then compounds were removed, cells were washed and cultured for further 72 hours. The cytostatic effect was calculated with the following formula:

$$\text{Cytostasis [\%]} = (1 - A_{\text{treated}}/A_{\text{control}}) \times 100$$

IC_{50} values were calculated from sigmoidal curves fitted on the cytostasis data using Origin2018 software.

Results indicate that most of the cinchona-chalcone hybrids studied proved to be effective anti-tumor agents under the conditions described above. Overall, MCF-7 human breast cancer cell line proved to be the most sensitive to the cinchona-chalcone hybrids (IC_{50} values were $< 3 \mu\text{M}$, except for one compound), but in case of some hybrids, lower IC_{50}

values could be obtained on HT-29 human colon carcinoma and A2058 human melanoma cells. The most effective compounds were JT-226 with a quinine skeleton, 1,4-disubstituted triazole linker carrying a 3,4,5-trimethoxybenzoyl substituent in the chalcone moiety ($IC_{50} = 0.57 \pm 0.23 \mu\text{M}$ on HT-29 cells), and JT-227 with a quinidine skeleton, and also a 1,4-disubstituted triazole linker and a 3,4,5-trimethoxybenzoyl group in the chalcone moiety ($IC_{50} = 0.52 \pm 0.06 \mu\text{M}$ on A2058 cells (Table 1., Figure 1).

Table 1. *In vitro* cytostatic effect of cinchona-chalcone hybrids JT-181–JT-227 on HT-29, HepG2, A2058, MDA_MB_231 and MCF-7 tumor cell lines

code	HT-29		HepG2		A2058		MDA-MB-231		MCF-7	
	IC_{50} [μM]	\pm SD								
JT-181	4.07	0.77	8.92	0.08	8.15	0.34	5.70	4.70	2.9	0.50
JT-182	3.28	0.48	8.03	0.38	2.51	0.43	6.80	5.10	3.1	0.60
JT-218	9.25	0.48	12.25	1.10	3.35	0.08	11.15	0.40	2.3	0.10
JT-219	8.99	1.08	34.18	0.00	3.36	0.26	6.05	2.10	3.1	0.60
JT-220	7.92	0.28	10.37	0.38	3.67	0.46	12.40	5.10	8.4	0.40
JT-221	3.66	0.72	9.34	0.07	2.31	0.01	6.60	4.50	3.1	0.20
JT-222	27.40	9.50	24.25	9.00	2.59	0.06	6.56	4.20	2.6	0.60
JT-223	8.14	0.56	6.88	3.86	1.49	0.33	9.15	2.10	2.8	0.30
JT-224	2.88	0.09	6.62	0.82	2.50	0.06	2.80	0.00	1.8	0.60
JT-225	10.86	0.99	n.d.	n.d.	7.27	0.90	2.60	0.10	1.4	0.40
JT-226	0.57	0.23	0.99	0.52	1.10	0.08	2.15	0.40	1.6	0
JT-227	1.32	0.04	2.98	0.70	0.52	0.06	5.70	4.70	2.9	0.50

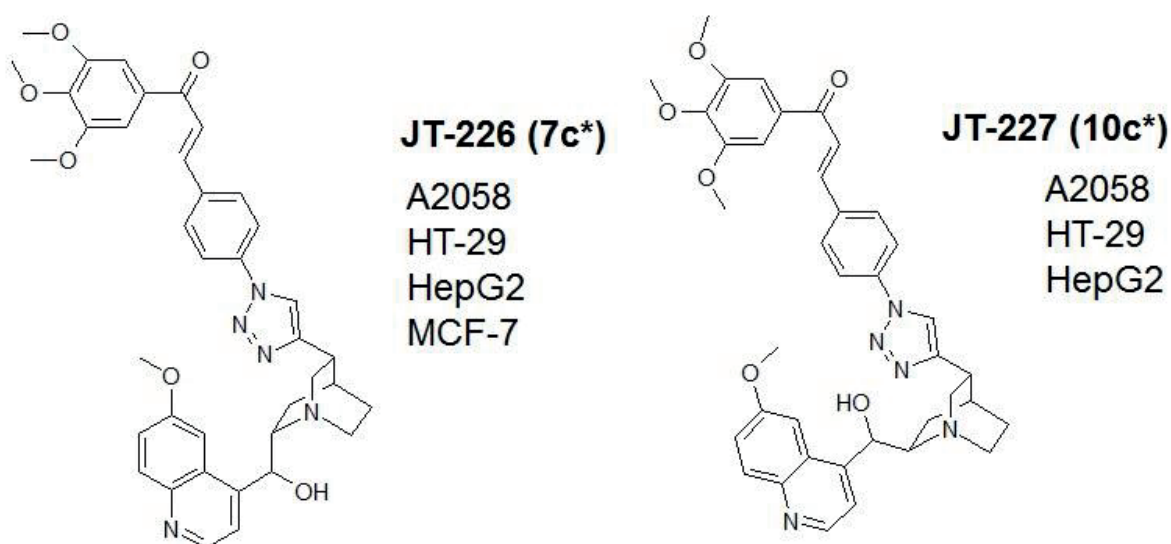


Figure 2. Structure of cinchona-chalcone hybrids elicited the most effective anti-tumor effect on HT-29 and A2058 cells (*numbering according to *Jernei et al.*⁵).

Based on these results, another set of compounds were tested on HT-29 and A2058 cells under the same conditions. We found two similarly effective compounds, with epiquinidine skeleton and 1,5-disubstituted triazole linker and 3,4,5-trimethoxybenzoyl group in the chalcone moiety (JT-382) or 3,5-dimethyl-4-hydroxybenzoyl derivative (JT-387) (Table 2)

Table 2. *In vitro* cytostatic effect of cinchona-chalcone hybrids JT-230–JT-387 on HT-29 and A2058 cell lines

code	HT-29		A2058	
	IC ₅₀ [μM]	± SD	IC ₅₀ [μM]	± SD
JT-230	10.27	2.34	9.86	0.49
JT-334/1	25.75	23.72	9.26	2.04
JT-334/2	9.71	0.17	10.04	1.51
JT-335/1	18.22	11.63	9.80	2.28
JT-335/2	>100	-	9.80	1.98
JT-354	25.24	18.37	23.11	15.36
JT-355	>100	-	52.72	10.51
JT-381	9.42	1.15	8.06	1.30
JT-382	4.48	2.59	2.78	0.06
JT-386	23.66	1.40	45.92	4.57
JT-387	3.54	0.11	4.40	0.16

Finally, a third group of hybrid compounds, four of them with quinuclidine skeleton, was also investigated on U87 human glioblastoma, A2058 human melanoma, A431 human skin carcinoma and HepG2 human hepatocarcinoma cell lines. Among these compounds, we found that JT-450 and JT-475 with 1,4-disubstituted triazole linker and 3,4,5-trimethoxybenzoyl substituent proved to be the most promising anti-tumor agents (IC₅₀ < 3 μM) on three of the four cell lines. The effect was cell dependent, A431 cells proved to be the most sensitive for these compounds (Table 3).

Table 3. *In vitro* cytostatic effect of cinchona-chalcone hybrids with quinuclidine skeleton on U87, A2058, A431 and HepG2 cell lines

code	U87		A2058		A431		HepG2	
	IC ₅₀ [μM]	±SD						
JT-446	11.51	-	9.19	-	11.00	-	14.11	-
JT-450	12.94	0.30	3.13	0.54	2.79	0.27	2.97	0.30
JT-471	9.56	-	7.26	-	4.41	-	8.54	-
JT-475	2.76	0.11	10.45	1.16	2.32	0.16	2.65	0.08
JT-521	14.74	0.18	3.14	0.45	5.33	0.35	11.78	0.65

In conclusion, we can state, that cinchona-chalcone hybrid compounds elicited an effective antitumor effect. The efficacy of these compounds was influenced by the skeleton as well as the position of the substituents on the linker, or the substituent in the chalcone moiety. Some hybrids showed outstanding effect with lower than micromolar IC₅₀ values; these molecules can be promising candidates for drug development for further clinical application.

References

1. Kacprzak K, Ruszkowski P, Valentini L, Huczyński A, Steverding D. *Biol Drug Des* **92**: 1778-1787 (2018)
2. Qi Y, Zhao X, Chen J, Pradipta AR, Wei J, Ruan H, Zhou L, Hsung R P, Tanaka K. *Biosci Biotechnol Biochem* **83**: 1011-1026 (2019)
3. Károlyi BI, Bősze S, Orbán E, Sohár P, Drahos L, Gál E, Csámpai A. *Molecules* **17**: 2316-2329 (2012)
4. Tsuruo T, Iida H, Kitatani Y, Yokota K, Tsukagoshi S, Sakurai Y. *Cancer Res* **44**: 4303-4307 (1984)
5. Jernei T, Duró C, Dembo A, Lajkó E, Takács A, Köhidai L, Schlosser G, Csámpai A. *Molecules* **24**: 4077 (2019)
6. Kocsis L, Szabó I, Bősze S, Jernei T, Hudecz F, Csámpai A. *Bioorg Med Chem Lett* **26**: 946-949. (2016)
7. Podolski-Renić A, Bősze S, Dinić J, Kocsis L, Hudecz F, Csámpai A, Pešić M. *Metallomics* **9**: 1132-1141 (2017)
8. Stoll R, Renner C, Hansen S, Palme S, Klein C, Belling A, Zeslawski W, Kamionka M, Rehm T, Mühlhahn P, Schumacher R, Hesse F, Kaluza B, Voelter W, Engh R A, Holak T A. *Biochemistry* **40**: 336-344 (2001)
9. Zsoldos-Mády V, Csámpai A, Szabó R, Mészáros-Alapi E, Pásztor J, Hudecz F, Sohár P. *ChemMedChem* **1**: 1119-1125 (2006)
10. Mosmann T. *J Immunol Methods* **65**: 55-63 (1983)

***In vitro* antitumor effect and structure–activity relationships of ferrocene-containing imipridone hybrids**

Rita Oláh-Szabó¹, Péter Bárány², Imre Kovács², Tamás Czuczi², Szilvia Bősze¹,
Antal Csámpai²

¹MTA-ELTE Research Group of Peptide Chemistry, Hungarian Academy of Sciences, Eötvös
L. University, Budapest, Hungary

²Institute of Chemistry, Eötvös L. University, Budapest, Hungary

Introduction

ONC201 (TIC10, TRAIL-inducing compound 10) is an effective small molecular antitumor agent that is able to induce apoptosis in tumor cells (Figure 1).

The mechanism of action is based on activating TRAIL, tumor necrosis factor (TNF)-related apoptosis-inducing ligand. It was explored that TIC10 and its derivative, ONC212 inhibit Akt and Erk signaling, in this way induce translocation of the transcription factor Foxo3a into the nucleus (Figure 1 and Figure 2). The transcription factor Foxo3a enhance the TRAIL gene expression and stimulates TRAIL and death receptor-5 (DR5) transcription, finally activating TRAIL-mediated apoptosis pathway.^{1,2}

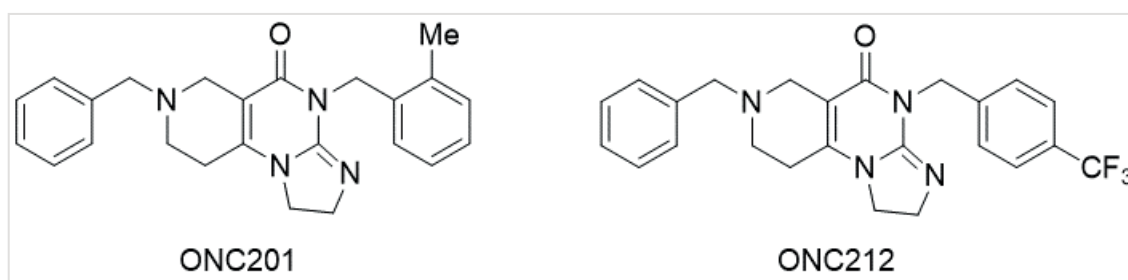


Figure 1. Structure of ONC201 (TIC10) and ONC212

Apoptotic effect of ONC201 was demonstrated on hepatocellular carcinoma, including HepG2 cells,³ whereas ONC212 showed an anti-tumor effect via blocking Akt/Erk pathway in a glioblastoma cell line² and its apoptosis induction was demonstrated on pancreatic tumor cell lines and xenografts as well.⁴

The organometallic ferrocene (*bis*(cyclopentadienyl)iron) is also known as an antitumor agent; several ferrocene derivatives proved to be effective against HL-60 human leukemia cells⁵⁻⁷ and cisplatin-resistant ovarian cancer cells.⁸ Ferrocene can cause cell death via different mechanisms: *e.g. via* inhibition of COX-2 isoenzyme that is frequently

overexpressed in various tumor cells,⁹ but topoisomerase II inhibition of different ferrocene derivatives was also described.⁵

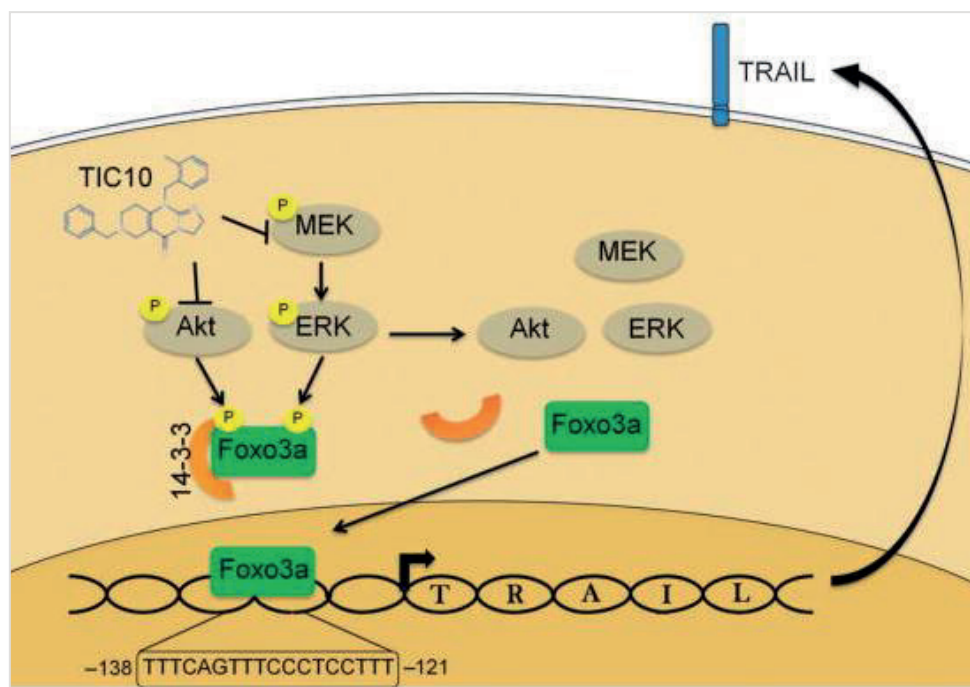


Figure 2. Mechanism of action of ONC201 and ONC212 initiating cell death

In these studies, we investigated antitumor effect of novel ONC201 hybrids with imipridone core and one or two differently positioned ferrocenylalkyl groups or halogenated benzyl groups on different human tumor cell lines, including melanoma, epithelial skin cancer, glioma, colon carcinoma and hepatocellular carcinoma.¹⁰

Results

Synthesis of the compounds was described in details by Bárányi *et al.*¹⁰ Novel compounds were characterized by ¹H- and ¹³C-NMR methods.

In vitro cytostatic effect of the compounds was measured by MTT assay¹¹ on A2058 human melanoma, A431 human epithelial skin carcinoma, U87 human glioblastoma, HT-29 human colon carcinoma and HepG2 human hepatocellular carcinoma cell lines. Cells were treated with the compounds at 0.8-100 μ M, 0.4-50 μ M or 0.2-25 μ M concentrations. Highest concentration for the treatment was determined with a preliminary solubility probe in serum free medium (RPMI-1640 or DMEM). Highest concentration for the treatment was determined with a preliminary solubility probe in serum-free medium (RPMI-1640 or DMEM). Cells were incubated with the compounds overnight, then the agents were removed and after several washing steps, cells were cultured for further 72 hours at 37 °C. The cytostatic effect was calculated with the following formula:

$$\text{Cytostasis [\%]} = (1 - A_{\text{treated}}/A_{\text{control}}) \times 100$$

IC₅₀ values were calculated from sigmoidal curves fitted on the cytostasis data using Origin2018 software.

First, we tested a set of new compounds on A2058 human melanoma and HT-29 human colon carcinoma cell lines. We found 10 compounds that showed a moderate cytostatic effect ($8.82 < \text{IC}_{50} < 69.43$) including three ferrocene containing derivatives. Two compounds, however, proved to be markedly effective, the hydrochloride salt of 7-benzyl-4-(4-iodophenylmethyl)-2,4,6,7,8,9-hexahydroimidazo[1,2-a]pyrido[3,4-e]pyrimidin-5(1H)-one (NZS-009·HCl, IC₅₀ = 2.7±1.1 μM on HT-29 colon carcinoma cells) (Table 1, Figure 3)

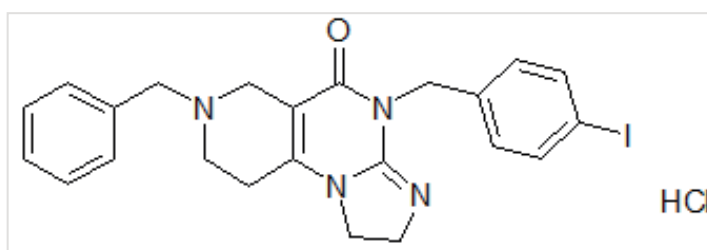


Figure 3. Chemical structure of the most effective compound, 7-benzyl-4-(4-iodophenylmethyl)-2,4,6,7,8,9-hexahydroimidazo[1,2-a]pyrido[3,4-e]pyrimidin-5(1H)-one

The second group of compounds was tested on A431 human skin carcinoma and U87 glioblastoma cells (Table 2). Of these substances, several compounds showed significant anti-tumor effect and two compounds induced extraordinary activity on 431 cells (IC₅₀ < 0.2 μM). For the most active compounds a patent application have been submitted.¹²

A third group of compounds was tested on four tumor cell lines, including the HepG2 human hepatocarcinoma cell line, A2058 human melanoma, A431 human skin carcinoma, and U87 human glioblastoma cells (Table 3). The results show that HepG2 cells were found to be much more sensitive to the compounds than the other cell lines, which is in consistence with the effect described for of ONC201.³ Among the highly cytostatic compounds we found azide, fluoro- and iodine-substituted derivatives as well as imipridone-gemcitabine hybrids (reference compound gemcitabine, CT-059G also showed a remarkable antitumor effect on three cell lines, except for U87 glioblastoma). Compound TBP-274 (7-(4-azidobenzyl)-4-(4-iodophenylmethyl)-2,4,6,7,8,9-hexahydroimidazo[1,2-a]pyrido[3,4-e]pyrimidin-5(1H)-one) showed an outstanding effect on A2058 cells. (Table 3, Figure 4.).

Table 1. Cytostatic effect of impiridone hybrids on HT-29 human colon carcinoma and A2058 human melanoma cells

code	HT-29		A2058	
	IC ₅₀ [μM]	±SD	IC ₅₀ [μM]	±SD
NZS-009 B·HCl	16.9	8.6	5.28	0.86
NZS-009·HCl	2.7	1.1	8.82	7.14
TBP-038·HCl	>100	-	>100	-
TBP-039·HCl	>100	-	>100	-
TBP-040·HCl	>100	-	>100	-
KIM-011·HCl	>100	-	>100	-
TBP-052·HCl	>100	-	47.365	23.50
TBP-053·HCl	>100	-	>100	-
TBP-054·HCl	33.0	23.3	20.91	12.46
TBP-055·HCl	34.0	21.9	17.64	6.65
NZS-009 B	>100	-	27.57	33.88
NZS-009	>100	-	>100	-
TBP-038	>100	-	>100	-
TBP-039	58.6	18.6	>100	-
TBP-040	>100	-	>100	-
KIM-011	>100	-	>100	-
TBP-052	35.6	0.5	31.22	8.98
TBP-053	11.6	3.5	13.51	8.49
TBP-054	>100	-	>100	-
TBP-055	>100	-	>100	-
NZS-033	22.08	9.43	9.53	8.14
NZS-034	>100	-	>100	-
NZS-036	>100	-	>100	-
TBP-116	45.35	38.56	35.12	30.64
TBP-117	69.43	7.83	>100	-
TBP-118	14.33	7.81	14.16	8.05
TBP-125	40.16	5.32	28.73	11.92
TBP-126	>100	-	49.84	13.56
TBP-127	39.86	16.50	32.33	22.82
TBP-128	>100	-	57.23	20.24
TBP-129	40.87	2.37	28.12	13.31
TBP-130	>100	-	42.00	26.85
CZT-016	55.68	3.77	45.4	2.60
CZT-016·HCl	54.69	9.21	43.6	2.97
CZT-018	72.40	13.02	52.0	1.12
CZT-018·HCl	45.97	3.12	45.0	0.98
NZS-022	26.52	15.25	36.3	13.35
TBP-029	24.82	4.46	>100	-
NZS-033	22.1	9.4	9.5	8.1
NZS-034	>100	-	>100	-
NZS-036	>100	-	>100	-

Table 2. Cytostatic effect of impiridone hybrids on A431 human skin carcinoma and U87 human glioblastoma cells.

code	IC ₅₀ [μM]	
	A431	U87
TBP-072	>25	>25
TBP-073	>25	>25
TBP-098·HCl	>25	>25
TBP-098	>25	>25
TBP-109	>25	>25
TBP-134	3.55	>25
TBP-135	7.29	>25
TBP-136	>25	>25
TBP-161	>25	>25
TBP-162	>25	>25
TBP-163	>25	>25
TBP-183	>25	>25
KIM-074/E	3.63	3.51
KIM-075/E	8.95	5.99
KIM-056/E	1.39	6.02
KIM-061/E	>25	>25
KIM-072/E	>25	>25
KIM-073/E	2.66	17.44
TBP-149	<0.2	4.48
TBP-150	6.16	>25
CZT-021	<0.2	4.16
CZT-022	<0.2	>25

Table 3. Cytostatic effect of impiridone hybrids on HepG2 human hepatocarcinoma cell line, A2058 human melanoma, A431 human skin carcinoma, and U87 human glioblastoma cells.

Code	IC ₅₀ [μM]			
	U87	A2058	A431	HepG2
TBP-272	6.1	1.25	11.1	<0.2
TBP-274	>25	0.7	>25	<0.2
CZT-054	>25	7.5	>25	0.6
CZT-059	>25	>25	>25	2.6
CZT-059G	>25	<0.2	2.7	<0.2
CZT-061	>25	>25	>25	0.6
CZT-069	>25	>25	>25	0.7
CZT-091	>25	>25	8.26	3.8
CZT-092	>25	7.25	4.4	3.4
CZT-097	10.6	1.6	9.3	0.8
CZT-099	>25	4.65	>25	8.1
CZT-100	22.3	1.7	>25	0.9
CZT-102	>25	6.3	>25	4.0

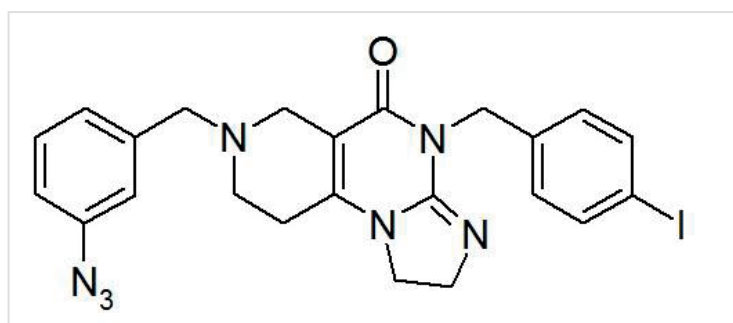


Figure 4. Structure of TBP-274 (7-(4-azidobenzyl)-4-(4-iodophenylmethyl)-2,4,6,7,8,9-hexahydroimidazo[1,2-a]pyrido[3,4-e]pyrimidin-5(1H)-one)

References

1. Allen JE, Krigsfeld G, Mayes PA, Patel L, Dicker DT, Patel AS, Dolloff NG, Messaris E, Scata KA, Wang W, Zhou JY, Wu GS, El-Deiry WS. *Sci Transl Med* **5**:171ra17 (2013)
2. Ishida C T, Zhang Y, Bianchetti E, Shu C, Nguyen TTT, Kleiner G, Sanchez-Quintero MJ, Quinzii CM, Westhoff MA, Karpel-Massler G, Prabhu VV, Allen JE, Siegelin MD. *Clin Cancer Res* **24**: 5392-5406 (2018)
3. Cheng L, Liu YY, Lu PH, Peng Y, Yuan Q, Gu XS, Jin Y, Chen MB, Bai XM. *Oncotarget* **8**: 28385-28394 (2017)
4. Lev A, Lulla AR, Wagner J, Ralff MD, Kiehl JB, Zhou Y, Benes CH, Prabhu VV, Oster W, Astsaturov I, Dicker DT, El-Deiry WS. *Oncotarget* **8**: 81776-81793 (2017)
5. Vashisht Gopal YN, Jayaraju D, Kondapi AK. *Arch Biochem Biophys* **376**: 229-235 (2000)
6. Zsoldos-Mády V, Csámpai A, Szabó R, Mészáros-Alapi E, Pásztor J, Hudecz F, Sohár P. *ChemMedChem* **1**: 1119-1125 (2006)
7. Miklán Zs, Szabó R, Zsoldos-Mády V, Reményi J, Bánóczy Z, Hudecz F. *Biopolymers* **88**: 108-114 (2007)
8. Pigeon P, Wang Y, Top S, Najlaoui F, Garcia Alvarez MC, Bignon J, McGlinchey MJ, Jaouen G. *J Med Chem* **60**: 8358-8368 (2017)
9. Farzaneh S, Zeinalzadeh E, Daraei B, Shahhosseini S, Zarghi A. *Anticancer Agents Med Chem* **18**: 295-301. (2018)
10. Bárány P, Oláh-Szabó R, Kovács I, Czuczi T, Szabó CL, Takács A, Lajkó E, Láng O, Kóhidai L, Schlosser G, Bősze Sz, Mező G, Hucecz F, Csámpai A. *Molecules* **23**: 2248 (2018)
11. Mosmann T. *J Immunol Methods* **65**: 55-63 (1983)
12. Patent Application No. 1292889-3119/MOI (2019)

The *in vitro* antitumor effect of ONC201 derivatives in pancreatic and in colorectal cancer cell lines

Angéla Takács¹, Zsófia Szász¹, Eszter Lajkó¹, Márton Kalabay¹, Diána Mező¹, Nóra Fekete¹, Éva Pállinger¹, Péter Bárány², Antal Csámpai², Orsolya Láng¹, László Kóhidai¹

¹Chemotaxis Research Group, Department of Genetics, Cell- and Immunobiology, Semmelweis University, Budapest, Hungary

²Institute of Chemistry, Eötvös L. University, Budapest, Hungary

Introduction

ONC201 (also called TIC10–TRAIL-inducing compound) is a new drug candidate that belongs to the family of small molecules.¹ It is water soluble, lipophilic (logP=2.3); thus it can be administered *per os* which is an important factor in the adherence of patients.¹ It is currently investigated in early-phase clinical trials aiming to cure solid tumors.

Although the mechanism of ONC201 is still not clear, from literature we know that it may be able to activate both intrinsic and extrinsic apoptosis.²

It can trigger apoptosis via p53-dependent ways by increasing the activation of caspases.³ By inhibiting the Akt and MAPK intracellular pathways independently from the p53-status of the cells, the FOXO3a transcription factor dephosphorylates and its activation increases.⁴ Due to the change in the conformation of this protein, it can easily penetrate into the nucleus, where it enhances the expression of the TRAIL protein (TNF-related apoptosis-inducing ligand). The TRAIL protein can then trigger apoptosis selectively in cancer cells upon the greater presence of TRAIL-R1 and TRAIL-R2 in the surface membrane of cancerous cells.⁵

The reference molecule, ONC201 can be modified with ferrocene, benzyl and halogenated benzyl group on the heterocyclic skeleton in order to optimize the pharmacokinetics of the molecule and to increase the antitumor effect (Figure 1).

Objectives of the present study were:

1. to study the antitumor effect of ONC201 and its 30 newly synthesized derivatives in PANC-1 and COLO-205 cell lines
2. to compare the efficacy of the derivatives with the parent molecule
3. to select the most effective 3 derivatives for further cell cycle analysis

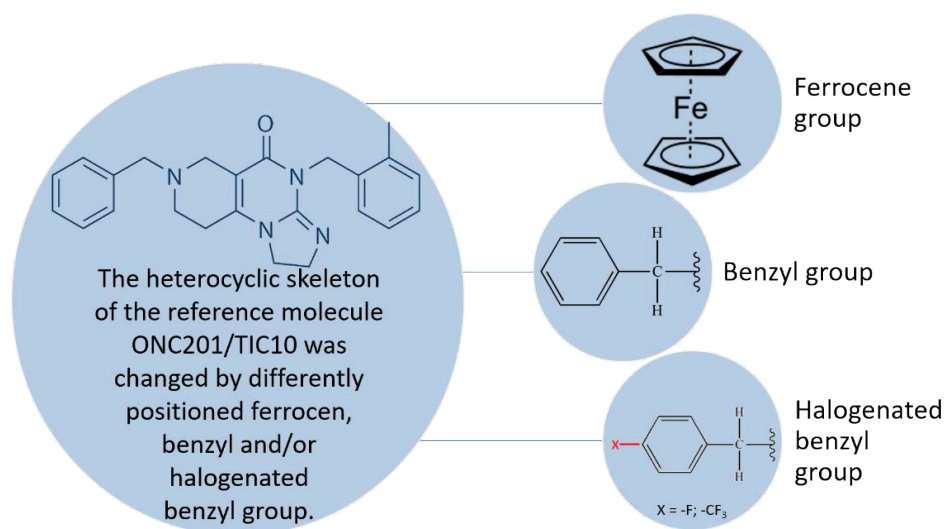


Figure 1. Groups of investigated TIC10 derivatives

Results

After evaluation of the cell viability assays, the IC₅₀ value of the reference molecule was not detectable on PANC-1 cells, but on COLO-205 it was 5 μM after a 72h long incubation (Figure 2). Table 1. shows that three derivatives were identified as more potent candidates than the reference molecule upon their lower IC₅₀ values. The most potent derivatives all belong to the group modified with a halogenated benzyl group.

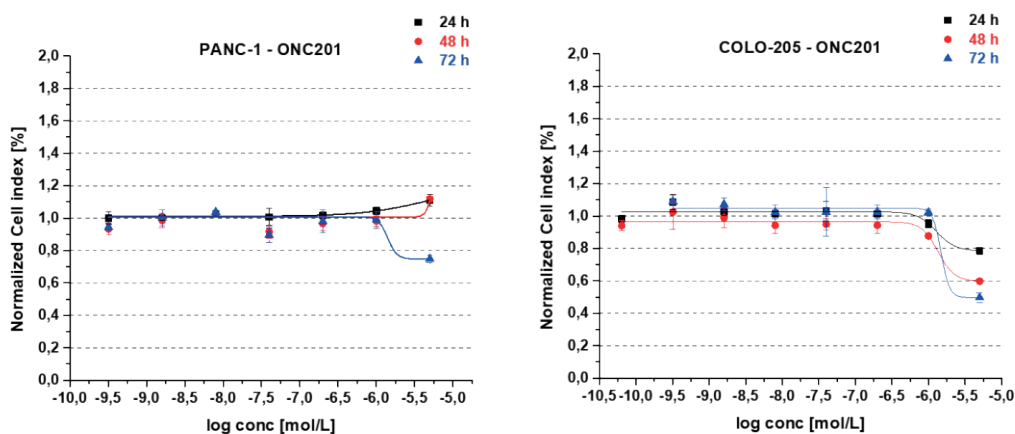


Figure 2. Normalized data and fitted dose-response curves of the reference molecule for PANC-1 and COLO-205 cell lines

As the upregulated TRAIL protein can act through the activation of death receptors, e.g. the TRAIL-R1 and TRAIL-R2, the status of the cell lines on these two receptors was determined by flow cytometry. The COLO-205 and the PANC-1 cells also seem to express both of the receptors, but COLO-205 cells tend to have a higher percentage of TRAIL-R1 and TRAIL-R2 than the PANC-1 cells (Figure 3).

Table 1. IC₅₀ values (μM) after 72 hours of treatment

	PANC-1	COLO-205
ONC201 (ref. molecule)	ND	5
Molecule 1	0.77	0.21
Molecule 2	0.16	0.25
Molecule 3	0.35	0.25

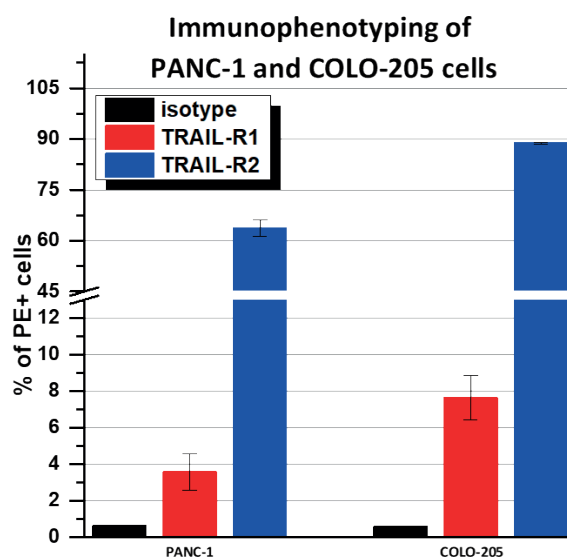


Figure 3. Levels of expression of TRAIL-R1 and TRAIL-R2 on the surface membrane of PANC-1 and COLO-205 cells

For further cell cycle analysis, the compounds were tested at 1.5 μM concentration. This concentration is the IC₂₀ value of the tested reference molecule for both tumorous cell lines. ONC201 and its 3 derivatives had a barely significant effect on the cell cycle phase distribution of PANC-1. In COLO-205, an increase in the number of the cells in the subG1 phase was detected after 48h long treatment. This increase correlates with the decrease of the cells in the G₀/G₁ phase. This idea suggests that the compounds can act independently from the cell division and can target resting cells in the G₀ phase (Figure 4).

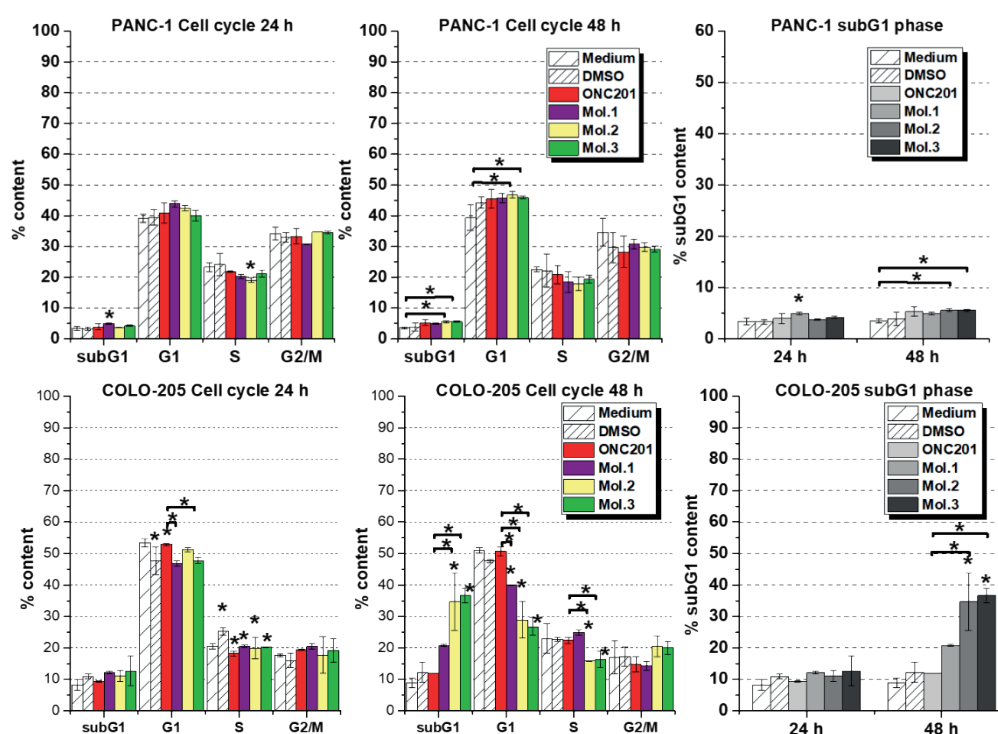


Figure 4. Cell cycle profile of PANC-1 and COLO-205 cells after 24 and 48 h long treatment with the different compounds at a concentration of 1.5 μ M

Conclusion

Our results show that ONC201 had a more potent effect on the colorectal tumor cell line COLO-205 than on the pancreatic adenoma cells PANC-1. Our results have a good correlation with the previous results of the literature.⁶ All of the tested compounds induced cell cycle arrest in the cell lines after 48 hours of the treatments, although no decrease in the cell viability was measured at this time point, which results confirm previous findings of the literature.⁷ As the COLO-205 tumorous cell line expresses a higher percentage of TRAIL-R2 than TRAIL-R1, our theory is supported that ONC201 can trigger cell death *via* the activation of TRAIL-R2.

In conclusion, our data suggest that the investigated derivatives are potentially good candidates for antitumor therapy of colorectal cancers in the future.

References

1. Greer YE, Lipkowitz S. *Oncoscience* **2**: 75-76 (2015)
2. Allen JE, Krigsfeld G, Mayes PA, Patel L, Dicker DT, Patel AS, Dolloff NG, Messaris E, Scata KA, Wang W, Zhou JY, Wu GS, El-Deiry WS. *Sci Transl Med* **5**: 171ra17 (2013)
3. Tu Y-S, He J, Liu H, Lee HC, Wang H, Ishizawa J, Allen JE, Andreeff M, Orlowski RZ, Davis RE, Yang J. *Neoplasia* **19**: 772-780 (2017)

4. Fang Z, Wang J, Clark LH, Sun W, Yin Y, Kong W, Pierce SR, West L, Sullivan SA, Tran AQ, Prabhu VV, Zhou C, Bae-Jump V. *Am J Cancer Res* **8**: 1551-1563 (2018)
5. Mohr A, Yu R, Zwacka RM. *BMC Cancer* **15**: 494 (2015)
6. Prabhu VV, Allen JE, Dicker DT, El-Deiry WS. *Cancer Res* **75**: 1423-1432 (2015)
7. Kline CLB, Van den Heuvel APJ, Allen JE, Prabhu VV, Dicker DT, El-Deiry WS. *Sci Signal* **9**: ra18 (2016)

Bortezomib has antitumor effect in melanoma cells that can be inhibited by alpha-lipoic acid

Angéla Takács¹, Eszter Lajkó¹, Orsolya Láng¹, Ildikó Istenes², László Kőhidai¹

¹Chemotaxis Research Group, Department of Genetics, Cell- and Immunobiology, Semmelweis University, Budapest, Hungary

²1st Department of Internal Medicine, Semmelweis University, Budapest, Hungary

Introduction

Bortezomib (BOZ), a targeted proteasome inhibitor, has become an unavoidable medicine in the treatment of multiple myeloma, a hematological malignancy. The U.S. Food and Drug Administration (FDA) approved BOZ for the treatment of progressive multiple myeloma in 2003. In addition, recently scientists have investigated the potential activity of BOZ and its probable combinations with the purpose of curing solid tumor malignancies, e.g. melanoma, the malignant transformation of melanocytes.^{1,2,3}

BOZ is a low molecular weight, hydrophilic dipeptide-boronic acid derivative. It acts as a reversible inhibitor of the chymotrypsin-like protease activity of the proteasome.⁴ It blocks the NF- κ B (nuclear factor kappa-light-chain-enhancer of activated B cells) pathway *via* inhibition of the degradation of the I κ B protein that binds to the NF- κ B and blocks its transport to the nucleus.^{5,6}

In general, chemotherapy-induced peripheral neuropathy (CIPN) is a severe side-effect of various chemotherapeutic agents, such as BOZ, cisplatin or paclitaxel.⁷ Unfortunately, bortezomib-induced peripheral neuropathy (BIPN) is a type of CIPN and belongs to the dose-limiting side effects of BOZ.^{8,9} The symptoms of BIPN are paresthesia, allodynia, hyperalgesia.⁷ These symptoms are usually presented in stocking-and-glove-shaped distribution, and thus dose reduction or discontinuation can be required.⁸ To optimize the quality of life of the patients, different types of CIPN can be treated with antiepileptic agents such as gabapentin, antidepressants such as amitriptyline and neuroprotective or antioxidant vitamins such as Vitamin C.^{10,11} These antioxidant vitamins are over-the-counter (OTC) products and are part of the cancer supportive care that has a growing market nowadays. However, cancer supportive care is aimed to focus on the quality of life during the treatments of cancerous illnesses, but many times it may also decrease the antitumor effect of the chemotherapeutic agent.

Other neuroprotective agents, *e.g.* alpha-lipoic acid (ALA) and Vitamin B1 (vit B1) are also applied as advantageous agents for cancer supportive care; previous studies have

shown the positive effect of these compounds mentioned above in different neurodegenerative conditions, *e.g.* diabetic neuropathy or anticancer drug-related peripheral neuropathy.¹²⁻¹⁴

Objectives

Based on the aforementioned findings, we hypothesized that the antioxidants may counteract the antitumor activity of BOZ. In the present work our aim was (i) to verify the anti-proliferative effects of BOZ in melanoma and myeloma cell lines, (ii) to test the influence of the ALA and vit B1 on the tumor growth inhibitory effect of BOZ, as well as (iii) to study the mechanisms of the effects of BOZ + antioxidants co-treatments.

Results

First, we determined the IC₅₀ values in the 24th hour of the BOZ treatment on both cell lines (A2058 - IC₅₀: 158 nM; U266 - IC₅₀: 2.17 nM). Based on these IC₅₀ values, the A2058 melanoma cell line showed a 72-fold lower sensitivity to BOZ compared with the U266 myeloma cells (Figure 1A and B). In the further experiments with the binary combination of BOZ and antioxidant vitamins, these compounds were tested only in representative concentrations (BOZ: 20, 100, 300 ng/mL; ALA: 10, 100 µg/mL and vit B1: 150, 300 nM).

Figure 1C-D shows the BOZ-induced anti-proliferation on myeloma and melanoma cells following 24 h exposure with 20, 100 and 300 ng/mL BOZ. The BOZ was anti-proliferative on the melanoma cell line A2058 in a dose-dependent manner (Figure 1C), while on the myeloma cell line U266, in all tested concentrations with the same extent (Figure 1D). It is clearly shown in Figure 1C that the number of viable melanoma cells was significantly increased following 20 ng/mL BOZ + 100 µg/mL ALA co-treatment compared to the only-BOZ treated cells. In the case of U266 cells, the antioxidants could not influence the antitumor effect of any BOZ treatment (Figure 1D).

As shown in Figure 1E, dose-escalated BOZ treatment induced remarkable p53-activation (phosphorylation of p53) even at lower concentrations on melanoma cell line compared to the control group (RFI = BOZ treated cells p53 MFI/control cells p53 MFI; RFI: ratio of the mean fluorescence intensity; MFI: mean fluorescence intensity). However, BOZ did not stimulate p53-activation in U266 cells.

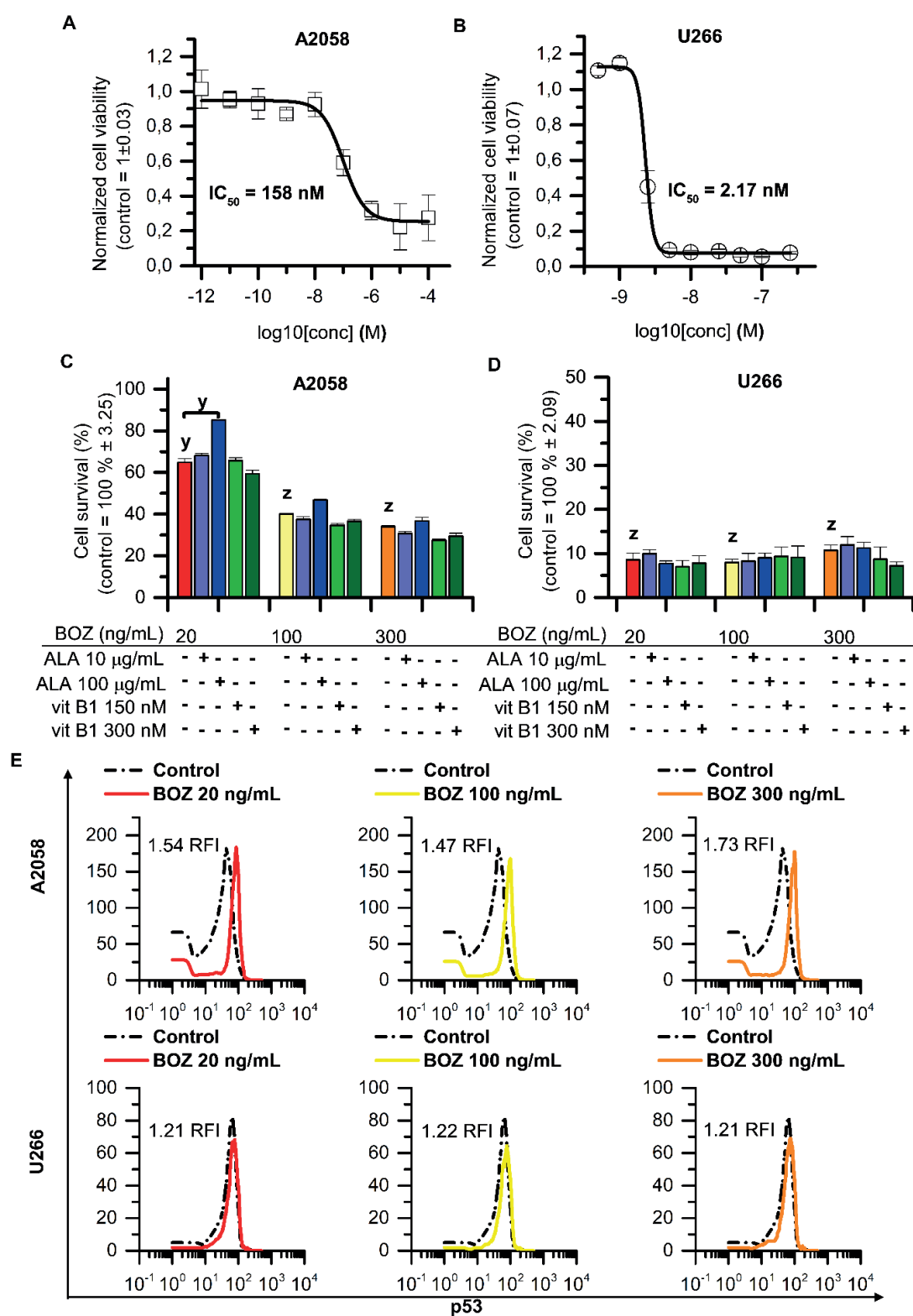


Figure 1. Concentration-response curves for (A) A2058 and (B) U266 cells treated with BOZ for 24 h. The data are normalized to the control wells. The IC₅₀ value of BOZ was determined by fitting a sigmoidal dose-response curve to the data, using Origin Pro 8.0. Influence of alpha-lipoic acid and vitamin B1 on bortezomib mediated cell death on A2058 (C) and U266 cells (D) after 24 h incubation. (E) Analysis of the level of the activated p53 of A2058 and U266 cells after 24 h incubation with 20, 100 and 300 ng/mL bortezomib (BOZ). The levels of significance are shown as follows: x: P < 0.05; y: P < 0.01; z: P < 0.001, determined by the One-way ANOVA test followed by Fishers LSD *post hoc* test.

As it can be seen in Figure 2, the percentage of the Annexin V (Ax V) positive cells was increased by every BOZ treatment in both cell lines. Surprisingly, the antioxidants were able to further increase the percentage of the early apoptotic cells compared to the matching BOZ-treated control in many instances, *e.g.* A2058 cell: 100 ng/mL BOZ + 100 µg/mL ALA or 150 nM vit B1; U266 cell: 20, 100, 300 ng/mL BOZ + 10 or 100 µg/mL ALA, respectively. Both concentrations of vit B1 could reduce the percentage of Ax V positive A2058 cells, however, no significant decrease was observed in the 20 ng/mL BOZ + 100 µg/mL ALA combination compared to the 20 ng/mL BOZ-treated cells (Figure 2A).

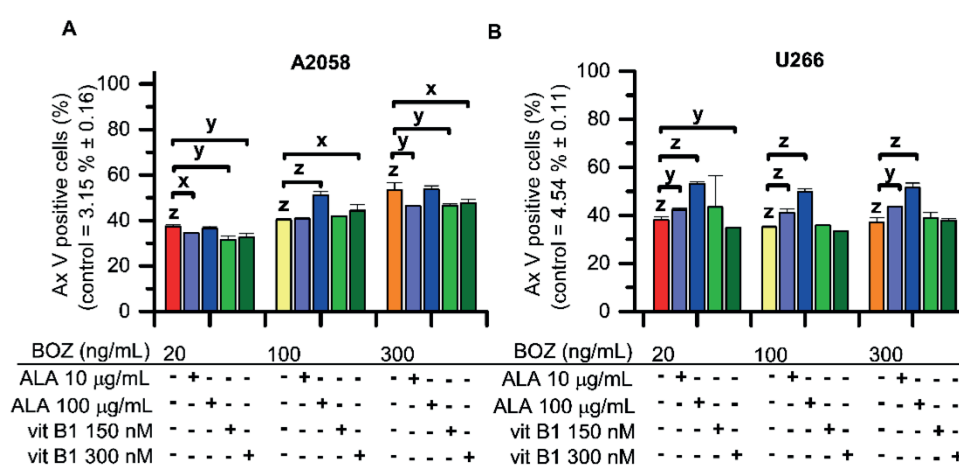


Figure 2. Apoptosis in A2058 (A) and in U266 (B) cells after 24 h long incubation with 20, 100 and 300 ng/mL bortezomib and combinations of BOZ + 10 or 100 µg/mL ALA and 150 or 300 nM vit B1 analyzed by Annexin V assay. Data are given as mean values ± standard deviation (SD) (n=2). The levels of significance are shown as follows: x: P < 0.05; y: P < 0.01; z: P < 0.001, determined by the One-way ANOVA test followed by Fishers LSD *post hoc* test.

We then hypothesized that BOZ may affect the cell cycle of the myeloma and melanoma cells. The cell cycle profile was evaluated after 24 h in the presence of BOZ (Figure 3). The percentage of A2058 cells in the sub G1 phase increased following the treatment with all the BOZ concentrations, along with a decrease in the proportion of the resting cells from G0/G1 phase (Fig. 3A). The treatment with 20, 100 and 300 ng/mL BOZ resulted in a tendentious increase in the proportion of cells in the S phase and G2/M phase. In contrast to our cell viability results, ALA could not significantly inhibit the effect of 20 ng/mL BOZ on the sub G1 phase (Figure 3B). The effect of the antioxidant co-treatments was insignificant on the G2/M arrest induced by 20 ng/mL BOZ treatment.

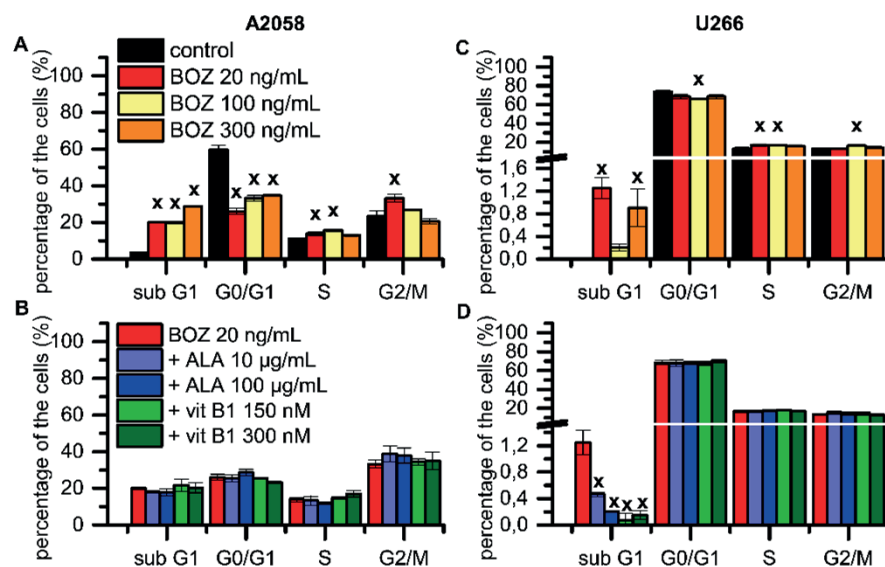


Figure 3. Cell cycle analysis of A2058 (A-B) and U266 (C-D) cell lines after 24 h long incubation with 20, 100 and 300 ng/mL bortezomib (BOZ) and combinations of 20 ng/mL BOZ + 10 or 100 $\mu\text{g/mL}$ alpha-lipoic acid (ALA) and 150 or 300 nM vitamin B1 (vit B1) analyzed by NucleoCounter. The levels of significance are shown as follows: x: $P < 0.05$; y: $P < 0.01$; z: $P < 0.001$, determined by the One-way ANOVA test followed by Fishers LSD *post hoc* test.

Conclusions

Bortezomib, the first FDA approved proteasome inhibitor drug, is very important for the first-line therapy of multiple myeloma.¹⁵ There is a large volume of studies attempting to explain the effects of BOZ on U266 myeloma cells.¹⁶⁻¹⁸ As Chen pointed out, BOZ increased Ax V positivity and inhibited the growth of the U266 cells. In 2013, Selimovic *et al.* published a paper in which they described BOZ induced apoptosis- and autophagy-related pathways in melanoma cells, too.¹⁹

According to Larsson *et al.*,²⁰ the IC_{50} values of drugs are suitable drug response metrics to predict the sensitivity of cells. In the present work, we report that U266 myeloma cells were (IC_{50} : 2.17 nM) more sensitive to BOZ than A2058 melanoma cells (IC_{50} : 158 nM). Our data demonstrate a tumor-specific antitumor effect of BOZ, because p53 activation was observed only on melanoma but not on myeloma cell lines. These results are consistent with other studies and suggest that, depending on the tumor type, BOZ may act independently of p53 phosphorylation.²¹

The detection of the early apoptotic cells developed by the BOZ treatments confirms our initial results on the cell viability of both cell lines. Dose-dependent apoptotic effect of BOZ was observed in the melanoma cells, whereas dose-dependency could not be detected in the myeloma cells. In contrast, other experiments carried out in this field,^{22,23} we could detect

a cell cycle arresting effect of BOZ on myeloma cells in the S-phase, while our results showed a G₂/M-phase arrest on melanoma.

This work calls the attention that BOZ may alter different pathways in the investigated melanoma and myeloma cell lines *in vitro*. Further data collection is required to unfold the dose-dependent correlation, how ALA affects the antitumor effect of BOZ. To sum up, the fact that 100 µg/mL ALA was able to disrupt the antineoplastic effect of 20 ng/mL BOZ in melanoma cells *in vitro*, should point towards the proper use of cancer supportive care that must be in accordance with evidence-based medicine and must be under medical control.

References

1. Markovic SN, Geyer SM, Dawkins F, Sharfman W, et al. *Cancer* **103**: 2584-2589 (2005)
2. Poklepovic A, Youssefian LE, Winning M, et al. *Invest New Drugs* **31**: 937-942 (2013)
3. Aghajanian C, Soignet S, Dizon DS, Pien CS, et al. *Clin Cancer Res* **8**: 2505-2511 (2002)
4. Bladé J, Cibeira MT, Rosiñol L. *Acta Oncol* **44**: 440-448 (2005)
5. Hideshima T, Chauhan D, Richardson P, Mitsiades C, et al. *J Biol Chem* **277**: 16639-16647 (2002)
6. Chen D, Frezza M, Schmitt S, Kanwar J, Dou QP. *Curr Cancer Drug Targets* **11**: 239-253 (2011)
7. Han Y, Smith MT. *Front Pharmacol* **4**: 156 (2013)
8. Starobova H, Vetter I. *Front Mol Neurosci* **10**: 174 (2017)
9. Areti A, Yerra VG, Naidu V, Kumar A. *Redox Biol* **2**: 289-295 (2014)
10. Mohty B, El-Cheikh J, Yakoub-Agha I, Moreau P, et al. *Haematologica* **95**: 311-319 (2010)
11. Gedlicka C, Kornek GV, Schmid K, Scheithauer W. *Ann Oncol* **14**: 339-340 (2003)
12. Golbidi S, Badran M, Laher I. *Front Pharmacol* **2**: 69 (2011)
13. Luong K, Nguyen LTH. *J Clin Med Res* **17**: 1115-1124 (2012)
14. Maschio M, Zarabla A, Maialetti A, Marchesi F, et al. *Integr Cancer Ther* **17**: 1115-1124 (2018)
15. Grethlein SJ. Multiple Myeloma Treatment Protocols (2019)
16. Chen L-J, Li J-Y, Qian S-X, et al. *Zhongguo Shi Yan Xue Ye Xue Za Zhi* **14**: 696-699 (2006)
17. Hu X, Xuan H, Du H, Jiang H, Huang J. *PLoS One* **9**: e95765 (2014)
18. Chudasama VL, Ovacik MA, Abernethy DR, Mager DE. *Pharmacol Exp Ther* **354**: 448-458 (2015)
19. Selimovic D, Porzig BBOV, El-Khattouti A, Badura HE, et al. *Cell Signal* **25**: 308-318 (2013)
20. Larsson P, Engqvist H, Biermann J, Werner Rönnerman E, et al. *Sci Rep* **10**: 5798 (2020)
21. Strauss SJ, Higginbottom K, Jülicher S, Maharaj L, Allen P, et al. *Cancer Res* **67**: 2783-2790 (2007)
22. Shen L, Au W-Y, Wong K-Y, Shimizu N, et al. *Mol Cancer Ther* **7**: 3807-3815 (2008)
23. Russo A, Bronte G, Fulfarò F, Cicero G, et al. *Curr Cancer Drug Targets* **10**: 55-67 (2010)

Design and synthesis of novel apoptosis-inducing cytotoxic drug leads for conjugation with carrier molecules and development of Tumor Targeting Drug Conjugates

Béla Bertók¹, György Dormán¹, László Kőhidai², Orsolya Láng², Csaba Magyar³

¹ComInnex Inc. Budapest, Hungary

²Semmelweis University, Budapest, Hungary

³Institute of Enzymology, Research Centre for Natural Sciences, Hungarian Academy of Sciences, Budapest, Hungary

Introduction

During the last 10 years, ComInnex specialized on developing high-quality drug-like molecules in order to cover novel chemical space of potential biological targets. ComInnex's original strategy focuses on non-flat 3-dimensional templates. The new compounds are prepared *via* hydrogenation of diverse heterocycles resulting in screening libraries with more favorable physicochemical properties and various functionalities. That approach, which was combined with up to date, *in silico* methods to generate focused Target Oriented Libraries *via* a complex platform (Figure 1), was an excellent starting point to synthesize novel compounds that might be applied as original drug leads alone or in combination with carrier compounds to develop novel Small Molecule Targeting Drug Conjugates (SMTDCs).

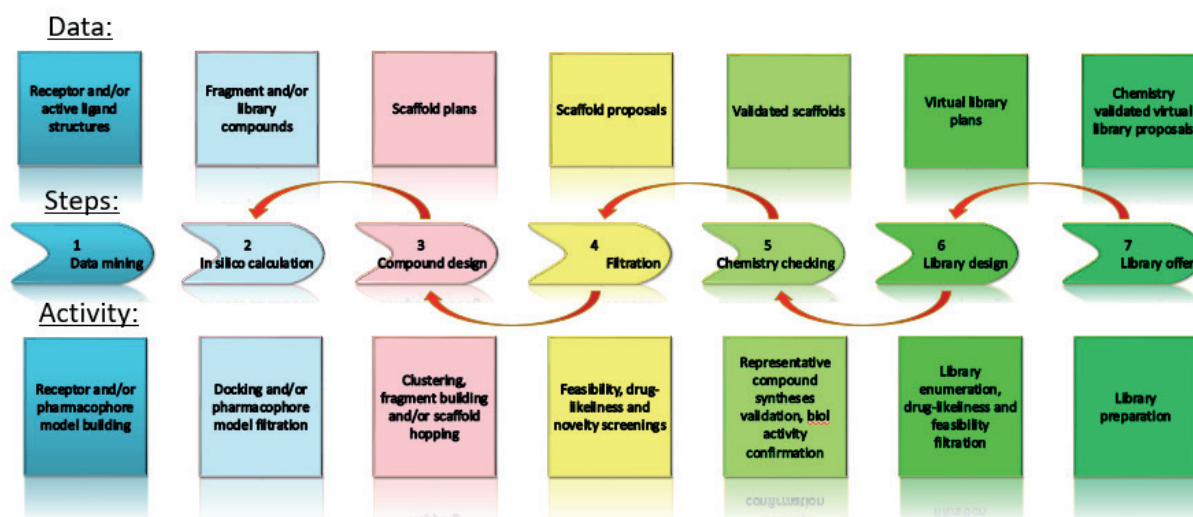


Figure 1. Target Oriented Library platform (TOL) general workflow and steps

Cancer is still one of the most challenging lethal diseases in medicinal chemistry with no or reduced surviving rate. Albeit some types of tumors already have potential treatment, there are still many tumor types without effective therapy. Our focus turned to pancreatic cancer, since it has a particularly high mortality rate (the general 5-year survival rate for

people with pancreatic cancer is 9%). The applied chemotherapies have several problems such as high resistance factor for anticancer drugs and low tolerability. The cytotoxic compounds applied in tumor treatment typically induce necrosis with toxic side-effects and inflammation, which is in contrast with the natural control mechanism of elimination and utilization of the malfunctioning cells regulated by programmed cell death (apoptosis) (Figure 2).¹

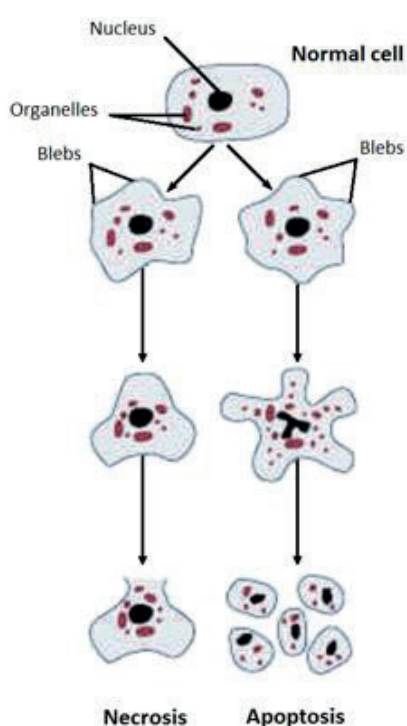


Figure 2. Main differences in necrotic and apoptotic elimination of cells

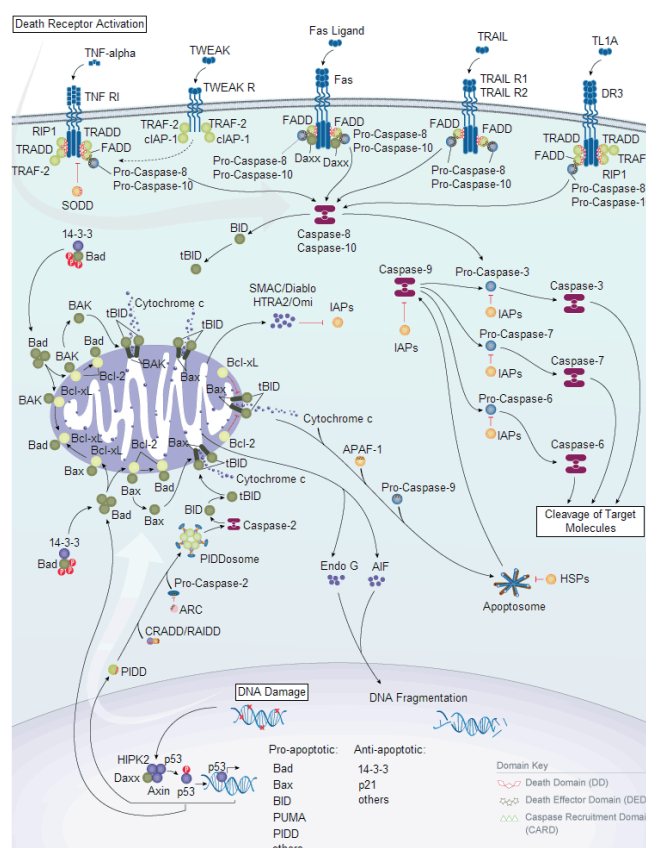


Figure 3. Apoptosis signalling pathways

Cancer is associated with the damage of the programmed cell death regulation, resulting in blocked elimination of the tumor cells, together with the resistance developed to chemotherapy. In cancer, the apoptotic signaling is de-regulated, particularly by the activation of an anti-apoptotic system, which allows cancer cells to escape this program leading to uncontrolled proliferation and tumor survival.²

Apoptosis has a complex regulation mechanism (Figure 3), since on one hand, it has a vital role in removing malignant cells, on the other hand, the uncontrolled or released apoptosis might result finally in killing the patient. The goal we targeted was, therefore, to develop novel apoptosis-inducing or regulating cytotoxic lead compounds, which might also be conjugated with specific carrier molecules to ensure selectivity only on cancer cells. Our strategy can be summarized as Triple Action Magic Bullet approach (Figure 4).

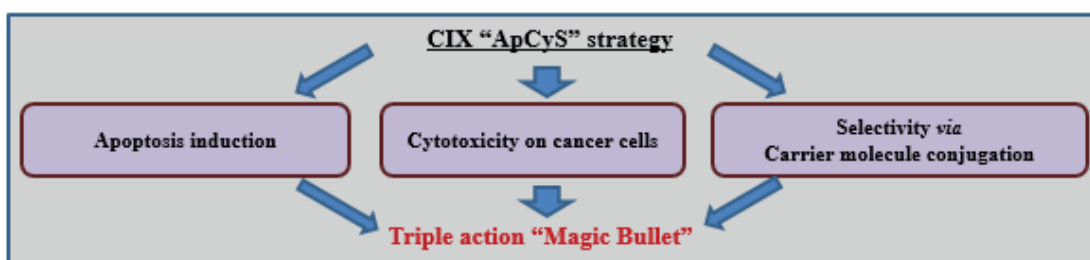


Figure 4. Triple Action Magic Bullet strategy

Design, synthesis and filtration of a diversified focused library

Several hundred diverse compounds were designed applying the ComInnex TOL platform. The compounds were filtered *via* chemical feasibility and physicochemical properties. The parameters were set according to the ADME properties characteristic to the existing small molecule drug developments:

MW	<350
clogP	<3.5
HBD	<5
HBA	<9

Finally, more than 200 compounds of different heterocycles were delivered and screened for cytotoxic activity on various cancer cell lines in the focus of two pancreatic cancer cell lines, PANC-1, and MiaPaCa-2. Six *structures* having cytotoxic activity higher than 10^{-4} were found from which 5 skeletons are illustrated in Figure 5. Two molecule cores which had more hits were picked for further development as starting points.

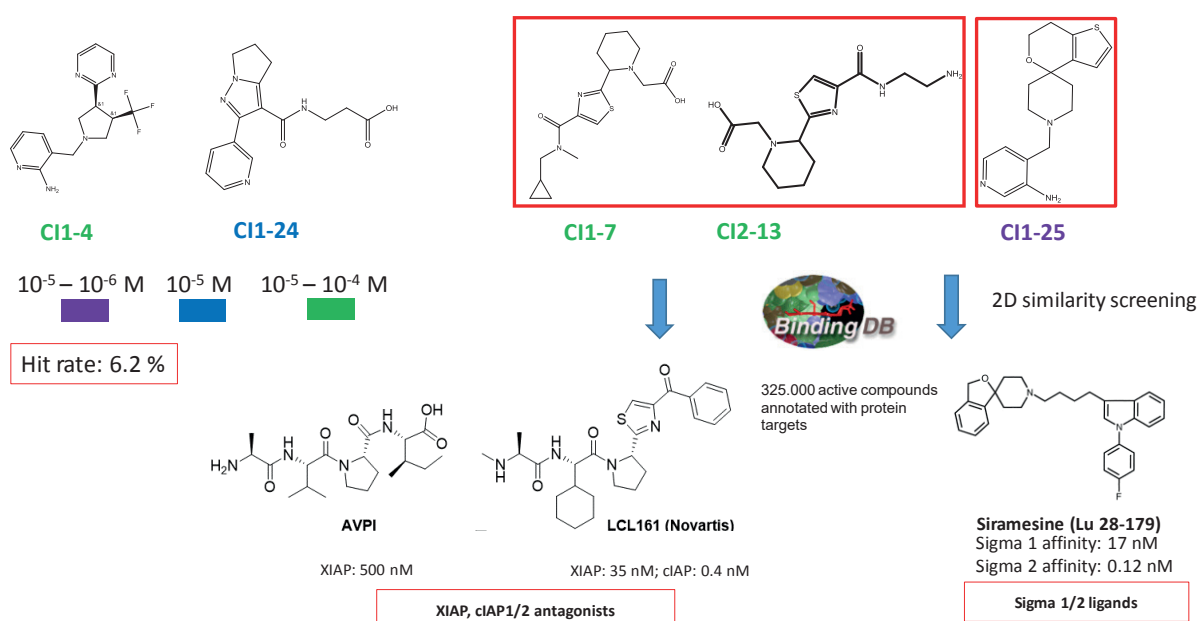


Figure 5. 1st round *in vitro* cytotoxicity screening: best hits/ *in silico* protein target prediction

2D similarity search based on the structure of active compounds applying annotated databases (*e.g.* BindingDB) confirmed the biological potency and revealed the potential proteins targets. Compound group of CI1-7/CI2-13 and CI1-25 showed similarity to existing bioactive compounds in development as XIAP antagonists (member of the Inhibitor of Apoptosis Protein family) and sigma-1,2 ligands, respectively.

The physiological function of Inhibitor of Apoptosis Protein family (IAP) and their antagonists^{3,4}

Natural anti-apoptotic proteins play an important role in the regulation of the programmed cell death (apoptosis). Those proteins regulate (inhibit) the activation of caspases. One of the most important protein groups in that regulation pathway is the Inhibitors of Apoptosis Proteins, comprising various proteins with high similarity (XIAP: X-linked IAP, cIAP1/2: cellular IAP1/2). XIAP inhibits initiator (Caspase-9) and effector caspases (Caspase-3 and -7), through the interaction of its BIR domains (BIR3 and BIR2) with the N-terminal tetrapeptide (AVPI) of the SMAC (Second Mitochondria-derived Activator of Caspases) or in other term, DIABLO (direct IAP-binding protein with low pI) protein. (Figure 6)

The IAP or XIAP antagonists such as SMAC/DIABLO and their mimetics temporarily suspend the inhibition of caspases. Intensive research activity is going on the field. Several SMAC mimetics were developed in the last couple of years,^{5,6} and 7 of them reached clinical phases. One of the first compounds, the Novartis' LCL161 (Figure 6) is particularly promising and has recently entered Phase II. clinical trials. That compound has not only hung up the inhibition of apoptosis but in parallel directly induces apoptosis by activating TNF α . The compound mimics the AVPI tetrapeptide, which is the protein binding motif of the natural SMAC peptide.

SMAC/AVPI is able to bind to the BIR3 domain of cIAPs as well and this interaction induces auto-degradation of the protein through E3 ligase mediated ubiquitination by the UBA/RING domain. However, if SMAC mimetics (compounds having AVPI-like structural motifs) are linked to specific binders of a POI (Protein of Interest) the conjugate could induce ubiquitination and degradation of this protein. Auto-ubiquitination and targeted ubiquitination can be balanced by achieving binding selectivity towards XIAP *vs.* cIAPs.

sigma ligands conjugated to various IAP antagonists showed increased cytotoxic activities in several cell-lines compared to the parent, separate small molecules.¹² While in these small-molecule drug conjugates the IAP antagonist serves as a cytotoxic “warhead”, attachment of the targeting sigma ligand has multiple actions:

- a.) increases the internalization of the conjugate into the cell,
- b.) contributes with its intrinsic antiproliferative effects.

On the other hand, recent TMEM97 knock-out studies revealed that the transmembrane receptor is not needed for the cytotoxic effects of sigma-2 ligands,¹³ thus, further studies are required to elucidate the molecular mechanism of the exact mode of action. The synergistic effect could also be attributed to the IAP antagonist’s protein degradation capability, therefore such conjugates were defined as SNIPERs (Specific and Non-genetic Inhibitor of apoptosis protein (IAP)-dependent Protein Erasers).¹⁴

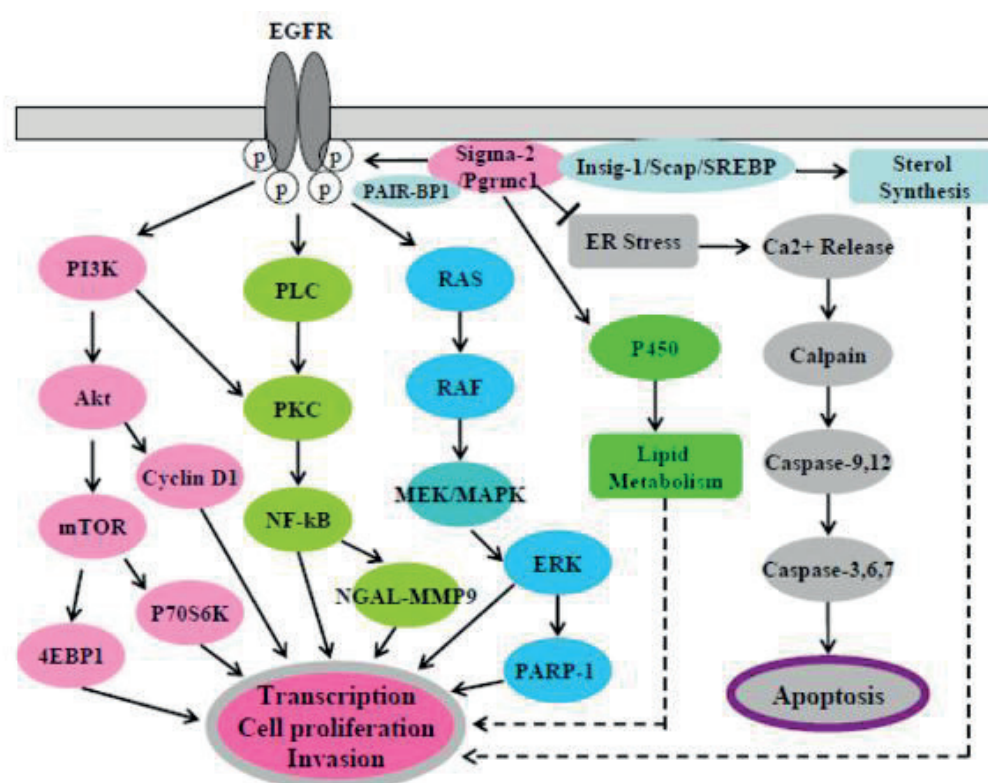


Figure 7. A hypothetical scheme of sigma-2 receptor/PGRMC1 signaling pathways in cancer cells¹⁵

Rational analog design of XIAP antagonist compounds

During the last couple of years, several structure – activity caveats were revealed. Looking at the structure of the natural ligand AVPI (alanine-valine-proline-isoleucine) tetrapeptide, 4 structural motifs (amino acids) were (P1, P2, P3, P4) determined.¹⁶ The relevance and the optional structural replacement for each motif is summarized in Figure 8.

As it was also reported, the P1, P2 dipeptide plays a critical role in binding to BIR3, thus, it acts as an “anchor”. The ring-embedded structure of the P2, P3 interface is similarly important and only isosteric replacements are allowed. Thus, P4 module offers the highest variability for novel compound design. During our rational design process, we identified the common or similar structural elements with LCL161 and applied the above modular approach for successively change the P3 and P4 motifs. In summary, we preferred changing the thiazole ring at 2,4 and 5 position. (Figure 9)

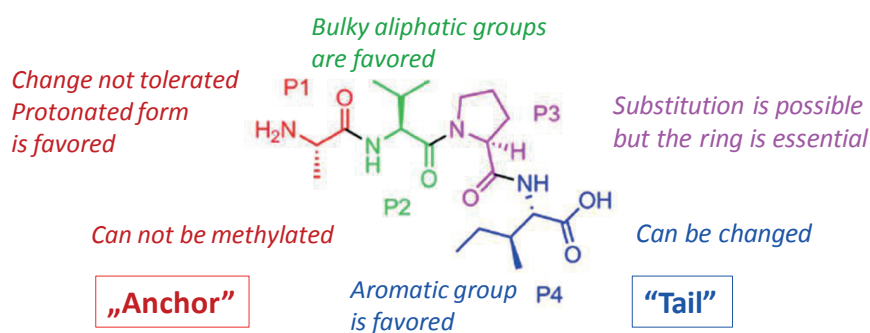


Figure 8. AVPI-based structure – activity relationships

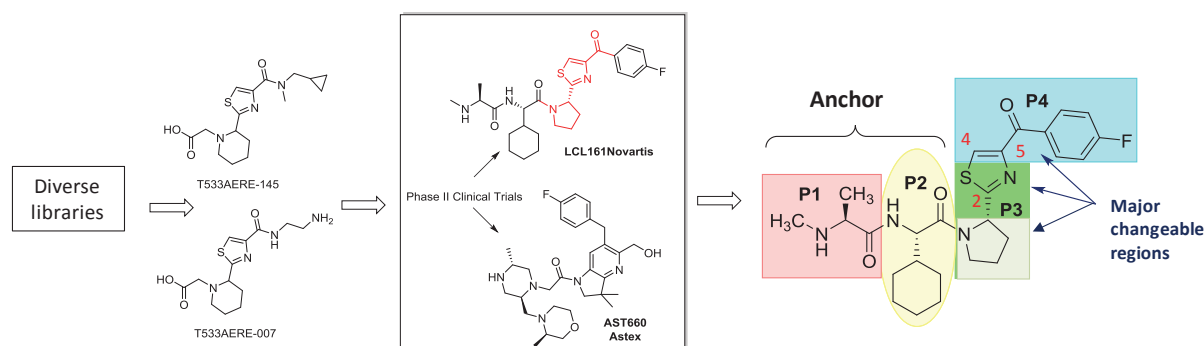


Figure 9. Rational design of novel XIAP antagonists

2D/3D chemoinformatics approaches. Virtual screening of the thiazole library

Based on the above rational design approach, a substituted thiazole library was generated (Figure 10).

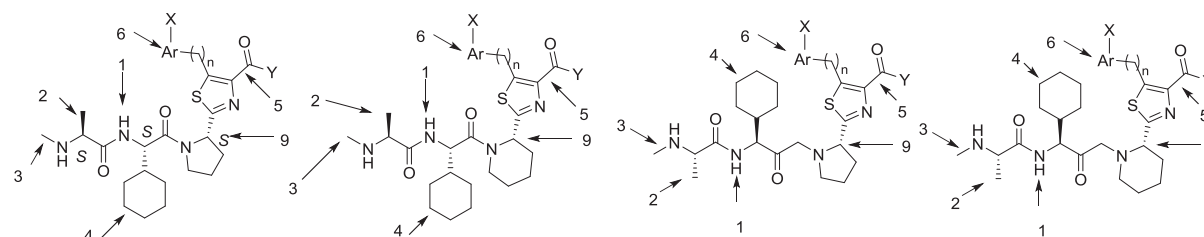


Figure 10. Major structural variations of the thiazole virtual library

The virtual library was first filtered for drug-likeness using the standard physicochemical parameter ranges followed by docking to the 3D structure of XIAP BIR3 domain. The available crystal structures of XIAP BIR3 (3HL5, 3CM2, 2OPY, 2JK7, 4HY0) allowed to generate 3D models in order to identify the major interactions of the known hit compounds and allowing to select the most effective XIAP antagonists.

For 3D modelling Schrödinger "Small Molecule Drug Discovery Suite" software package was used. Based on the results of cross docking calculations, the 4HY0 crystal structure was selected leading to the best performing model of XIAP BIR3 domain. To incorporate flexibility of the receptor, the Induced Fit Docking module was applied, followed by MM-GBSA binding free energy calculations.

The ΔG free energy values correlated with the biological activities of the reference compounds (XIAP-BIR3 K_d values: AVPI: 580 nM; AVPF (AVPI Ile \rightarrow Phe) 290 nM; LCL161: 52.7 nM). Some of the library members (e.g. Lead 1 (S)) showed lower free energy values (Figure 11).

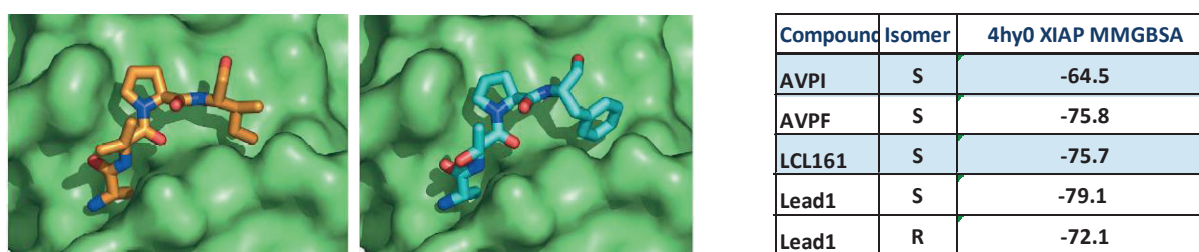


Figure 11. a.) 3D modelling for virtual screening (AVPI- and AVPF-XIAP complex – 4hy0) b.) ΔG free energy values (kcal/mol) of the reference and CIX lead compounds. (Note: Lead 1 = CI6_7 see later)

In vitro screening later confirmed that even the R/S diastereomeric mixture of Lead1 (CI6-7) showed increased cytotoxicity compared to LCL161. Additional cheminformatics methods were applied to improve the performance of the virtual screening. The possible binding features of the small molecules can be assessed by their 3D conformational flexibility and shape (ChemAxon MarvinSketch Screen3D).¹⁷ Applying flexible alignment analysis and molecular dynamics, the statistically average conformations generated allows to rapidly compare the 3D similarity between two compounds. The 3D similarity measures are expressed in 3D Tanimoto coefficient (T3D). 3D similarity helps the analog design revealing close 3D shape between the active compounds and the candidates in rational design (3D similarity of LCL161 and AVPF, T3D= 0.7) as it is illustrated in Figure 12.

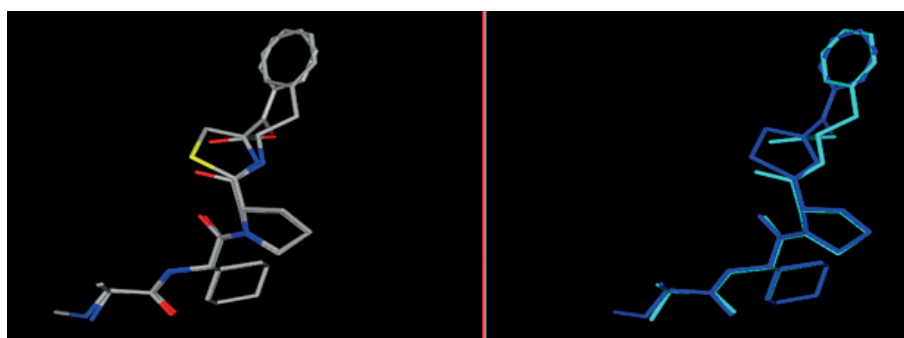


Figure 12. 3D similarity of LCL161 vs. AVPF 3D similarity (T3D = 0.7)

In addition, based on the structure of available XIAP-BIR3 binding ligands (20) a consensus pharmacophore model was developed. For model validation, LCL161 was used as a “required match”. The ADHHR_4 model was selected as the best performing consensus pharmacophore arrangement (BEDROC α 160.9: 0.98) (Figure 13). This model has sufficient capacity for *in silico* screening of an extended virtual thiazole library (72k).

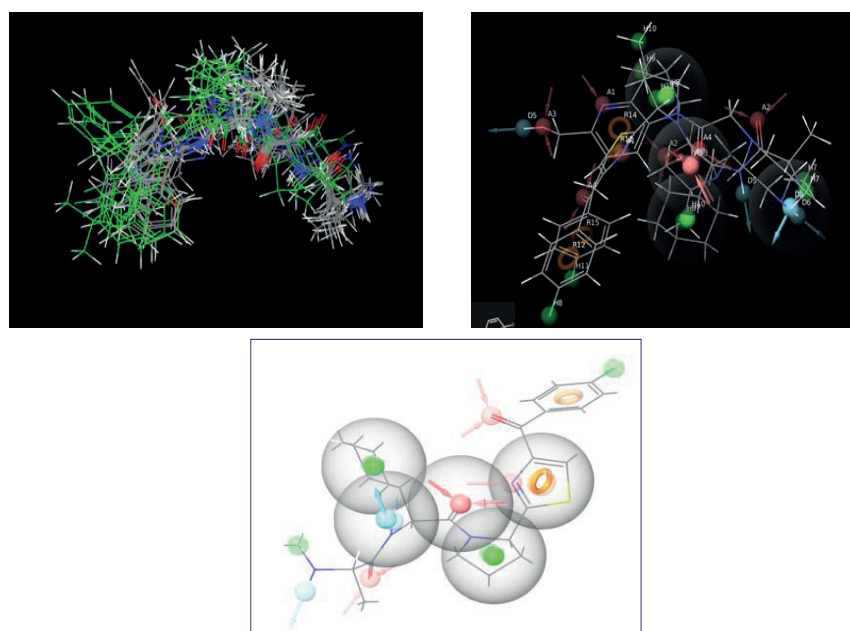


Figure 13. Generation of pharmacophore models for XIAP BIR3 binding ligands: Matching 20 compounds; identification of the major pharmacophoric features; ADHHR_4 as best performing model (LCL161 is shown as the best match).

Scaffold hopping

Using our established pharmacophore model and 3D similarity comparisons of known IAP ligands applying MarvinSketch Screen 3D, novel compounds were designed (Figure 14).

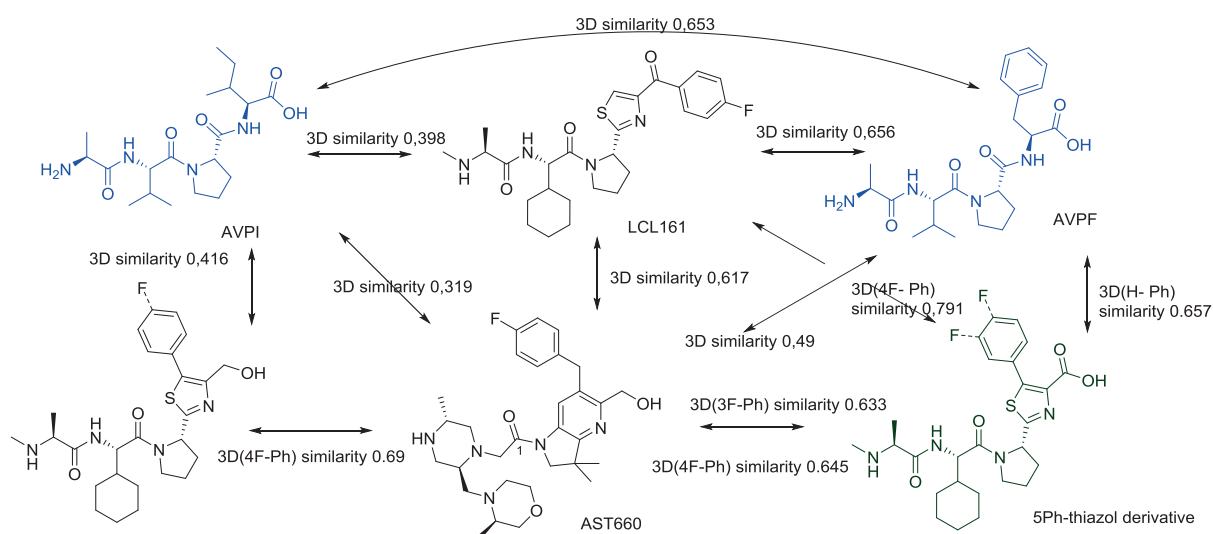


Figure 14. 3D similarity correlations of IAP ligands

Based on the similarity results, the substitution and the modification of the position of the phenyl group in the thiazole ring showed further possibility. Increasing the freedom on the phenyl ring by inserting a methylene group had even better fitting and potential, as shown by the respective *Tanimoto* coefficients: T3D=0.86 vs 0.78 as illustrated in Figure 15.

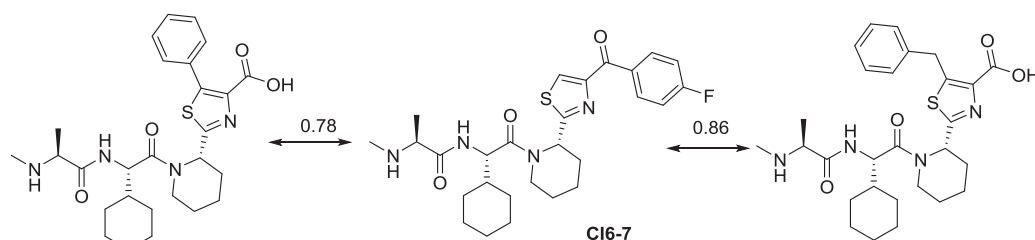


Figure 15. Scaffold hopping via 3D similarity of phenyl and benzyl substituted thiazole

The possibility of the modifications was confirmed by the biological results (Tables 1 and 7). The introduction of a new functional group in the molecule allowed us to develop new derivatives and a new possibility to conjugate the molecule with linkers and carrier compounds.

Cytotoxicity of novel XIAP antagonists

The best-fitting compounds were prepared and tested. The results confirmed the expected binding and cytotoxicity. The results are summarized in Table 1.

The following conclusions have been drawn from the biological data:

1. There is a long-lasting dogma in the publications that replacement of the pyrrolidine ring to piperidine decreases the XIAP antagonist activity. „At the proline position (*of AVPI*),

replacement with a variety of amino acids leads to a dramatic loss in binding affinity. ...piperidine, bearing a six-membered ring, exhibits ...10-fold decreases in the K_d value....” (Cong *et al.*).⁶ We found that such replacement (LCL161 → CI6_7) led to 2-4-fold cytotoxic activity increase and with this “irrational” modification we entered a patent-free area. Our modification was supported by the 3D modelling studies.

2. We identified a novel substitution pattern on the thiazole ring (CI12_3 and CI12_7) that showed improved or equal cytotoxic activities compared with LCL161. These novel analogs opened new opportunities for further analog design.

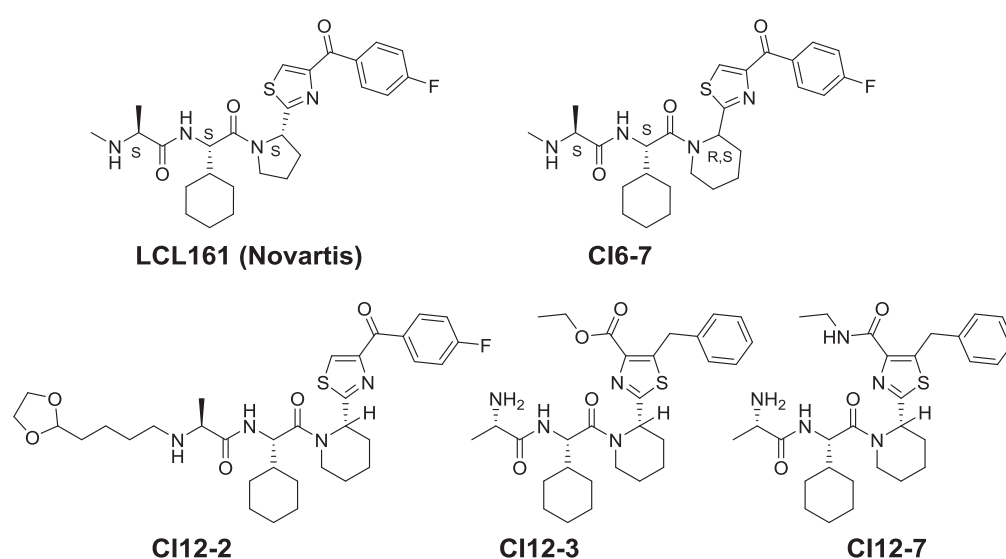


Table 1 shows that the different forms of the CIX Lead1 (CI6-7) are 2-4-fold more active than LCL161, particularly on pancreatic tumor cells, the IC₅₀ value of CI6-7 2xTFA (SSS) on PANC-1 cell line is 11 μM – 72 h, while LCL161 base is cytotoxic at 58 μM concentration on the same cell line and 72 h incubation period.

Table 1. The IC₅₀ values are shown in μM concentration

Compounds (form/isomer)	Test ID	PANC-1 – xCELLigence SP (Pancreas)			A2058 (Melanoma)		
		24 h	48 h	72 h	24 h	48 h	72 h
LCL161 base (SSS)	CI4-49	54.9	79.5	58.5			
LCL161 xHCl(SSS)	CI6-6	100	100	67.5	99	55	52
CIX CI6-7 xHCl (RS,SS)	CI6-7	32	37	31	18	21	14
CIX CI6-7 base (RS,SS)	CI9-4						9
CIX CI6-7 2xTFA (RS,SS)	CI10-2			14.3			13.9
CIX CI6-7 2xTFA (SSS)	CI10-3			11.7			14.6
CIX CI6-7 2xTFA (RSS)	CI10-4			23.2			11.8
CIX CI12-2, base (SSS)	CI12-2	18.2	17.6	19.9	22	46.4	12.8
CIX CI12-3 base (SSS)	CI12-3	26.4	32.7	36.4	21	13.6	8.19
CIX CI12-7 base (SSS)	CI12-7	93	54.6	60	50.4	27.3	35.8

Compounds (form/isomer)	Test ID	EBC1 (Lung)			Colo205	MiaPaca (Pancreas)	MdaMb231 (Breast)
		24 h	48 h	72 h	72 h	72 h	72 h
LCL161 base (SSS)	CI4-49				39.4	16.8	
LCL161 xHCl(SSS)	CI6-6	> 100	84	54			
CIX CI6-7 xHCl (RS,SS)	CI6-7	29.5	25	25			
CIX CI6-7 base (RS,SS)	CI9-4			7.7	7.4	8.8	1.5
CIX CI6-7 2xTFA (RS,SS)	CI10-2				14.7	6.5	
CIX CI6-7 2xTFA (SSS)	CI10-3				13.3	6.2	
CIX CI6-7 2xTFA (RSS)	CI10-4				11.9	10.3	
CIX CI12-2, base (SSS)	CI12-2	30.3	34.7	41.1	15		
CIX CI12-3 base (SSS)	CI12-3	32.1	18.8	13.2	11		
CIX CI12-7 base (SSS)	CI12-7	70.5	38.2	28.2	24.6		

Property forecast and drug likeliness of the lead compound¹⁸

The measured and calculated physicochemical parameters listed in Table 2 were similar to the reference compounds, thus the predicted character of the lead compound is conformed with the drug-likeliness criteria needed for further development.

Table 2. Drug likeliness of Lead 1 compared with relevant drug in clinical trials

Parameter	LCL161	Lead 1 (CI6-7)	AST660
Mw	500.63	514.66	539.70
HBD	2	2	2
HBA	5	5	7
TPSA	91.4	91.4	81.17
CLogP (calculated)	3.78	4.22	2.62
ChromLogD (measured)	3.0	3.1	3.1*
Property Forecast Index ¹⁹	5.0	5.1	5.1

*Literature data²⁰

Development of further XIAP antagonist hit compounds

The new molecules have potential modification possibilities in the P3 and P4 positions.

The key elements as the chirality and the size of the P3 ring, as well as the substitution possibilities of the thiazole ring were systematically checked. The potential development directions are shown in Figure 16.

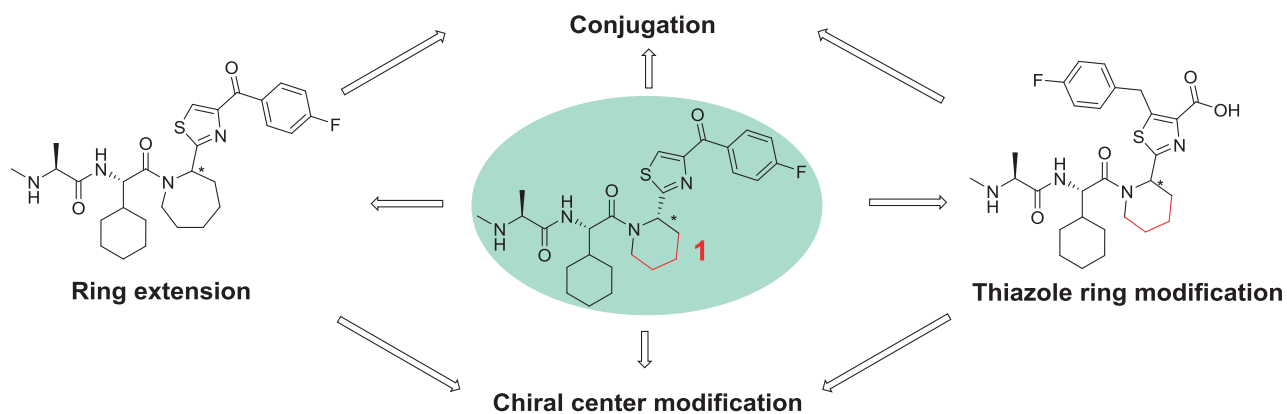
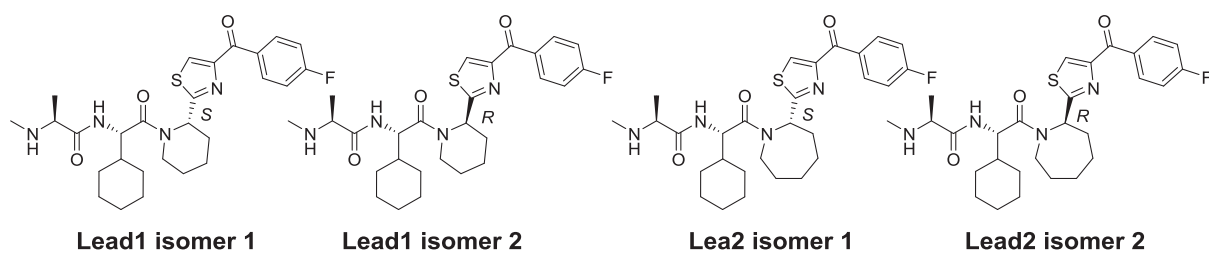


Figure 16. Development possibilities of the Lead 1 compound

Effect of the chirality and extension of the P3 ring

The piperidine ring was enlarged to azepane and the epimers of the stereoisomers of the molecules were docked in our *in silico* model. Both compound pairs fit in the receptor with high binding energy.



#	Compound	Isomer	XIAP BIR3 (4HY0) MMGBSA (Kcal/mol)
1	AVPI	1	-64.5
2	AVPI	2	-63.3
3	AVPF	1	-75.8
4	AVPF	2	-58.8
5	LCL161	1	-75.7
6	LCL161	2	-77.0
7	Lead1	1	-79.1
8	Lead1	2	-72.1
9	Lead2	1	-80.6
10	Lead2	2	-72.8

Figure 17. *In silico* binding values of the epimers and the ring extension

The results listed in Figure 17 showed that the new compounds and epimers were fitting well in the model; therefore the molecules were prepared and tested. The results summarized in Table 7 confirmed that the modification is possible, serving a novel set of compounds.

Rational analog design and development of Sigma 1/2 ligands

Rational analog design of Sigma-1 or Sigma-2 receptor ligands started from the initial hit compound CI1-25.

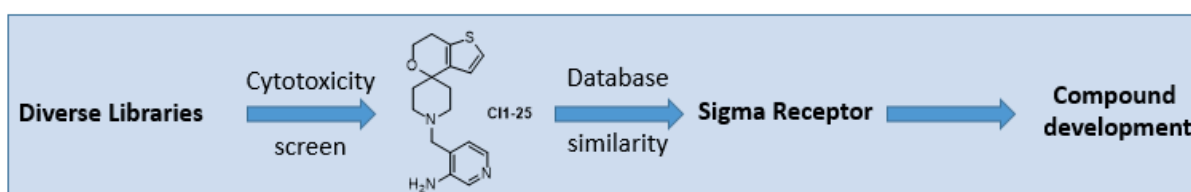


Figure 18. Development scheme of novel Sigma Receptor ligands

Retaining the spiro ring system, R_1 (alkyl, aryl) and R_2 substituents were varied and systemically designed applying the TOL platform.

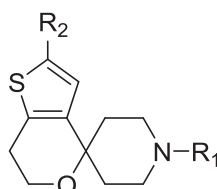


Figure 19. Rational design of dihydrospiro[piperidine-4,4'-thieno[3,2-c]pyran] library

A two-dimensional compound library was generated applying *in silico* methods and compound development based on the cytotoxicity screen results.

Cheminformatics methods to support the rational design of the sigma-1,2 ligands

The 3D modelling is very challenging, since crystal structure is only available for sigma-1 proteins, furthermore, similar structures could act as agonists or antagonists and often allosteric interactions could also be predominant. Therefore, 3D and homology methods were only used for fragment screening or confirmation of the biological activities. The 5HK1 sigma-1 receptor crystal structure was selected for the 3D model building based on the results of cross-docking experiments of sigma-1 ligands with various receptors. The binding site was optimized by using Induced Fit Docking calculation with selected ligands. The fragment library was docked to the optimized binding site using the Schrödinger Glide SP program.

The best-performing fragments were selected and used in analog design. The novel virtual structures were first filtered for drug-like properties and synthetic feasibility, and followed by virtual screening using pharmacophore models (Figure 20). After ranking the compounds, the promising virtual hits were docked to 5HK1 (Figure 21) and ranked again based on the free energy values.

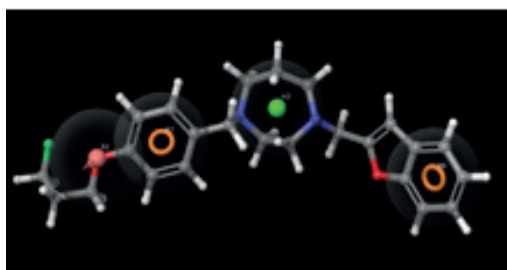


Figure 20. Pharmacophore model based on the structure of Haloperidol

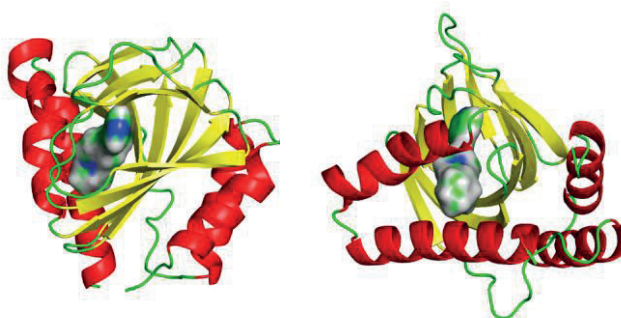


Figure 21. Binding model of CI7-8 lead compound to 5HK1 S1 receptor

Development of Sigma receptor ligands

Based on the rational analog design strategy and virtual screening, more than 50 compounds were synthesized and pre-screened for cytotoxicity (Figure 22).

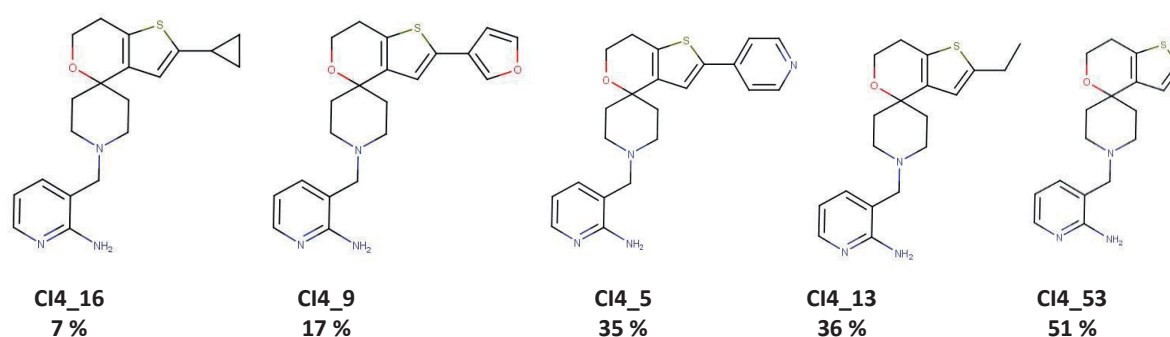
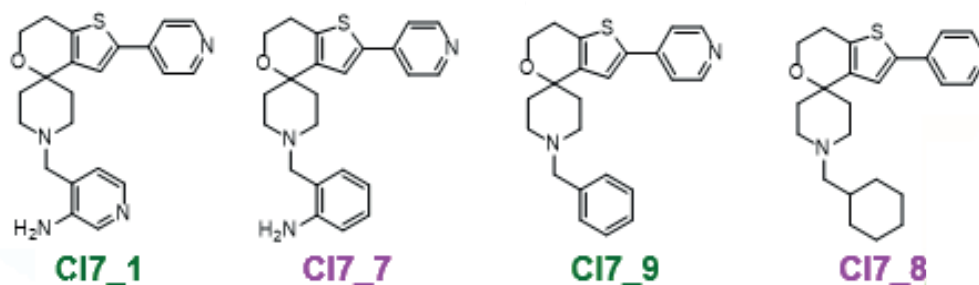


Figure 22. Cytotoxicity results of the first rounds of sigma-1,2 ligands (PANC1 cell line; cell viability %, 72 h, at 10^{-4} M concentration)

Based on the results, a second analog set was prepared according to the original rational design plan. The pyridine-substituted dihydrospiro[piperidine-4,4'-thieno[3,2-c]pyran] series, by removing the *N* atom and the amino group from the pyridinyl-methyl side chain; plus saturating the aromatic ring, led to the identification CI7_8 as a potential lead compound.



The cytotoxic effect of the new compounds was tested on different cell lines (Table 3). The modifications showed a robust correlation with the *in silico* model (Table 4). For hit validation, a new batch of CI7_8 was synthesized (ID: CI9_1); the concentration dependency was measured and the IC_{50} values were determined. (Table 5)

Table 3. Cytotoxicity results of selected sigma 1-2 ligands (various cell lines; cell viability %, at 24, 48, 72 h, in 10^{-4} M concentration).

ID	PANC1			A2058 - Melanoma			EBC1 - Lung			Colo205- Colon		
	24	48	72	24	48	72	24	48	72	24	48	72
CI7_1	53	62	80	68	67	67	78	44	26	72	39	23
CI7_7	17	16	16	23	11	9	62	23	14	39	18	14
CI7_8	11	10	9	27	15	13	48	22	14	37	18	14
CI7_9	69	76	41	30	35	37	55	31	34	88	53	64

Table 4. The free energy values and the physicochemical parameters of sigma lead compounds (PDB: 5HK1)

Compound	MM-GBSA ΔG (kcal/mol)	MW	HBA	HBD	LogP	Fsp3	TPSA	Rotable Bonds
CI7-7	-81.8	391.5	4	1	3.07	0.35	51.4	3
CI7-8	-89.0	382.6	3	0	4.29	0.61	25.4	3
Haloperidol	-84.4	375.9	3	1	3.66	0.38	40.5	6

Table 5. IC₅₀ values of CI9_1 lead compound using various cancer cell lines measured at 24, 48 and 72 hrs (values are in μM).

ID	PANC1			A2058 - Melanoma			EBC1 - Lung			Colo205- Colon		
	24	48	72	24	48	72	24	48	72	24	48	72
CI9_1 (CI7_8)	76.6	71.2	53.1	55	48.1	3.37	66.2		8.3	66.2	24	8.7

CI9_1 was particularly efficient in melanoma, lung cancer and colon cancer cell lines, showing low micromolar cytotoxicity. Although the scaffold was the same, these compounds were significantly different from the Esteve compounds, which were reported earlier as sigma ligands.^{21,22} Depending on the substituent pattern around the above core the compounds show affinities to both Sigma-1 and Sigma-2 receptors with varying ratio. The synthesized novel dihydrospiro[piperidine-4,4'-thieno[3,2-c]pyran] derivatives (CI7_8 or CI9_1) showed equal cytotoxicity to the reference XIAP antagonist LCL161.

Generating Small Molecule Targeting Drug Conjugates by linking novel XIAP antagonists and novel sigma-1,2 ligands

Since one of the major objectives of the project was to connect the apoptosis inducer “warhead” to targeting molecules, the CI6-7 compound was extended with a linker at the P1 alanine site (CI12-2).

Hawkins and his coworkers previously reported sigma-2 conjugates with XIAP antagonists. Since sigma-2 receptors are overexpressed in many proliferating tumor cells and the complexed ligands were internalized in the cancer cells, they assumed that sigma-2 receptor was an attractive target for drug delivery.¹² They attempted to conjugate apoptosis-inducing compounds (“warheads”) such as XIAP antagonists with sigma-2 ligands as a targeting or delivering tool. They constructed a typical Small Molecule Targeting Drug Conjugate compound.

Similarly, novel conjugates were rational to design and test since we identified both novel XIAP antagonist and sigma receptor ligands. Based on the above analogy we assume that our sigma ligands act also as at least partially sigma-2 binding ligands. (Figure 22)

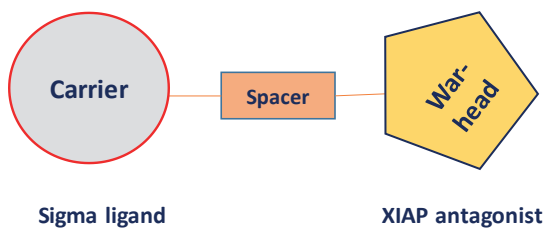


Figure 23. General structure of the XIAP antagonist sigma-2 ligand conjugates

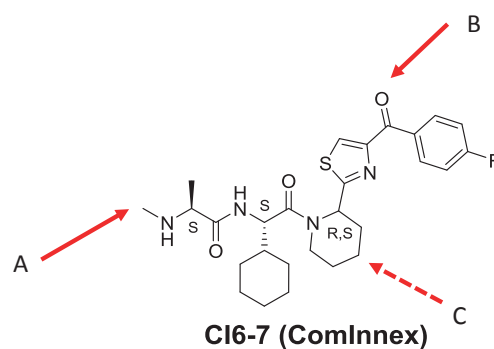


Figure 24. Possible conjugation sites in CI6-7

it has been established that the XIAP antagonist sigma-2 ligand conjugate exhibited higher cytotoxic activities than either of the parent (monomeric) compounds. More significant cytotoxicity increase was observed with the XIAP antagonist portion, while the cytotoxic activity was doubled for the sigma-2 ligand. In order to design a XIAP antagonist sigma-2 ligand conjugate, the optimal linker position should be identified. For the XIAP antagonist portion there were several options based on literature analogies:

Since previously we have already synthesized CI12-2 for possible multipurpose conjugation and the compound showed reasonable activity, we have the A-variation in hand. For the sigma-2 ligand portion, only limited connection site was feasible through the spiro-piperidine substructure. These two linkers, containing compounds with the dioxolane masked aldehyde functionality, are shown in Figure 25. Surprisingly, CI11_4 had poor cytotoxic activity, which accounted for some uncertainty for the expected activity of the conjugate. The linker length was predicted by *in silico* modelling studies as 5 carbons. (Figure 26)

The biological activity of the SMDT conjugate showed excellent cytotoxic activities on several cell lines, interestingly, with little time dependency. The conjugate doubled the biological activity towards the XIAP antagonist and showed more than one order of magnitude cytotoxicity increase compared with the sigma-2 ligands (Table 6).

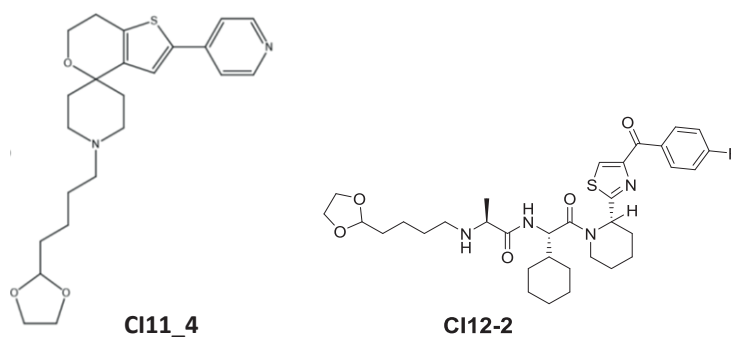


Figure 25. Two halves of the linker-containing portion as potential compounds for assembly

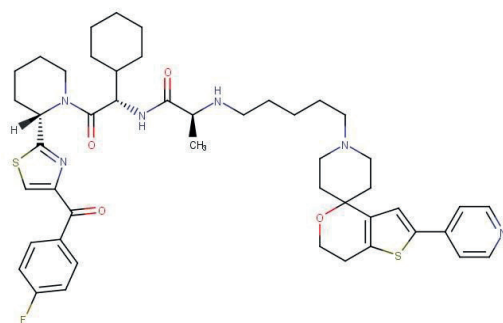


Figure 26. The XIAP antagonist sigma-2 ligand conjugate (CI12_1)

Table 6. Comparative IC₅₀ (μM) of the Chimera compound on tumor cells

	ID	PANC1			Melanoma			EBC1 - Lung			Colo205- Colon			
		Time	24	48	72	24	48	72	24	48	72	24	48	72
XIAP antagonist	CI10-3			11.7			14.6							13.3
XIAP antagonist with linker	CI12-2	18.2	17.6	19.9	22	46.4	12.8	30.3	34.7	41.1	15			15
Sigma ligand	CI9_1 (CI7_8)	76.6	71.2	53.1	55	48.1	3.37	66.2		8.3	66.2	24		8.7
Sigma - XIAP ant. Conjugate	CI12_1	6.5	6.71	6.56	5.18	5.54	3.44	6.85	6.97	6.58	6.73	5.93		3.17

Cytotoxicity screening of XIAP antagonists and sigma-1,2 ligands

Impedimetric assay

Biological tests were performed on different tumor cell lines, PANC1 (pancreatic adenocarcinoma), COLO-205 (colon cancer), A2058 (melanoma), EBC1 (lung cancer), Miapaca (pancreatic ductal adenocarcinoma) and MDA MB231 (breast cancer). Cytotoxicity was measured by impedance-based technique²³ in an xCELLigence SP (ACEA) system.

Colorimetric assay

In the case of COLO-205, A2058 and EBC-1 cell lines, a colorimetric assay (alamarBlue- or MTT-test) was used to determine the antiproliferative/cytotoxic effects of the ONC201 derivatives as references. These colorimetric assays were chosen because for these cell lines there was no stable plateau phase (A2058) or there was only a weak/negligible adhesion (COLO-205 and EBC-1), therefore detection with the xCELLigence System was not feasible.

Summary of the cytotoxicity results

The results of the representative compounds are listed in Table 7.

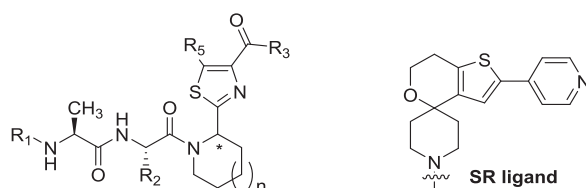


Table 7. The IC₅₀ results of selected IAP binders indicating the sensitive cells among the 6 tested cancer lines (Pancreas, lung, breast, colon and melanoma)

Code	R ₁	R ₂	R ₃	R ₅	n	* isomer	Salt	IC ₅₀ μM (72h)	Cell line
CI6-7	Me	cHex	pFPh	H	1	RS	HCl	14	Melanoma
CI9-4	Me	cHex	pFPh	H	1	RS	Base	2	Brest
CI10-2	Me	cHex	pFPh	H	1	RS	TFA	7	MiaPaca
CI10-3	Me	cHex	pFPh	H	1	S	TFA	6	MiaPaca
CI10-4	Me	cHex	pFPh	H	1	R	TFA	10	MiaPaca
CI11-1	H	cHex	pFPh	H	1	S	HCl	40	Panc1
CI11-2	H	cHex	pFPh	H	1	RS	HCl	33	Panc1
CI12-5	Me	cHex	NHEt	Ph	0	RS	Base	35	Panc1
CI12-1	-(CH₂)₅-SR ligand	cHex	pFPh	H	1	S	Base	0.8	Melanoma
CI12-2	-(CH ₂) ₅ -2-dioxolane	cHex	pFPh	H	1	S	Base	20	Panc1
CI12-3	H	cHex	NHEt	Bn	1	RS	Base	25	Colo205
CI12-4	H	cHex	OH	Bn	1	RS	Base	>100	
CI12-7	H	cHex	OEt	Bn	1	RS	Base	8	Melanoma
CI12-6	H	BuNH ₂	pFPh	H	1	S	Base	54	Melanoma
CI14-1	-CH ₂ (CH ₂) ₂ CO ₂ CH ₃	cHex	pFPh	H	1	S	Base	7	Brest
CI14-2	-CH ₂ (CH ₂) ₄ CH ₂ OH	cHex	pFPh	H	1	S	Base	6	Brest
CI14-3	-(CH₂)₅-SR ligand	cHex	pFPh	H	1	R	Base	0.8	Melanoma
CI15-3	-(CH ₂) ₃ -CO ₂ -(CH ₂) ₆ -SR ligand	cHex	pFPh	H	1	S	Base	25	Colo205
CI15-4	Me	cHex	O ⁻ -(CH ₂) ₅ -SR ligand	Bn	1	S	Base	2	Colo205
CI15-6	Me	CH ₂ (CH ₂) ₂ CO ₂ CH ₃	pFPh	H	1	S	Base	>100	
CI15-5	Me	CH ₂ CH ₂ SCH ₃	pFPh	H	1	S	Base	34	Colo205
CI15-7	Me	cHex	pFPh	H	2	RS	Base	14	Colo205

Collateral sensitivity determination of XIAP antagonists and sigma-1,2 ligands

Collateral sensitivity was identified by Gottesman and Szakács in the early 2010s. Collateral sensitivity is a “phenomenon in drug-resistant cells whereby the development of resistance in cells to one agent can confer higher sensitivity to an alternate agent than seen in the original (parental) line”. In other words, the resistant cell line is more sensitive to a cytotoxin than the parental line from which it is derived.²⁴ Abate and co-workers reported that the cytotoxicity of sigma-2 ligands²⁵ is increased in multi-drug resistant cells, thus the multiresistant cells are sensitized to the cytotoxic agents. Based on these findings we initiated to test our hit compounds in cancer cells together with their multidrug-resistant counterparts. In order to identify the cytotoxicity difference, two cell lines were selected: Mes-Sa parental and Mes-Sa/Dx5 multidrug-resistant uterine sarcoma cell lines.

Cytotoxicity measurements on MES-SA and MES-SA/Dx5 multiresistant cell lines

In the co-culture system, after trypsinization, suspensions of MES-SA mCherry²⁶ and MES-SA/Dx5 eGFP were tested. Measurements were also performed with MES-SA/Dx5 (*in the Tables 'Dx5'*) cell lines in the presence of the P-gp inhibitor tariquidar (TQ) in order to identify whether the selective toxicity of the compounds (the collateral sensitivity) is linked to the glycoprotein P (P-gp) efflux pump. Our compounds are presumably not interacting with ABCB1, since no significant change in IC₅₀ occurs in the case of tests against cancer cell lines when TQ is present, compared with LCL161, where a significant effect was detected. The two XIAP antagonists – the reference compound LCL161 and particularly our lead compound (CI6-7 SSS) – showed increased sensitivity towards the multidrug-resistant cell line. **Notably, the cytotoxicity of CI6-7 SSS on DX5 cell line was 4.14 μM.**

Table 8. IC₅₀ measurements on MES-SA and MES-SA/Dx5 cell lines (in μM).

	Mes-Sa- mCherry	Mes-Sa- mCherry	Mes-Sa- mCherry	Mes-Sa average IC50	Messa- mCh(TQ)	Dx5- eGFP	Dx5- eGFP	Dx5- eGFP	Dx5 average IC50	Dx5- eGFP(TQ)
Compound	72h	120h	144h	72-120-144h	144h	72h	120h	144h	72-120-144h	144h
CI7-8 2HCl	12.95	13.40	14.34	13.56	12.65	9.04	7.22	10.01	8.75	8.52
LCL161	19.53	21.97	34.61	25.37	16.69	16.95	17.19	17.10	17.08	13.18
CI12-1	1.93	1.98	1.39	1.77	1.96	2.33	2.21	2.11	2.22	1.82
CI7-7 HCl	18.33	19.39	20.78	19.50	18.11	15.54	15.84	17.01	16.13	16.41
CI6-7 SSS	14.96	16.28	13.95	15.06	11.11	3.04	3.25	6.12	4.14	5.65
Values: IC50 in [uM]										
Mes: Human uterus sarcoma drug sensitive cell line										
Dx5: multidrug resistant cell line										
TQ: tariquidar, ABCB1 inhibitor										

Table 9. Collateral sensitivity determination on MES-SA and MES-SA/Dx5 cell lines (IC₅₀ values are shown in μM).

	Mes-Sa average IC50	Dx5 average IC50	Selectivity Ratio (Mes/Dx5)	Dx5-eGFP	Dx5-eGFP(TQ)	Selectivity Ratio (Dx5/Dx5)(TQ)
	72-120-144h	72-120-144h	72-120-144h	144h	144h	144h
CI7-8 2 HCl	13.6	8.75	1.55	10	8.523	1.17
CI7-7 HCl	19.5	16.13	1.21	17.1	13.2	1.29
LCL161	25.4	17.1	1.85	17	16.4	1.04
CI6-7 SSS	15.06	4.136	3.64	6.123	5.649	1.08

Collateral sensitivity measurements revealed that the two sigma 1,2 ligands show moderate collateral sensitivity (Selectivity Ratio - Mes/Dx5 = 1.2-1.5). While the two sigma ligands show moderate collateral sensitivity, our XIAP antagonist lead compound (CI6-7 SSS) indicated increased sensitivity towards the multidrug-resistant cell line (**Selectivity Ratio - Mes/Dx5 = 3.64**).

The presence of the P-gp inhibitor tariquidar (TQ) in a multidrug-resistant cell line (Dx5) does not influence the selective toxicity of the compounds (Selectivity Ratio = $(Dx5/Dx5)(TQ) \sim 1$), which suggests that the observed collateral sensitivity could be linked to other, cell line-specific factor(s).

PAMPA modelling assay

The potential absorption of the compounds was tested by PAMPA test.²⁷

Table 10. Permeability test results of lead compounds

Compound	Calc (nm)	C ₀ (μM)	C _d (μM)	C _a (μM)	C _e (μM)	P _e (cm/s*10 ⁻⁶)	R (%)
Caffeine	270	50	42.4	11.2	29.9	10.4	0.33
LCL161	270	50	40.9	8.6	28	8.2	6.64
CI7-8	310	50	23.7	9.9	18.2	17.5	39.34
CI12-1	295	50	10.4	0.6	6.5	2.3	78.38
CI7-7	310	50	20.5	8.7	15.8	17.8	47.29
CI6-7	275	50	33.1	14.3	25.5	18.2	14.85
Calc: the characteristic absorption peak in UV							
Pe: permeability							
R: recovery							

The results showed that CI7-7, CI7-8 and CI12-1 had high, CI6-7 medium and LCL161 low permeability compared to caffeine as a reference compound. That means that the permeability of our IAP antagonist was increased significantly and the sigma ligand serves as a carrier molecule which might exploit the active transport in the sigma receptor. It is also interesting that LCL161 has lower penetration than our lead CI6-7.

Synthesis of the compounds by applying innovative procedures

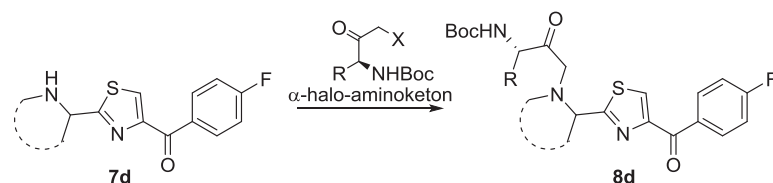
The reactions were carried out according to the best practice of comprehensive organic chemistry in standard chemical laboratory environment following the general rules and conditions of compound preparations.

Analytical methods

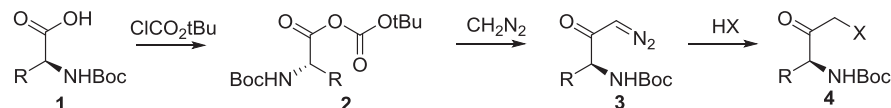
Purity analyses and molecular weight determination of the samples were performed on a Waters 2695 HPLC/ Waters ZQ MS system or on a Waters Acquity H-class/ Qda MS system. The optical purity was determined by chiral HPLC tests applying YMC CELLULOSE-SB 250*4.6, 5 μM column and Heptane-IPA 95-5 eluent at ambient temperature. The structures were confirmed by ¹H, ¹³C and 2D NMR tests at ambient or elevated temperatures.

Preparation α -halo-aminoketones in flow reactor

The first active compound contained $-\text{CH}_2-$ derived structure of amino acids. These types of compounds were prepared by coupling α -halo-aminoketones with the piperidine ring of the intermediate **7d**.



The direct preparation of the reagent from amino acids utilizes *Arndt-Eistert* reaction, which requires dry diazomethane. The safe and effective method worked out by Kappe's group at University Graz²⁸ was adapted in our laboratory for the derivatization of oligopeptides as well.²⁹



The key to the reaction was the special membrane coil Teflon AF-2400, which was permeable for diazomethane and delivered dry diazomethane in the activated amino acid solution. Reaction in continuous conditions gave the required halo-ketone in a safe and simple way, which is illustrated in Figure 27.

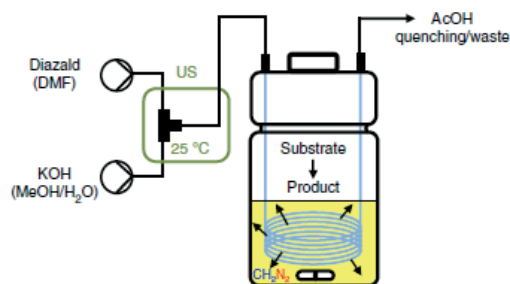


Figure 27. Simplified scheme of the diazomethane flow reactor

Synthesis of XIAP antagonists

Albeit the synthesis of the LCL161 was published by the Novartis researchers,³⁰ several synthetic steps and novel reactions were worked out and used in the preparation of the novel molecules. The synthesis of the compounds is summarized in Figure 28.

The individual routes could be combined since they had several common intermediates. The versatility of the syntheses allowed us to get a high number of different derivatives and complex libraries. The optical isomers of the starting amino acids **1** were

commercially available in pure form and were convenient starting points of the synthesis. The synthetic steps were carried out both with the *S* and the *R* optical isomers in a similar way to get finally the two epimers of the target compounds **10** and **10a**.

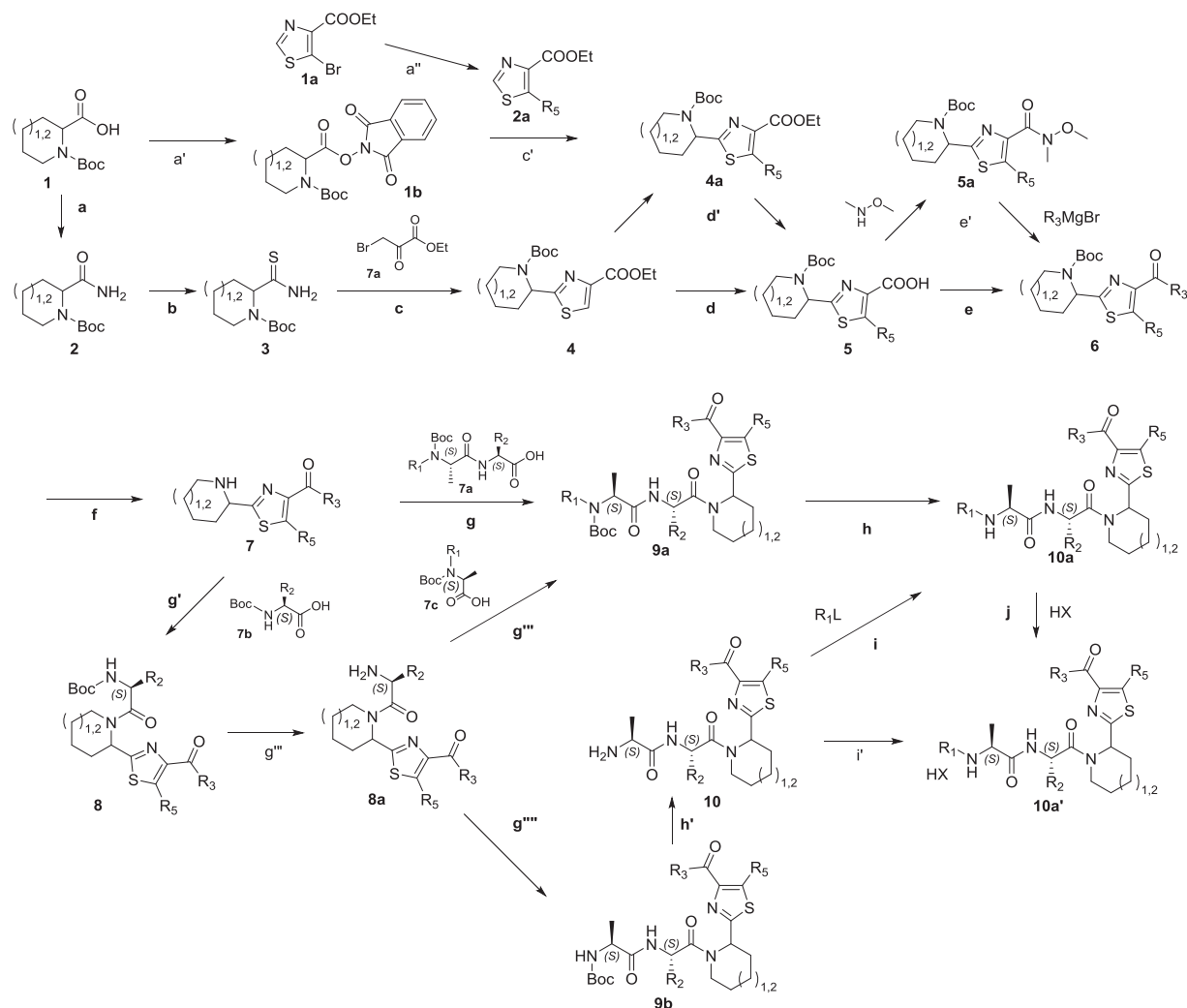


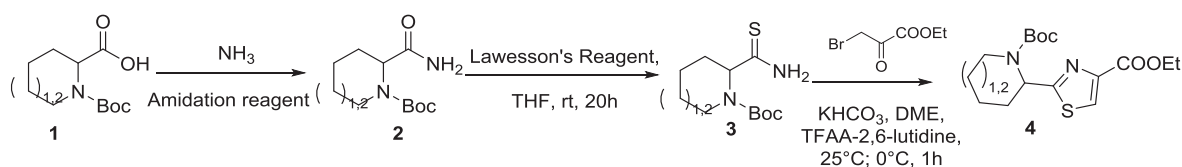
Figure 28. General synthetic scheme of XIAP antagonist library

Stereoselective synthetic methodology was applied to isolate the compounds in optically pure forms, which were confirmed during the synthesis by continuous analytical monitoring and structure confirmations applying chiral HPLC, LCMS and NMR methods. The amide bond was prone to form stable tautomer/rotamer forms, which were elucidated by 2D and heated NMR tests. The syntheses of individual target compounds were basically linear and had around 8 linear steps, thus it had to be started in a relatively big scale to ensure the needed amount of the final compounds. T3P (Propylphosphonic anhydride) as reagent was selected for amidation, which proved to be optimal, since using it in dichloromethane showed high enantio- and diastereo-selectivity and could be washed out from the reaction mixture by

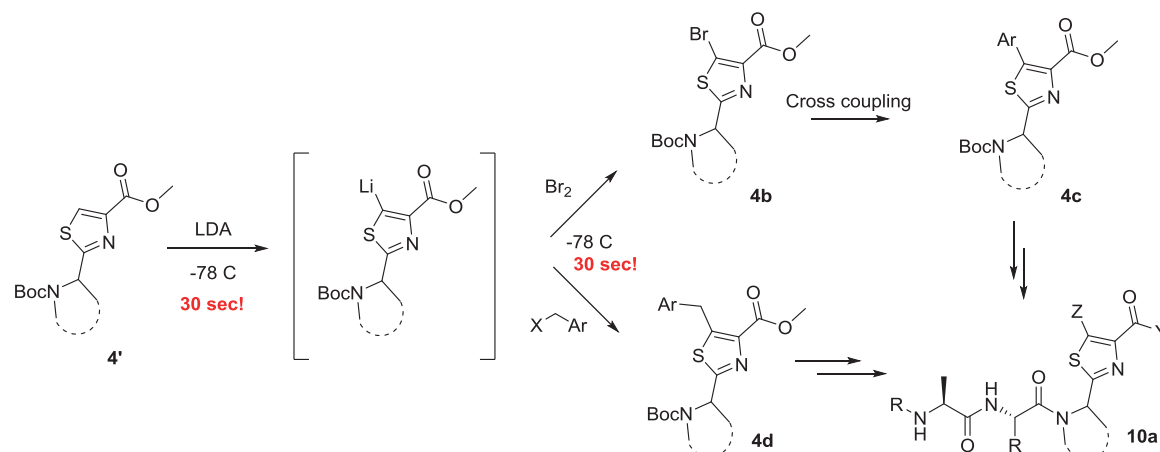
extraction. The products were purified by crystallization or in smaller scale by flash or by preparative HPLC chromatography.

Novel reactions and methodologies for the preparation of substituted thiazoles

Key intermediate thiazole ester **4** was prepared by the reproduction of the LCL161 synthesis; however, the published route was not appropriate for expanding the preparation to get compound libraries, therefore novel reactions were worked out for the substitution of the thiazole-4-carboxylate ring either at *C2* or *C5* position.



In the described approach³¹ compound **1** was transformed to the corresponding amide **2** by applying routine amidation reaction. The formation of thioamide **3** needed careful operation, since over 50°C the molecule racemized. Ring closure of thioamide **3** had to be carried out in neutral conditions otherwise the compound racemized again or lost the Boc protecting group. The classical methodology to transfer intermediate **4** to **4a** thiazole derivatives was based on lithiation reaction.³²



The reaction published in the literature was hardly reproducible since both the lithiation and the transformation of the lithium salt requested quick operations at low temperature, otherwise the sensitive intermediates decomposed. Applying IceCube continuous reactor supplied by ThalesNano, the reaction was carried out stereoselectively in good yields. The reactor set-up is illustrated in Figures 29 and 30.

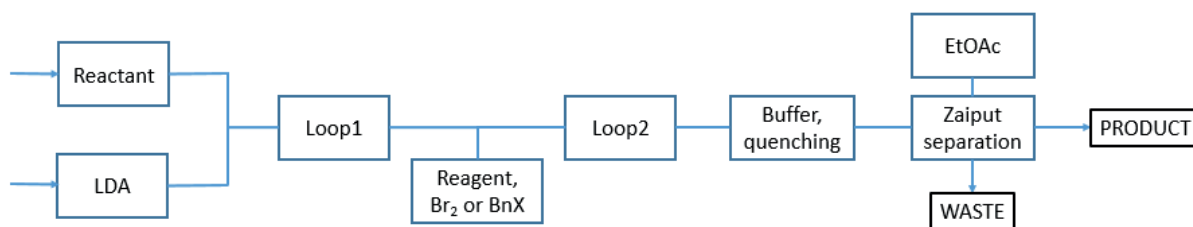
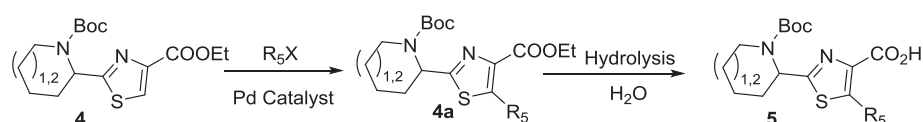


Figure 29. Continuous preparation of 5 substituted thiazole carboxylates using IceCube



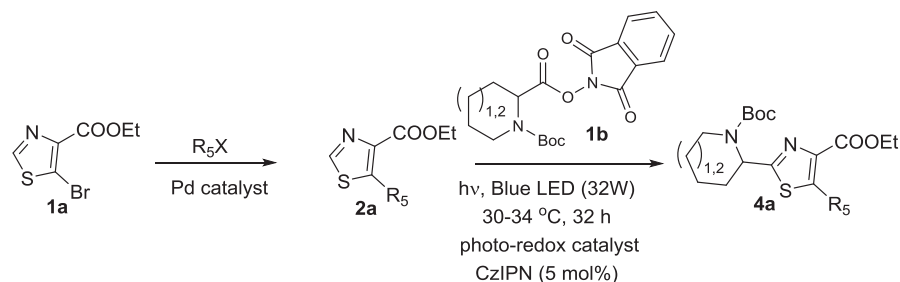
Figure 30. ThalesNano IceCube and PhotoCube reactor

Starting from intermediate **4** a novel reaction was worked out for the direct substitution of the thiazole ring in position *C5* to get the new derivative.³³



Activation of compound **4** using palladium catalyst then substitution with benzyl-halide gave **4a**, which delivered the acid **5** after hydrolysis using mild conditions. The isolated compounds had over 90% ee. Fortunately, after coupling the acid with chiral amino acids the formed diastereomers could be separated and optically pure compounds were isolated.

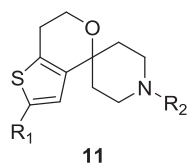
To increase the chemical possibilities a new route was worked out for the substitution of thiazole ring in *C2* position as well. The reaction was developed by applying the *Minisci* photo-redox reaction³⁴ using the photoreactor supplied by ThalesNano Inc (Figure 30). For the successful reaction, 5-bromo-thiazolate **1a** had to be converted to aryl-substituted derivative **2a** applying classical coupling reactions.



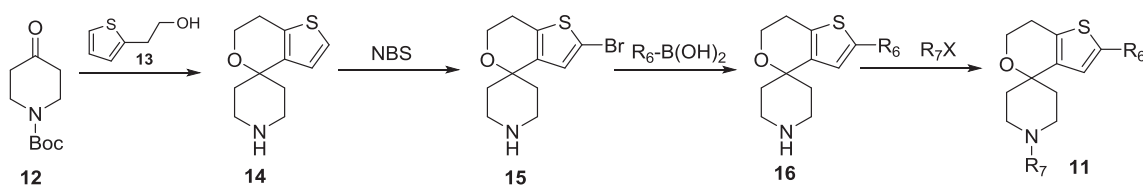
The stereoselective conversion of optically active pipecolic acid reagent still needs further development.

Synthesis of Sigma receptor ligands

The core structure of the active Sigma Receptor ligand of compound **11** was systematically derivatized and tested to have SAR data and to find correlations to confirm the *in silico* modelling results.



Albeit the general core structure was known and published,³⁵ we worked out a simple method for the synthesis of the skeleton which allowed us to generate a two-dimensional compound library.



Starting from piperidone **12** the spiro-condensation was carried out in acidic conditions with thiophene-ethanol **13**. The thiophene ring was then selectively brominated with *N*-bromosuccinimide forming the key intermediate **16**, which was transformed in two steps to the **11** derivatives *via* cross-coupling and *N*-substitution reactions. The free amine function of compound **16** allowed us to connect the compound to linkers and IAP binding warheads.

Conjugation of Sigma and IAP binding ligands, preparation the conjugated chimeras

The two types of compounds were connected with linkers to bridge the two active sites resulting in bifunctional chimeras, where the sigma ligand served as a carrier molecule and the IAP antagonist as an apoptosis inducer “warhead”. The IAP molecule had two connection points to conjugate either at the *N*-terminal function in the peptide chain or at the *C*-terminal functional group on the thiazole ring. The compounds were stable both in base or salt forms. The solubility of the compounds was good, however, when it was possible, the salt form was preferred to prepare to increase their physicochemical and ADME properties.

(cIAP1/2 and XIAP) and the Sigma-1,2 receptors are key elements of the apoptosis regulation.

Our best IAP antagonist compound (31 μ M, 72 h, PANC-1) showed two-fold higher cytotoxic activity than the structurally related Novartis compound LCL161, which is under clinical trials. The replacement of the pyrrolidine ring of the reference compound to piperidine (LCL161 \rightarrow CI6_7) resulted in the increase of cytotoxic activity even though previous reports argued against such change.

We also identified and developed novel sigma receptor ligands with promising cytotoxic activities (51 μ M, 72 h, PANC-1). Sigma receptors have also important roles in apoptosis regulation and cell proliferation. They are characteristic motifs on the cancer cell surfaces, thus, are targeted as tumor markers in the cancer diagnosis.

Both structure groups have proper physicochemical properties and were promising starting points for the development of novel anticancer drug leads.

Based on the role played by sigma receptors in the active internalization of the complexed compounds, we connected the apoptosis-inducing XIAP antagonist compound (“warhead”) with sigma-2 ligands serving as a targeting or delivering tool forming a Small Molecule Targeting Drug Conjugate compound. The resulting chimeras, comprising the in-house discovered best IAP antagonist compound and the novel sigma ligand, multiplied the biological activity compared to the parent XIAP antagonist and showed more than one order of magnitude cytotoxicity increase compared to the reference compounds (3.0-6.6 μ M, 72 h, COLO-205, A2058, PANC-1). The results proved our concept that the targeted transport is feasible. The preliminary *in vivo* data showed positive signs of activity, however, further studies are planned to confirm the results. For the novel compound family a patent has already been filed.

During the project execution, we developed a novel 3D docking and virtual screening technology to identify potential IAP antagonists and sigma ligands based on the available protein structures. During the preparation of the novel structures, innovative synthesis technologies were developed and applied, such as novel *CH* activation reaction, flow chemistry, flow photochemistry and membrane technology.

In summary, by the integration of the biology, chemistry and chemoinformatics we set the foundation of a novel integrated drug discovery platform.

Acknowledgement

We thank all past and present members of the ComInnex management and participating teams for their backing and outstanding scientific and experimental contributions that have enabled us to develop the new promising anticancer compounds and innovative chemistry, especially Gellért Sipos and Gergő Ignác for the flow chemistry solutions and for the development of the photoredox reaction, Dániel Kócsi for the development of the new thiazole substitution reaction based on CH activation. We are grateful to NKFIH for the NVKP16-1-2016-0036 grant and the financial support of the project. We thank the ELTE and the Semmelweis teams for their work and the excellent collaboration especially Gábor Mező for his coordination of the grant consortium and for backing the preliminary in vivo tests of our compounds. We appreciate very much and say a big thank you for Schrodinger Co. for letting us to use the state-of-the art modelling and simulation platform free of charge. We thank András Simon for the 2D NMR structure assignment of compounds, Szilárd Tóth and Gergely Szakács for the collateral testing, József Murányi for the PAMPA experiments and József Tóvári for the mouse xenograft tests. We express our thanks for ThalesNano Inc. for supplying us the flow reactors.

References

1. Apoptosis Physiology and Pathology (Eds.: Reed JC, Green DR, Cambridge University Press, 2011)
2. Mohammad RM, Muqbil I, Lowe L, Yedjou C, Hsu H-Y. *Semin Cancer Biol* **35**: 78-103 (2015)
3. Tewari KM, Dhaneshwar SS. *J Cancer Res* **1**: 213 (2012)
4. Lalaoui N, Vaux DL. *F1000Res* **7**: 1889 (2018)
5. Fulda S. *Clin Cancer Res* **21**: 5030-5036 (2015)
6. Cong H, Xu L, Wu Y, Qu Z, Bian T, Zhang W, Zhuang C. *J Med Chem* **62**: 5750-5772 (2019)
7. Tesei A, Cortesi M, Zamagni A, Arienti C, Pignatta S, et al. *Front Pharm* **9**: 711 (2018)
8. Kim FJ, Pasternak GW. *Proc Nat Acad Sci* **114**: 6888-6890 (2017)
9. Riad A, Zeng C, Weng CC, Winters H, Xu K, Makvandi M, Mach RH. *Sci Reports* **8**: 1-12 (2018)
10. Zeng C, Rothfuss JM, Zhang J, Vangveravong S, Chu W, et al. *Anal Biochem* **448**: 68-74 (2014)
11. Longhitano L, Castracani CC, Tibullo D, Avola R, Viola M, et al. *Oncotarget* **8**: 91099 (2017)
12. Hashim YM, Spitzer D, Vangveravong S, Hornick MC, et al. *Mol Oncol* **8**: 956-967 (2014)
13. Zeng C, Weng CC, Schneider ME, Puentes L, Riad A, et al. *Cell Death Discovery* **5**: 1-12 (2019)
14. Naito M, Ohoka N, Shibata N. *Drug Discovery Today: Technologies* **31**: 35-42 (2019)
15. Huang Y-S, Lu H-L, Zhang L-J, Wu Z. *Med Res Rev* **34**: 532-566 (2014)
16. Finlay D, Teriete P, Vamos M, Cosford ND, Vuori K. *F1000Res* **6**: 587 (2017)
17. Kalászi A, Szisz D, Imre G, Polgar T. *J Chem Inf Model* **54**: 1036-1049 (2014)

18. Leeson PD, Young RJ. *Med Chem Lett* **6**: 722-725 (2015)
19. Young RJ, Green DVS, Luscombe CN, Hill AP. *Drug Discovery Today* **16**: 822-830 (2011)
20. Johnson CN, Ahn JS, Buck IM, Chiarparin E, Day JEH, et al. *J Med Chem* **61**: 7314-7329 (2018)
21. Oberdorf C, Schepmann D, Vela JM, Buschmann H, et al. *J Med Chem* **55**: 5350-5360 (2012)
22. Oberdorf C, Schepmann D, Vela JM, Diaz JL, et al. *J Med Chem* **51**: 6531-6537 (2008)
23. Giaever I, Keese CR. *Proc Nat Acad Sci* **81**: 3761-3764 (1984)
24. Szakács G, Hall MD, Gottesman MM, Boumendjel A, et al. *Chem Rev* **114**: 5753-5774 (2014)
25. Niso M, Riganti C, Abate C. *Receptors Clin Invest* **1**: 208-216 (2014)
26. Pape VFS, Tóth S, Füredi A, Szebényi K, Lovrics A, et al. *Eur J Med Chem* **117**: 335-354 (2016)
27. Di L, Kerns EH, Fan K, McConnell OJ, Carter GT. *Eur J Med Chem* **38**: 223-232 (2003)
28. Pinho VD, Gutmann B, Miranda LSM, et al. *J OrgChem* **81**: 5814-5823 (2016)
29. Sipos G, Ignác G, Bertók B (2019). Flow Chemistry Europe Conference, Cambridge (2019)
30. NOVARTIS AG; Thakur J, Yang D, Feng, L. WO2011/18474 (2011)
31. Deng S, Taunton J. *J Am Chem Soc* **124**: 916-917 (2002)
32. Deng S, Taunton J. *Org Lett* **7**: 299-301 (2005)
33. Kócsi D, Bertók B. unpublished results (2019)
34. Varga I, Balogh F, Ignác G, et al. *J Am Chem Soc* **258**: ACS National Meeting, SanDiego (2019)
35. Meyer C, Schepmann D, Yanagisawa S, Yamaguchi J, et al. *J Med Chem* **55**: 8047-8065 (2012)